UNIVERSITY OF OKLAHOMA

GRADUATE COLLEGE

REGIONAL VARIABILITY OF CANEY SHALE ELEMENTAL COMPOSITION, MINERALOGY, AND PETROPHYSICAL PROPERTIES, ARDMORE BASIN, OKLAHOMA

A THESIS

SUBMITTED TO THE GRADUATE FACULTY

in partial fulfillment of the requirements for the

Degree of

MASTER OF SCIENCE

BY

BRITTANY STROUD

Norman, Oklahoma

2022

REGIONAL VARIABILITY OF CANEY SHALE ELEMENTAL COMPOSITION, MINERALOGY, AND PETROPHYSICAL PROPERTIES, ARDMORE BASIN, OKLAHOMA

A THESIS APPROVED FOR THE

SCHOOL OF GEOSCIENCES

BY THE COMMITTEE CONSISTING OF

Dr. Matthew Pranter, Chair

Dr. Fnu “Ming” Suriamin

Dr. John Pigott

ACKNOWLEDGEMENTS

This research was funded by the Reservoir Characterization and Modeling Laboratory at the University of Oklahoma, the School of Geosciences at the University of Oklahoma, the Society of Petrophysicists and Well-Log Analysis Foundation (SPWLAF), the Oklahoma Geological Foundation (OGF), the Oklahoma Energy Resources Board (OERB), and the Oklahoma Geological Survey (OGS). Well data were provided through Andrew Cullen from Warwick Energy Group, and drill-cuttings were provided by the Oklahoma Petroleum Information Center (OPIC). Software was provided by Schlumberger (Petrel), LMKR (GeoGraphix), IHS (Petra), SAS (JMP Pro), and Paradigm (GEOLOG).

I thank Dr. Matthew Pranter for his assistance with Petrel and 3-D modeling, mentorship, advice, and encouragement. I thank Dr. Fnu Suriamin for assistance with GEOLOG and ρ_{maa}-U_{maa} analysis, Dr. Dean Richmond for his guidance and assistance with GeoGraphix and well-log normalization, Dr. Bill Full for his guidance and assistance with unsupervised machine learning, Dr. Jean-Yves Chatellier for his assistance with a short drill-cuttings "chip size" study, Dr. Bryan Turner for his guidance regarding elemental data, and Anna Turnini for her assistance with GeoGraphix and Petrel software.

Thank you to my mother, my father, and my sister Alia for all that you do, for all of your love and encouragement, and for always being my home. Thank you to my fiancé Dakota for your love and support, and for enduring this journey with me. I also thank my friends for their support, encouragement, and companionship throughout graduate school. Finally, a large thank you to God for this challenging and amazing opportunity, and for all of the valuable lessons it has taught me.

TABLE OF CONTENTS

ABSTRACT

The Mississippian-age Caney Shale of the Ardmore Basin, Oklahoma, consists of four chemofacies based on geochemical analyses of well drill cuttings. Chemofacies 1 and 3 represent a dominant detrital source into the basin, and chemofacies 2 is associated with periods of shallow-water conditions favorable to carbonate mineral formation. Chemofacies 4 represents intervals that are interpreted to have formed by reducing-bottom water conditions during deposition, with pyrite formation in an anoxic setting. The elemental proxies used to indicate carbonate minerals and detrital fluxes correlate with X-ray diffraction (XRD) derived mineralogical analyses. Based on XRD, the Caney Shale is primarily composed of mixed-clays, quartz, and carbonate minerals. The mixed-clay fraction consists of illite and kaolinite, while the carbonate fraction is composed of calcite and ankerite. These results are also consistent with ρ_{maa}-U_{maa} mineralogical analysis, constrained by XRD results, which revealed 3 rock types: mixed-clays, quartz, and carbonate. Rock-type models and vertical proportion curves illustrate an abundance of carbonate deposits within the central Ardmore Basin, suggesting a shallow-water environment and likely multiple shorefaces delivering sediment across the basin. A decreasing upward GR log response paired with an increasing upward carbonate abundance can be interpreted as transgressive sequences that correspond to 4 stratigraphic zones within the Caney Shale. Chemofacies also correlate with the transgressive sequences, suggesting that chemofacies are related to deposition. 3D total porosity models show an average porosity of approximately 20% per zone of the Caney Shale, with maximum porosity values of 61% occurring in Zone 4. Brittleness index models show brittleness within the quartz rock type, and greater ductility within the mixed clay rock type. This basin-scale characterization provides an understanding of Caney Shale elemental composition, mineralogy, and petrophysical properties and their regional variability.

INTRODUCTION

The Mississippian-age Caney Shale in the Ardmore Basin of south-central Oklahoma (Figure 1) primarily consists of interbedded shale and siltstone, and ranges in thickness from approximately 4 to 600 ft (61 to 183 m). Exposure of the Caney Shale are in the Arbuckle Mountains between the Ardmore and Arkoma basins. The Caney Shale is of interest for two reasons. (1) The lithological variability and stratigraphic architecture of the Caney Shale are poorly understood and (2) the structure and lithologies trap oil and natural gas, and therefore serve as petroleum reservoirs (Andrews, 2007). The Caney Shale within the Ardmore Basin has received minimal attention. The term "Caney", introduced by Taff (1901), was first used to describe black shales in the Coalgate quadrangle, which was then still Indian Territory as Oklahoma was not yet granted statehood. Much later, Elias (1956) studied the Caney Shale within the northern Arbuckle Mountains and divided the Caney Shale into three members based on lithological variations and fauna. The members are: lower Ahlosa Member, middle Delaware Creek Member, and upper Sand Branch Member. Elias (1956) described the members in detail and interpreted their ages. Harris (1971) conducted a palynological investigation within the upper Sand Branch Member of the Caney Shale within Johnston County. He determined the Sand Branch Member to be of late Mississippian age (middle to upper Chesterian) by comparing its palynomorph assemblage with similar assemblages reported from North America, Russia, and Europe. Schwartzapfel (1990) conducted the first comprehensive investigation of Late Paleozoic radiolaria within the Arbuckle Mountains of south-central Oklahoma. Schwartzapfel (1990) sampled the three members of the Caney Shale, proposed by Elias (1956), for radiolaria, conodonts, and goniatitesa in Phillips Creek and Hickory Creek in Carter County, as well as in Johnston County. In the Phillips Creek area, Schwartzapfel (1990) discovered pyritized

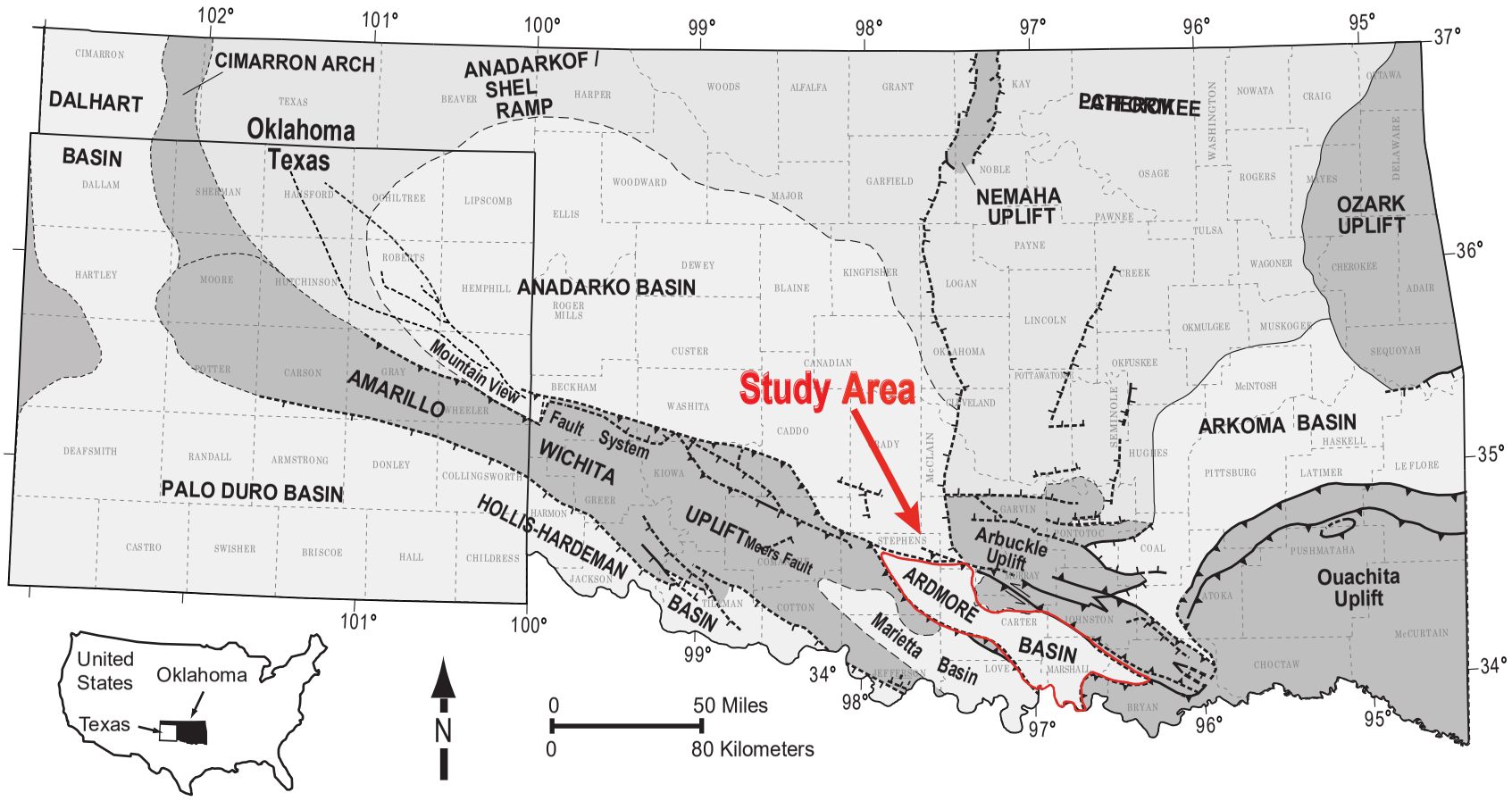

Figure 1: Regional map showing major tectonic provinces of Oklahoma. The study area is located in South Central Oklahoma within the Ardmore Basin and is outlined by the bold red polygon. (Modified from Johnson and Luza, 2008; Northcutt and Campbell, 1995; Campbell et al., 1988)

radiolaria and ammonoids in the Delaware Creek Member of the Caney Shale, which further confirmed a Chesterian age for the Caney Shale. Importantly, Schwartzapfel (1990) also suggested that Elias (1956) inappropriately divided the Caney Shale members in paleontological regards, according to commission guidelines. Kamann (2006) agreed with this argument and further refined the descriptions of these three members. Cullen (2019) investigated detrital zircon within the upper sandstone of the Caney Shale, located along the southern limb of the Arbuckle Anticline (Philips Creek outcrop). Petrographic analysis concluded that there were likely long-distant transport mechanisms delivering different sized detritus into the Ardmore Basin, and there is a possibility that the sand and silt fractions within the Caney Shale may not have a shared provenance. Cardott (2017) described the hydrocarbon potential of the Caney Shale within the Ardmore Basin and recorded that all "oil-producing Caney-only wells" are in south-central Oklahoma. According to Cardott (2017), the best gas-producing well within the Caney Shale was completed in the limestone and siltstone and sandy-siltstone facies of the combined Caney Shale and Sycamore Limestone, rather than the principal shale facies of the Caney Shale. There are limited studies focused on the Caney Shale within the Ardmore Basin. Previous research has focused on the palynology and biostratigraphy, which have been useful for age dating. Characterization of the Caney Shale in the Ardmore Basin has been limited since Elias (1956). Cullen's (2019) thin section analysis and Katende et al.'s (2021) micro- and nanoscale geochemical study are the next most recent records of Caney Shale characterization. Unrelated to mineralogy, Radonjic et al. (2020) studied pore types using SEM-EDS and noted that all porosity within the Caney is likely micro- to nanometer in scale. To contribute to the understanding of the Caney Shale in the Ardmore Basin, this study investigates its composition and how it varies laterally and vertically by answering four focused research questions:

1. What are the elemental abundances, mineralogies, chemofacies, and rock types?
2. What do chemofacies suggest about environmental conditions?
3. What is the stratigraphic zonation?
4. How do the rock types, porosity, and brittleness index vary spatially?

This work focuses on 305 selected well cuttings samples from 5 wells spanning the Ardmore Basin of south-central Oklahoma. Well-log data include digital log-ascii standard (LAS) data for approximately 117 wells (Figure 2). Characterization of well cuttings followed by elemental signature analysis provides an understanding of the lithologies, mineralogies, and elemental composition of the Caney Shale. XRF-derived chemofacies, generated using unsupervised machine learning, show vertical and lateral changes in the 5 key wells. The log dataset was used to model rock types, chemofacies, total porosity, and BI variability across the basin. Models provide an understanding of the spatial variability of these properties and allow for interpretations of depositional environment.

GEOLOGIC SETTING

The Ardmore Basin is located in south-central Oklahoma and has an elongate geometry that extends for approximately 100 mi (161 km) from the northwest to the southeast, and approximately 20 mi (32 km) from southwest to northeast (Suneson, 1996). The Ardmore Basin has a complexly folded and faulted nature (Figure 3) as it formed in conjunction with the Ouachita fold and thrust belt on the edge of the North American craton (Granath, 1989). Located within the foreland adjacent to the fold and thrust front, the Ardmore Basin is confined to the base of a Paleozoic trough known as the Southern Oklahoma Aulacogen (Shatski, 1947). The

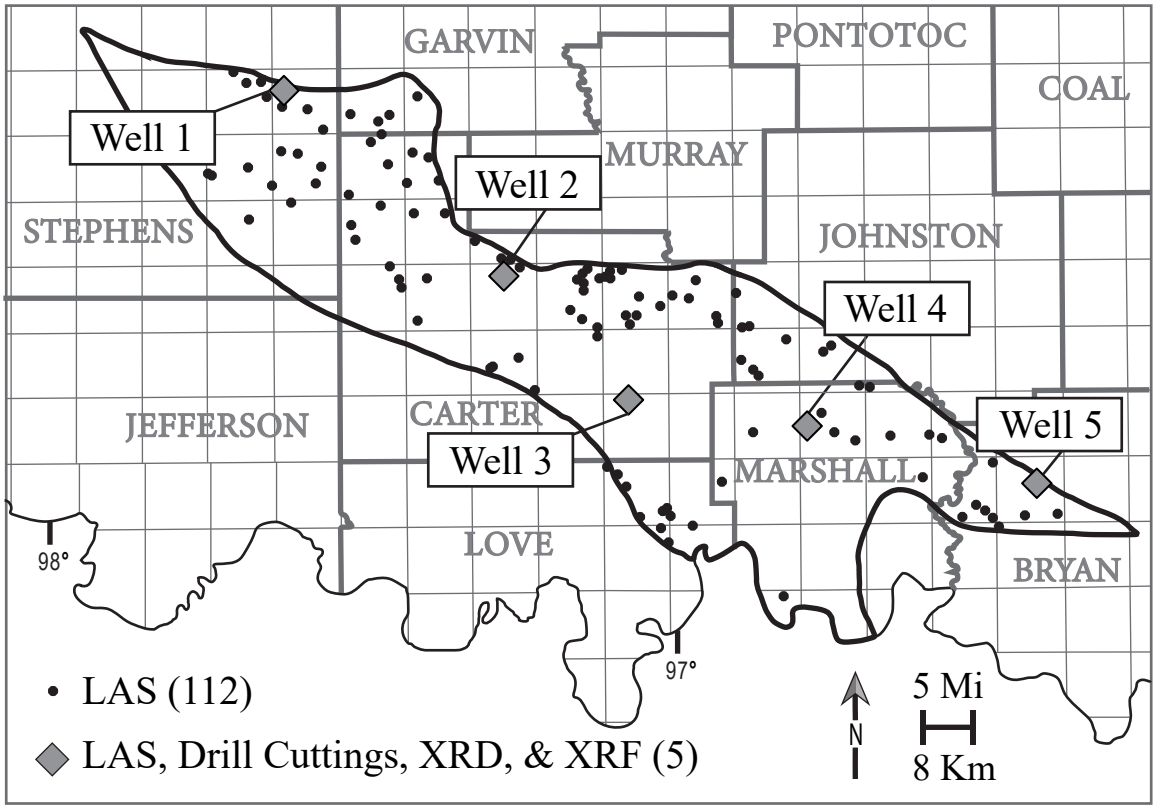

Figure 2: Detailed study area basemap displaying 11 total well locations with LAS data. Grey diamonds indicate the 5 key wells with drill-cuttings data, XRD samples, and XRF elemental data.

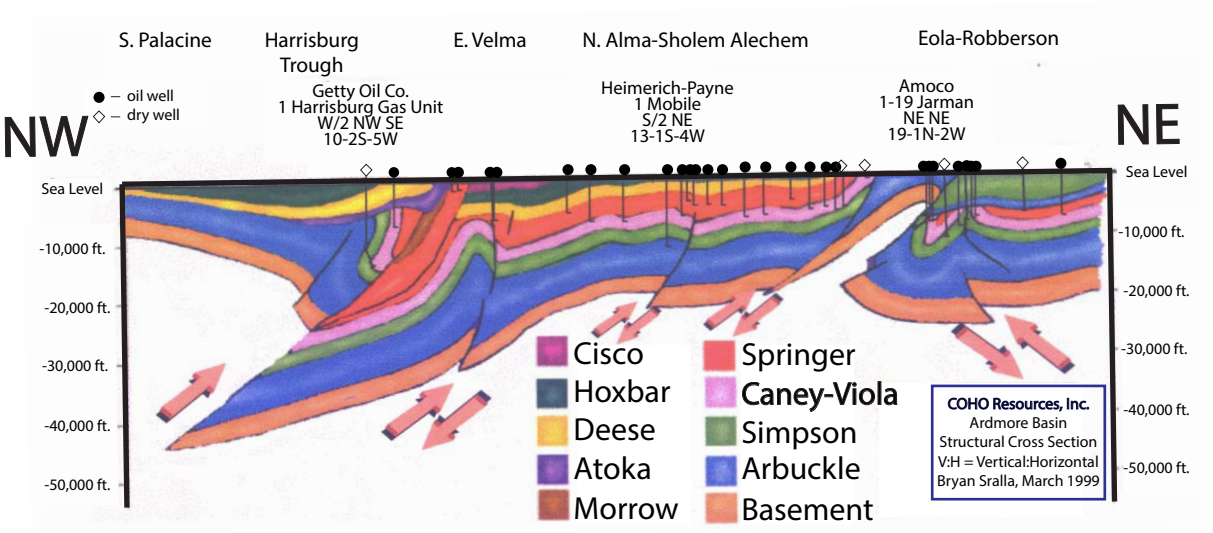

Figure 3: Northwest to northeast structural cross-section of the Ardmore Basin displaying faulting and deformation (Modified from Allen, 2000). The Caney Shale interval is colored pink, and the cross-section location is found on the map in the upper-right corner.

northwest to southeast aligned aulacogen formed during the early Cambrian period, and the resultant trough later filled with Paleozoic-age sediments (Harris, 1971). The lithostratigraphic units that comprise these sediments are (1) Late Cambrian-Early Devonian marine deposits, (2) Late Devonian-Early Mississippian shales (Figure 4), and (3) Pennsylvanian-Permian clastic deposits (Schwartzapfel, 1990). The Ardmore Basin once extended from Criner Hills to the Pauls Valley Uplift but was confined to its present-day geometry by the much later Middle Pennsylvanian Arbuckle Orogeny (Allen, 2002). The Ardmore Basin is bounded by a series of faults to the northeast and southwest, which are a result of a left-lateral shear belt that affected Oklahoma (Granath, 1989). The northeastern bounds of the Ardmore Basin are comprised of the Cambrian Arbuckle anticline, the Cambrian Washita Valley fault, and the early-Pennsylvanian Tishomingo-Belton uplift. The southwestern portion of the Ardmore basin is bounded by the early Paleozoic Criner Hills uplift –which separated the Ardmore basin from the Marietta Basin to the south –and the Paleozoic Waurika-Muenster uplift (Suneson, 1996). Towards the southeast, the Ardmore Basin is terminated by the covered Paleozoic Ouachita Thrust Belt. Toward the northwest, the Ardmore Basin meets the larger and deeper Anadarko Basin (Suneson, 1996).

The Mississippian strata within the Ardmore Basin are divided into 4 units (from oldest to youngest): Kinderhookian, Osagean, Meramecian, and Chesterian (Craig et al., 1979). During the Kinderhookian, a large epiric sea covered southeastern Oklahoma and the rest of the North American craton (Craig et al., 1979). This was a period of climatic transition, as temperatures were cooling, and the sea level was falling. The climate was likely tropical to subtropical, and the ocean temperatures ranged from 65° to 85° F (Buggisch et al., 2008). Due to the orientation of the land masses along the equator, the shallow warm sea that covered the North American

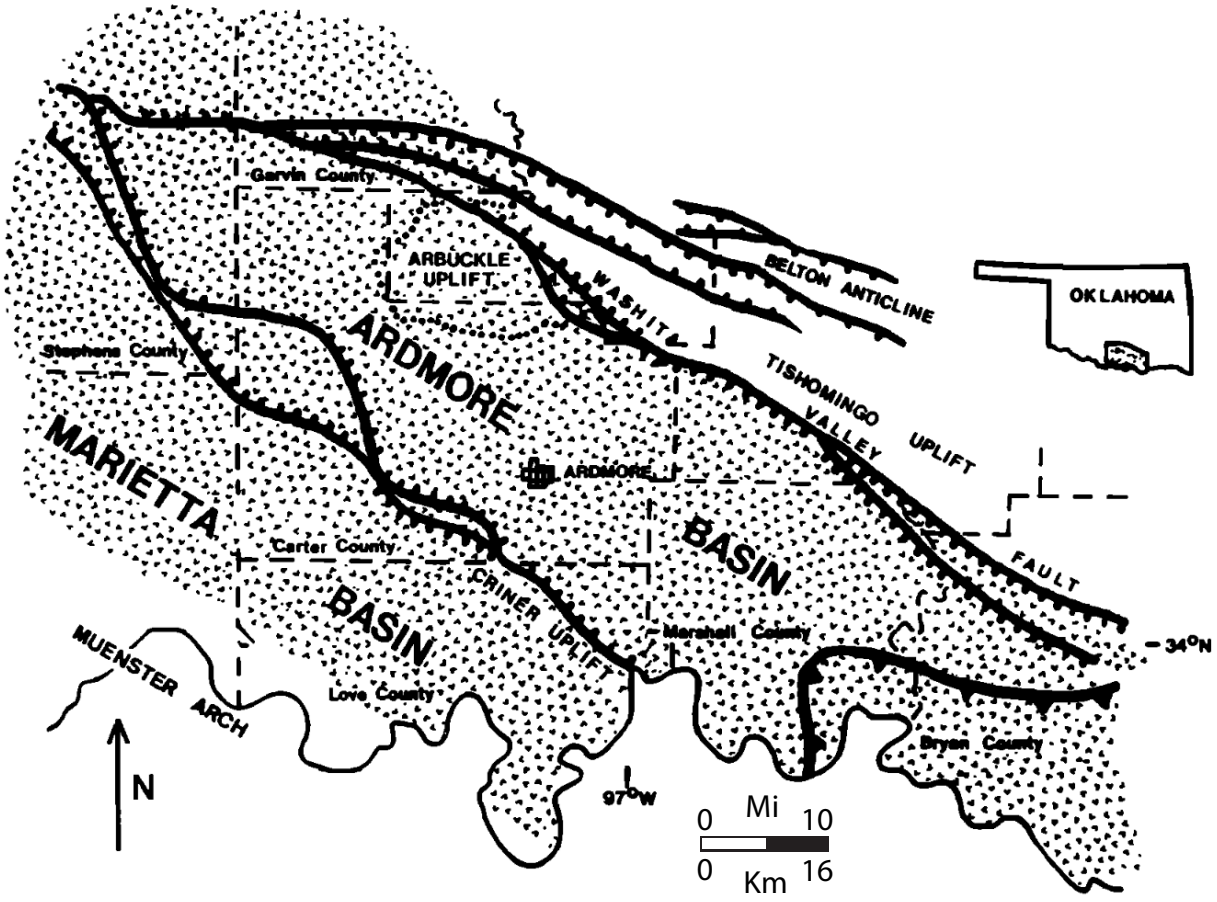

Figure 4: Depiction of the Ardmore Basin and its northeast and southwest bounding faults. The deposition of the Mississippian strata onto the floor of the aulacogen is represented by the dotted pattern. (Modified from Granath, 1989)

craton became anoxic in some cases, owing to the lack of ocean circulation from pole to pole (Schad, 2004). During this period of cratonic stability, the Mississippian-aged Caney Shale was deposited stratigraphically above the earlier Mississippian-aged Sycamore Formation and was later capped by the Pennsylvanian aged Springer/Goddard Group (Sloss, 1963; Schad, 2004) (Figure 5). The deposition of the entire Mississippian section represents a series of transgressive-regressive cycles (Sloss, 1963). The Caney Shale specifically corresponds to an overall period of transgression, as well as the progressing diminishment of clastic input into the Ardmore Basin (Miller et al., 2019; Milad et al., 2020). The Caney Shale composition of sandy siltstone, limestone, and shale units reflects the depositional history of transgression-regression patterns; however, the true source of its sandy siltstones is unclear (Cullen, 2019).

METHODOLOGY

Cuttings Selection and Descriptions

A detailed drill-cuttings description was conducted for 305 cuttings samples that included lithology, grain size, color, and general descriptions. The 5 wells with cuttings (Appendix A) were chosen based on availability, minimum vertical sample spacing, condition of cuttings chips, and lateral well spacing. Lithology, grain size, color, and general descriptions were recorded for each cuttings sample for all 5 wells (Appendix B).

Drill-cuttings chips often vary in size due to differing drill bits and drilling processes (Hayatdavoudi, et al., 1987). This non-geologic variation in chip size can affect XRF readings and alter results (J-Y. Chatellier et al., 2011). To ensure that the cuttings samples were analyzed

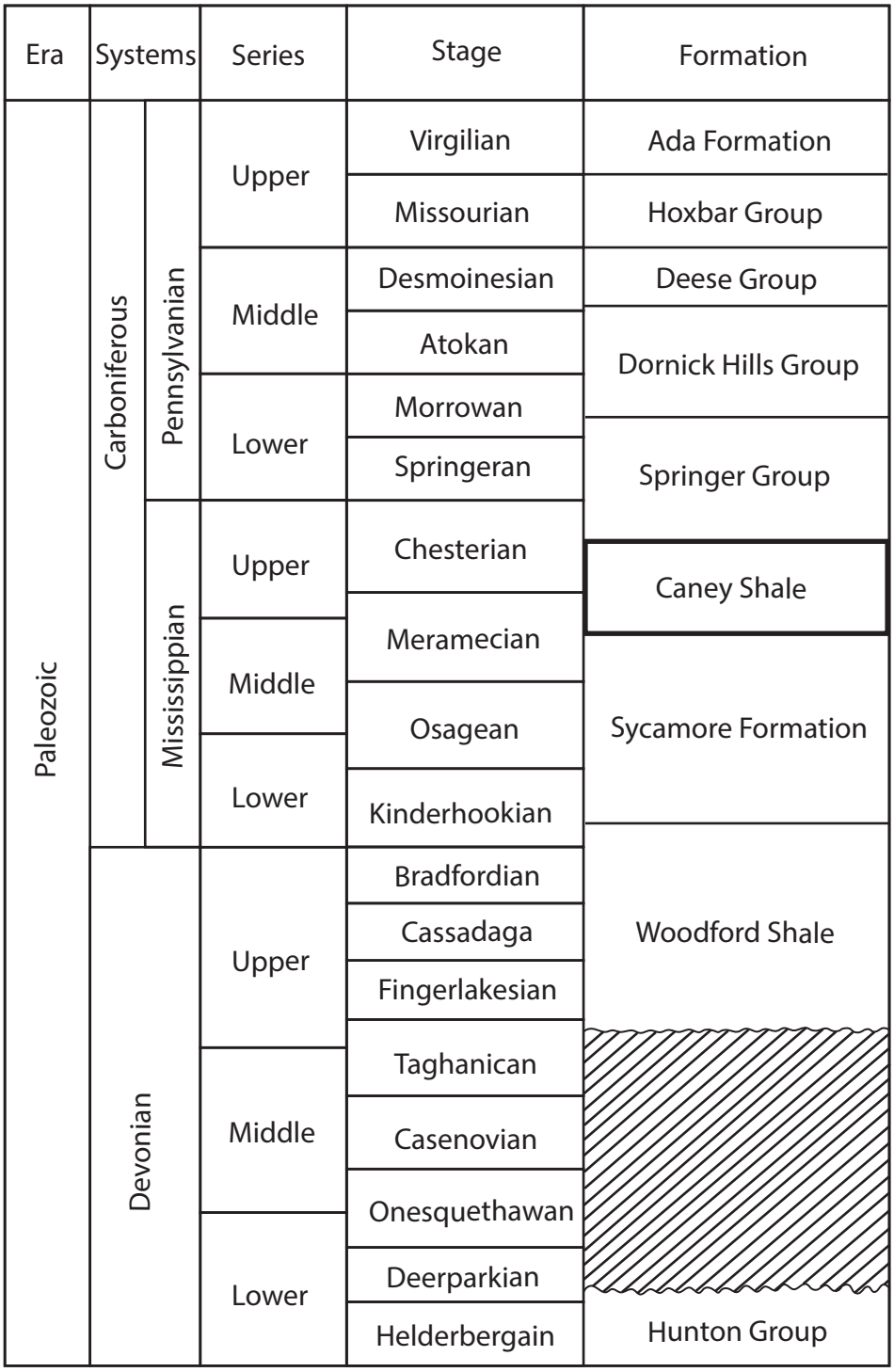

Figure 5: Stratigraphic column of the Arbuckle uplift. The 4th column corresponds to the regional North American nomenclature of stages. (Modified from Duarte, 2021)

with minimal error, a 1cm (0.4 in) sized sieve was used on all cuttings to provide a constant chip size before analysis.

XRF Data Acquisition

The elemental compositions and chemofacies of the Caney Shale are addressed through XRF analysis. Relative changes in sea level and environmental conditions can be interpreted from patterns in elemental data. To analyze the elemental composition of the Caney Shale, whole-rock elemental data were acquired and interpreted for 233 cuttings samples using the Bruker Tracer III-SD Handheld X-ray Fluorescence Analyzer in the bench-top set-up. 8 major element (Al, Si, Ti, Na, Fe, Mn, Ca, and K) and 21 minor and trace element (As, Ba, Cl, Co, Cr, Cu, Mo, Nb, Ni, P, Pb, Rb, S, Sb, Sn, Sr, Th, U, V, Zn, and Zr) concentrations were analyzed for the 5 wells with cuttings spanning the Ardmore Basin. Wells 1, 2, 3, and 4 were analyzed at 10-ft (3.1 m) vertical spacing, and Well 5 was analyzed at 5-ft (1.5 m) vertical spacing, using the S1PXRF analysis program.

Index Element Selection

To interpret the environmental conditions during deposition, 9 elements and 1 ratio (Figure 6) were used as proxies. The index elements were initially selected based of Principal Component Analysis (PCA) of all 29 major and minor elemental concentrations (Appendix C). Along with PCA biplots (Appendix C), eigenvalue heat maps produced from PCA (Appendix D) were helpful for visual evaluation of the dataset as well. Additionally, research of commonly used elemental proxies were utilized, accuracy charts of accepted versus measured XRF data

Element	Proxy	References
Silica (Si)	Detrital or biogenically derived quartz	Pearce and Jarvis, 1992; Pearce et al., 1999, Sageman and Lyons, 2004
Aluminum (Al)	Clay minerals or feldspar	Vine and Tourtelot, 1979; Timothy and Calvert, 1998; Tribovillard et al., 2006
Silica aluminum ratio (Si/Al)	Detrital quartz	Pearce and Jarvis, 1992; Pearce et al., 1999; Sageman and Lyons, 2004
Titanium (Ti)	Continentally derived source and aeolian fluxes	Li, 1982; Balsam et al. 1995; Sageman and Lyons, 2004
Zirconium (Zr)	Continentally derived source	Li, 1982; Sageman and Lyons, 2004
Potassium (K)	Clay minerals or feldspar	Weedib and Shckleton, 1997; Tribovillard et al., 2006
Calcium (Ca)	Carbonate source and phosphates	Vine and Tourtelot, 1979; Tribovillard et al., 2006
Strontium (Sr)	Carbonate source and phosphates	Vine and Tourtelot, 1979; Tribovillard et al., 2006
Cobalt (Co)	Pyrite formation indicator or detrital source	Tribovillard et al., 2006; Brumsack, 2006; Luther and Morse, 1999
Molybdenum (Mo)	Redox-sensitive, water anoxia/euxinia	Luther and Morse, 1999; Tribovillard et al., 2006

Figure 6: A list of XRF elemental proxies used for this study. The first column displays 9 elements and 1 ratio used for data analysis, the second column shows the proxy or significance of each element, and the third column outlines the references. (Modified from Milad et al., 2020)

were evaluated (Rowe, 2012), and visually identified patterns were assessed to refine the selection of index elements.

The 10 index element profiles are as follows: titanium (Ti), zircon (Zr), aluminum (Al), potassium (K), silica (Si), calcium (Ca), strontium (Sr), molybdenum (Mo), and cobalt (Co). Ti and Zr are used for identification of detrital influence and the possible presence of eolian deposition. Al and K are common clay proxies and may also indicate the presence of alkali feldspars. Al is fairly stationary during diagenesis, and therefore it represents the aluminosilicate fraction for most sedimentary deposits (Vine and Tourtelot, 1979; Tribovillard et al., 2006). Si serves as a proxy for both detrital and autogenic quartz (Pearce and Jarvis, 1992) as it can be both continentally and biogenically derived. The origin of quartz is often shown by the ratio of Si to a clay proxy, such as Si/Al. A positive correlation in concentration between Si and Al can indicate the presence of detrital quartz, while a decrease in Al paired with an increase in Si may indicate an autogenic influence (Pearce and Jarvis, 1992; Martin, 2019. Ca and Sr are commonly associated with a carbonate sources, which can originate from direct precipitation of sea water, calcareous algae, or the skeletons of marine organisms (Vine and Tourtelot, 1979; Tribovillard et al., 2006; Martin, 2019). Molybdenum (Mo) is a redox-sensitive trace element that is often found in organic-rich sediments, is fairly unreactive with seawater, and is associated with anoxic water conditions and a sulfide-rich (euxinic) water column (Emerson and Huested, 1991; Luther and Morse, 1999; Tribovillard et al., 2006; Dahl et al. 2013). The available O_2 and H_2S in the water column dictates the geochemical behavior of Mo. In sulfide-rich water columns, Mo-sulfide precipitates out of solution, resulting in strong sedimentary Mo enrichments (Emerson and Huested, 1991). Because of the relationship between Mo and seawater, it can be a useful paleoredox proxy. Cobalt (Co) abundance in sediments is strongly tied to the abundance of

clastic material, so it is not commonly used as a paleoredox proxy; however, when CoS is present in anoxic or euxinic environments, Co can precipitate readily into sediment through pyrite formation (Luther and Morse, 1999; Tribovillard et al., 2006; Simmons, 2019). Because of this, Co can be used as a paleoredox proxy in combination with other elements.

K-means Clustering and Chemofacies Classification

K-means clustering is an unsupervised machine learning algorithm used to distinguish natural associations in a dataset. This method creates "K" random centroids, or "clusters" scattered throughout the data, and assigns data points to nearby centroids based on the squared Euclidean distance (Macqueen, 1967; Trevino, 2016). The process of assigning data to various centroids repeats until the data points have become stationary to their respective cluster. The optimal number of clusters can then be determined using a variety of methods including elbow plots, cubic clustering criterion (CCC), or scree plots. Elbow plots display the sum of squared distances between (SSB) and within (SSW) for a particular number of clusters (Macqueen, 1967; Trevino, 2016). The optimal cluster value can then be determined by bends or "elbows" in the dataset. A scree plot shows the proportion of variation in the data explained by the principal components and is interpreted similarly by a bend in the dataset (Sarle, 1983). The CCC method estimates the error of k-means in the reference distribution and in the training data for all cluster values to test. The difference between these two error measures for each trial amounts to the value of CCC at that cluster value (k) (Sarle, 1983). High CCC values on a CCC plot indicate optimal cluster values.

To ensure that the most optimal cluster value was chosen, K-means was conducted multiple times, several cluster combinations were assessed, and other clustering methods were evaluated. To classify clusters into chemofacies, the data were additionally evaluated according to their geologic significance. Chemofacies were defined based on interpretations of elemental proxies for continental-sourced sediment, relative sea-level movement, and ocean-water conditions.

Powder X-Ray Diffraction

To determine the mineralogy and clay fraction of the Caney Shale, powder x-ray diffraction (XRD) analysis was conducted (Appendix E) for 1 sample per zone per well with drill-cuttings, amounting to 20 samples total. All samples were prepared for XRD as random mounts, which are generally used for bulk mineralogy analysis (Poppe et al., 2005). Powder x-ray diffraction analyses were performed in the School of Geosciences at the University of Oklahoma using a Rigaku Ultima IV diffractometer. Cu-K alpha radiation (40kV, 44mA) was used with a scintillation detector. Data analysis was completed by comparing d-spacings with standard tabulations (Poppe et al., 2005).

Log Normalization

The manual log-normalization method used for this study is effective because it does not remove anomalous, *geological* variations in log-curve responses. It is especially helpful for removing *non-geological* errors, which improves confidence in log correlation efforts, prospect analysis, and work involving computer processing (Shier, 2004). To normalize well-log curves,

cross-plots of log values (RHOB and GR) and formation thickness for 117 wells were evaluated to understand the data distribution and to find wells with outlier values (Appendix F). A "type well" was designated to represent the most ideal log values from the dataset. A minimum and maximum log value was defined from the type well and used as a boundary for each unnormalized log curve (Doveton and Bornemann, 1981; Shier 2004). For curves that match the type log character, but appear to be off-scale, a simple shift in the curve placement was applied. For logs that appeared inaccurately compressed or elongated, a new scaling factor, or "multiplier", was used to stretch or squeeze the curve until it was similar to the type log. Histograms of the type log values and the unnormalized log values were evaluated throughout the normalization process to visualize shifting and scaling of the well logs (Figure 7). The general log normalization equation by Doveton and Bornemann (1981) is as follows:

where,

$$V_{norm} = \frac{R_{min} + (R_{max} - R_{min})(V_{log} - W_{min})}{W_{max} - W_{min}} \quad (6)$$

V_{norm}, normalized log value
R_{min}, minimum log value
R_{max}, maximum log value
V_{log}, unnormalized log values
W_{max}, maximum unnormalized log value
W_{min}, minimum unnormalized log value

ρ_{maa}-U_{maa} Multi-mineral Estimation and Brittleness Index

A well-log derived, litho-density, multi-mineral estimation method called ρ_{maa}-U_{maa} analysis was used to calculate the volumetric proportion of mineralogy, rock types, and

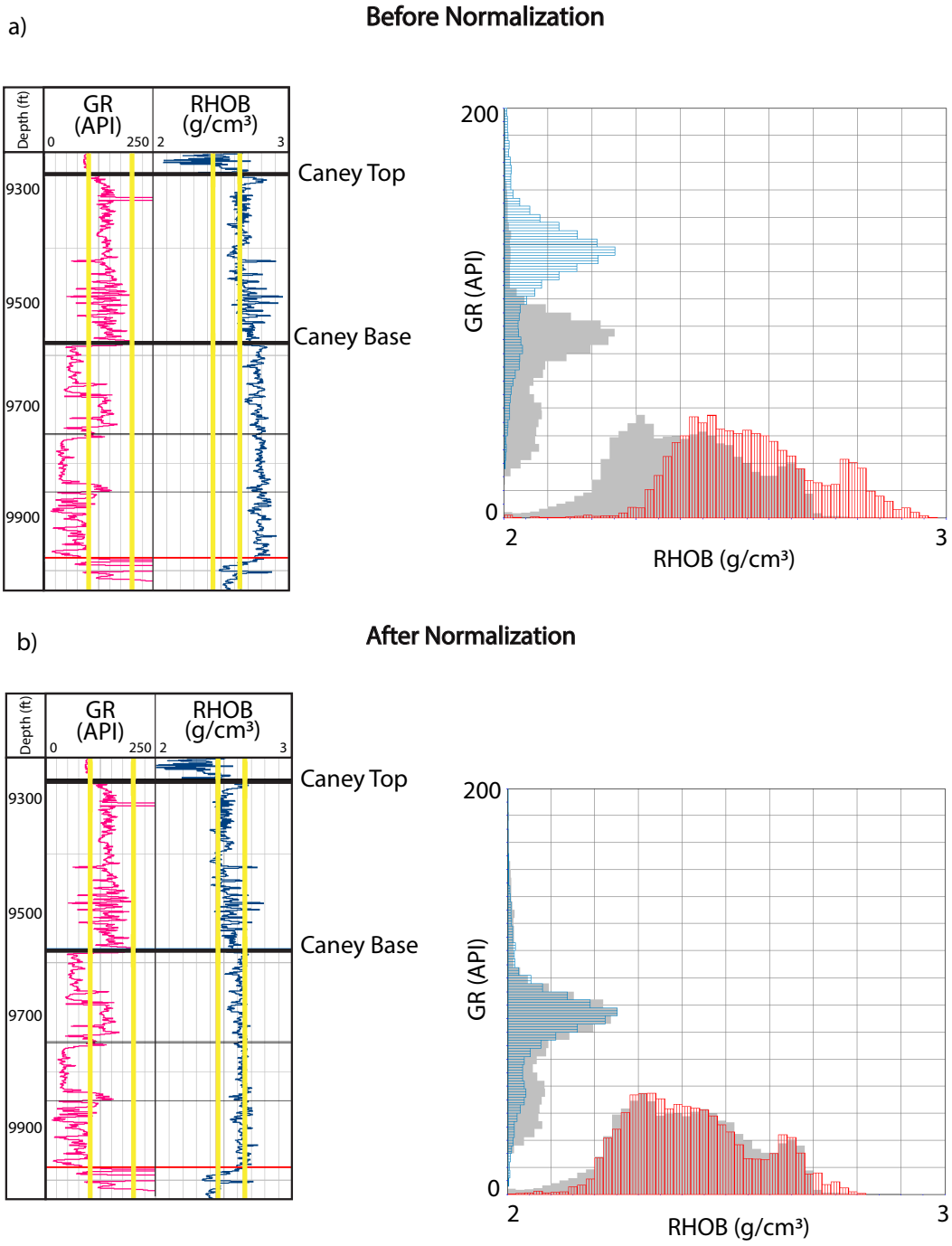

Figure 7: The manual log normalization process is displayed. Type-log minimum and maximum cut-offs are represented by the vertical yellow lines, and the type-log frequency histograms are displayed in grey on the graphs. a) displays the unnormalized GR and RHOB log curves (left) and their corresponding frequency histograms compared to the type-log histograms (right). b) displays the normalized curves now within the type log cut-off boundaries (left) and the corrected histograms fitted to the type-log histograms (right).

brittleness index for both the Caney Shale and the Sycamore Formation. The ρ_{maa} parameter is the apparent matrix grain density, calculated from the RHOB log (Equation 1 and 2), and the U_{maa} parameter is the apparent matrix volumetric cross-section, calculated from the PE log and the photo-electron density constant (Equation 3) (Doveton 1994). The ρ_{maa} and U_{maa} data points for each well are presented on a cross-plot, and a percentage scaled template is used to assign mineralogy to specific data points (Doveton 1994). The mineral end-members of the scaled template were assigned according to XRD mineralogical results and standard ρ_{maa}-U_{maa} values for those mineralogies. For each datapoint (each log depth), the most abundant estimated mineralogy was set as the rock type. The percentage scaled template was constrained by the XRD derived mineralogy.

where,
$$\rho_{maa} = \frac{\rho_b - \phi_{ta} * \rho_f}{1 - \phi_{ta}} \quad (1)$$

ρ_{maa}, apparent matrix grain density (g/cm^3)
ρ_b, bulk density (g/cm^3)
ϕ_{ta}, apparent total porosity (v/v)
ρ_f, flush zone pore fluid density (~1.0 g/cm^3 for fresh-water mud filtrate)

where,
$$\rho_e = \frac{\rho_b + 0.1883}{1.0704} \quad (2)$$

ρ_e, electron density (g/cm^3)
ρ_b, bulk density (g/cm^3)

where,
$$U_{maa} = \frac{P_e \rho_e - \phi_{ta} * U_f}{1 - \phi_{ta}} \quad (3)$$

U_{maa}, apparent matrix volumetric cross-section

(barns/cm^3)
P_e, photoelectron index (barns/electron)
ρ_e, electron density (g/cm^3)
ϕ_{ta}, apparent total porosity (v/v)
U_f, Volumetric photoelectric absorption of the flushed zone pore fluid (~0.398 barns/cm^3)

Brittleness index (BI) (Equation 4) was calculated using an equation by Jarvie et al. (2007). Brittleness index is a function of mineral composition; therefore, mineralogical data can be used to calculate BI. ρ_{maa}-U_{maa} derived, and XRD constrained, mineral logs were normalized, converted from volume percent to weight percent (Equation 5), and used to calculate BI logs.

where,
$$BI = \frac{Q}{(Q+C+Cl)} \quad (4)$$

BI, Brittleness Index
Q, quartz content (W_t%)
C, carbonate content (W_t%)
Cl, mixed clay content (W_t%)

where,
$$W_t\% = \frac{\rho_g * Vol\%}{\rho_b} \quad (5)$$

Wt%, Mineral weight percent (%)
ρ_g, grain density component (g/cm^3)
Vol%, mineral volume percent (%)
ρ_b, bulk density (g/cm^3)

Stratigraphic Correlation

The Caney Shale formation tops discussed in this section were interpreted based on geological interpretation, scout tickets from the Oklahoma Petroleum Information Center

(OPIC), and literature review (Andrews 2007; Cullen 2019; Milad et al., 2020). Caney Shale zones were interpreted and correlated across the Ardmore Basin based on continuous intervals of decreasing upwards GR responses, markers in the RT and porosity curves, and rock-type logs derived from ρ_{maa}-U_{maa} analysis.

3-D Geological Modeling

A 3-D model grid honoring structural-contour and isopach maps was generated to represent the stratigraphy of the Caney Shale. The grid dimensions were determined based on well spacing, preservation of the vertical resolution, and attention to a reasonable amount of cells for computer processing. The Caney Shale structural contour maps were used to define 4 model zones (1-4). Proportional layering was assigned to each zone, and the number of layers was determined based on the average thickness of each zone divided by the vertical cell height. The Sycamore Formation structural-contour maps were used to define additional zones for reference; however, these zones were not evaluated in detail for this study.

To capture the variability of rock types, porosity, and brittleness index (BI), 3-D rock type and petrophysical-property models were generated. Log properties were upscaled according to the resolution of the 3-D grid, and the accuracy of upscaling was evaluated through comparison of the original logs with the upscaled logs. Frequency histograms (for each log property) and cross sections were used to validate the accuracy of upscaling. Variogram ranges were set to capture variability of log properties with distance and direction.

The 3-D rock-type model was created using sequential-indicator simulation (SIS). The rock-type model was constrained by (1) the 3-D model grid (stratigraphic framework), (2) 59

upscaled rock-type logs, (3) rock-type percentages per zone, (4) rock-type vertical proportional curves, and (5) vertical and horizontal variogram parameters. Logs were upscaled such that the most abundant rock type in a particular cell was assigned to that cell. Assuming the deposition of sediment into the Ardmore Basin likely had multiple sources, horizontal variogram ranges were set with no preferred direction of anisotropy, with a value of 30,000 ft (9,144 m) in the major and minor directions, and a value of 15 ft (4.6 m) in the vertical direction. The nugget was set to zero to honor all upscaled facies. Multiple realizations of the rock-type model were computed to ensure accuracy of the model.

Similar to the rock type model, the brittleness index (BI) model was modeled as a continuous property using sequential-Gaussian simulation and constrained by (1) the rock-type model, (2) 59 upscaled BI logs, (3) vertical and horizontal variogram parameters, and (5) BI histograms. A model showing a classification of "brittle" and "ductile" areas was calculated from the BI model using BI cutoff values, where BI>50% was assigned as "brittle" and a BI<50% was assigned as "ductile". The major and minor vertical and horizontal variogram ranges were set equal to the rock-type ranges. The nugget was set to zero to honor all upscaled facies.

To capture the variability of chemofacies, a 2-D chemofacies model was generated independently of rock type and petrophysical properties. The chemofacies model was generated using sequential-indicator simulation and was constrained by (1) the upscaled chemofacies logs from the 5 wells with cuttings (Figure 2), (2) vertical proportion curves, and (3) chemofacies percentage per zone.

To model porosity, total porosity was first calculated using the root-mean-square of density porosity and neutron porosity (Asquith and Gibson, 1982):

where,

$$\phi_t = \frac{\sqrt{\phi_D{}^2 + \phi_N{}^2}}{2} \quad (6)$$

ϕ_t, total porosity (v/v)
ϕ_D, density porosity (v/v)
ϕ_N, neutron porosity (v/v)

Total porosity was modeled using sequential-Gaussian simulation (SGS) and was constrained by (1) the 3-D rock-type model, (2) 112 wells with upscaled total porosity logs, (3) vertical and horizontal variogram parameters, and (4) porosity values by zone and by rock type. The variogram ranges for the major and minor directions of anisotropy were not set to a preferred orientation, and the nugget was set to zero, similar to that of the previous modeling parameters.

RESULTS

Elemental Abundances, Mineralogies, Chemofacies, and Rock Types

The XRD mineralogical analysis of Caney Shale drill-cuttings revealed a composition of mixed-clays, quartz, carbonate minerals, plagioclase feldspar, and a small fraction of other minerals (Appendix G). The mixed clay fraction is comprised of illite and kaolinite. Kaolinite was present in every well except for Well 3. The carbonate fraction is composed of ankerite –a member of the Dolomite Group of minerals –and calcite. Plagioclase feldspar was mostly present in the form of albite and was recorded in all samples. A smaller fraction of other minerals includes siderite, pyrite, potassium feldspar minerals, and fluorapatite.

Several iterations of K-means were conducted on a combination of the elemental data and selected well-log data (RHOB, GR, and RES) to assess the impact on clustering. The associations of well log data (~1 ft [0.3 m] vertical sampling) and elemental data (10 ft [3 m] vertical sampling) proved to be poor, resulting in extremely large cluster values. This non-correlation is likely a result of low resolution XRF sampling, as well as the small-scale elemental variability that cannot be captured at the well-log scale.

The K-means clustering analysis of the 9 geochemical profiles and 1 ratio resulted in a range of 3 to 5 potential clusters. A cluster value of 4 (Figure 8; Appendix H) was deemed the most optimal after evaluating scree plots, elbow plots, CCC plots, and the geological significance of all potential cluster values. The following index element profiles were used for clustering and chemofacies interpretation: Si, Al, Si/Al, K, Ti, Ca, Sr, Zr, Mo, and Co. XRD mineralogy was evaluated per each chemofacies of the Caney Shale to determine the relationship between elemental and mineralogical data (Figure 9; Appendix I). The 4 chemofacies of the Caney Shale are defined as follows:

Chemofacies 1 represents conditions with an elevated detrital source. Major detrital proxies have a greater average abundance (12.5 wt% Si; 2.5 wt% Al; 1.1 wt% K) while carbonate proxies show a negative correlation (2.1 wt% Ca; 220 ppm Sr). XRD mineralogical analysis reveals cuttings designated as “Chemofacies 1” to be predominantly composed of mixed-clays (45%), with abundance of quartz (36%) as well (Figure 9; Appendix J1).

Chemofacies 2 is characterized by high average carbonate proxies (5.8 wt% Ca; 328 ppm Sr) and low detrital proxies (9 wt% Si; 1.7 wt% Al; 0.7 wt% K). XRD mineralogical analysis supports the elemental data, showing a majority composition of carbonate minerals (36%) and less mixed clays (30%) associated with Chemofacies 2 (Figure 9; Appendix J2).

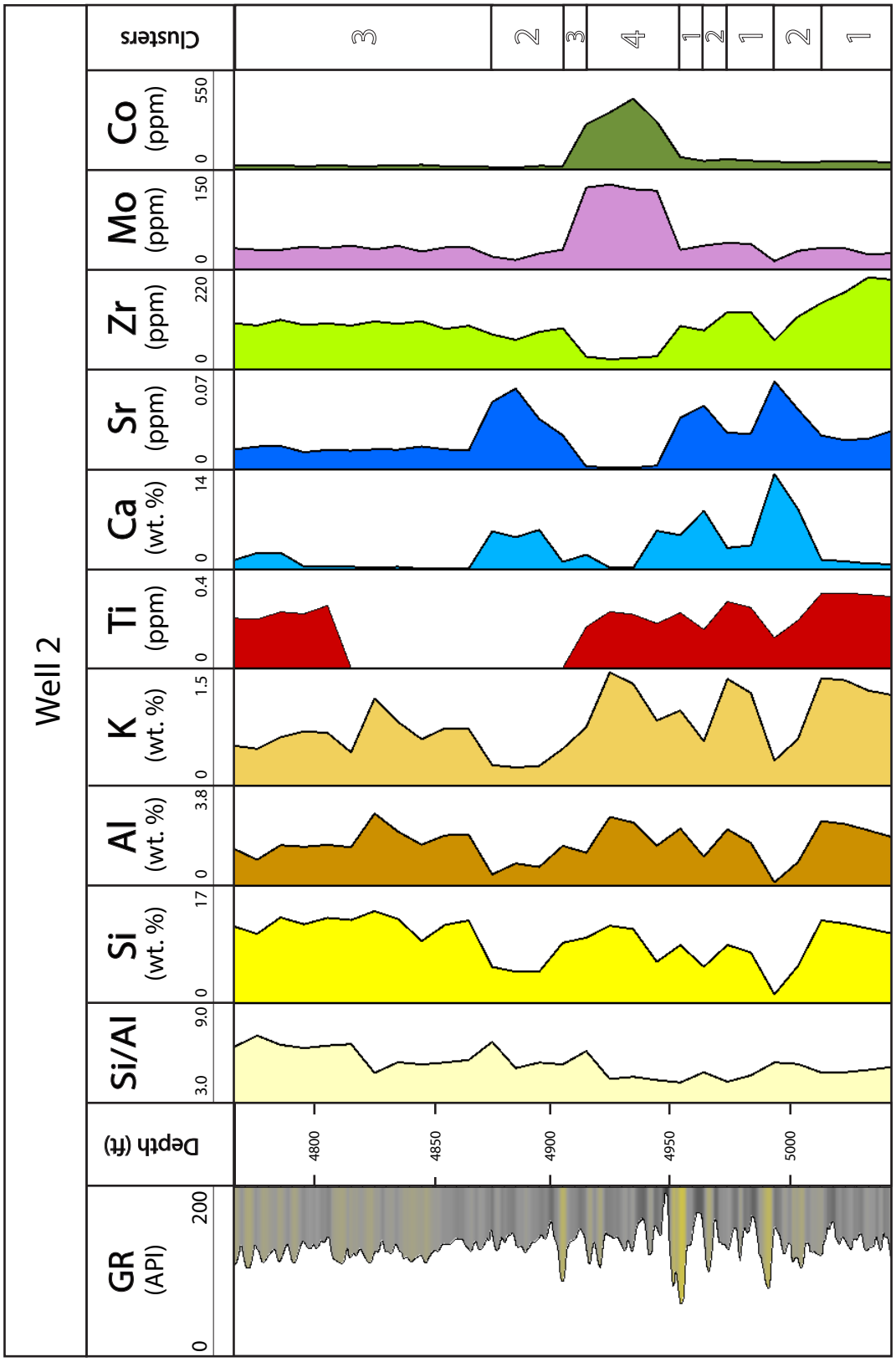

Figure 8: Example of index element curves and cluster identifications for Well 2. The GR log is displayed to the right. Major elements are presented in wt%, and trace elements are presented in ppm.

Chemofacies 3 is characterized by a moderate increase of detrital proxies (12 wt% Si; 2.1 wt% Al; 0.8 wt % K) and a negative correlation with the carbonate proxies (1.5 wt% Ca; 180 ppm Sr). Chemofacies 3 and Chemofacies 1 are similar, however the detrital and carbonate proxy abundances are slightly lower in chemofacies 3. The XRD mineralogy displays a quartz dominance (42%) for chemofacies 1, with abundance of mixed clays as well (40%) (Figure 9; Appendix J3)

Chemofacies 4 is characterized by a covarying abundance in molybdenum (122 ppm) and cobalt (334 ppm), which negatively correlate with the elemental concentrations of the carbonate proxies (1.67 wt% Ca; 12 ppm Sr) and zirconium (23 ppm). The major element detrital proxies are relatively abundant during intervals of chemofacies 4 (12 wt% Si; 2.3 wt% Al; 1 wt% K). The mineralogy analyses did not indicate a major trend and have a similar result to Chemofacies 1 and 3. Chemofacies 4 was apparent in all wells except for Well 1 (Figure 9; Appendix J4).

The rock types derived from the $\rho_{maa} - U_{maa}$ analysis consist of mixed clays which account for illite and kaolinite, carbonate which accounts for both calcite and ankerite, and quartz. Overall for the Caney Shale, ρ_{maa} *values are higher and* U_{maa} values are lower than that of the Sycamore Formation due to change in lithology and differing log character (Appendix K). The collective rock-type abundances of the entire Caney Shale formation are 55% mixed-clays, 24% quartz, and 21% carbonate (Figure 10).

Stratigraphic Framework

The Caney Shale log response is mainly characterized by a high gamma ray (GR), a separation between the neutron porosity (NPHI) and density porosity (DPHI) curves, and an

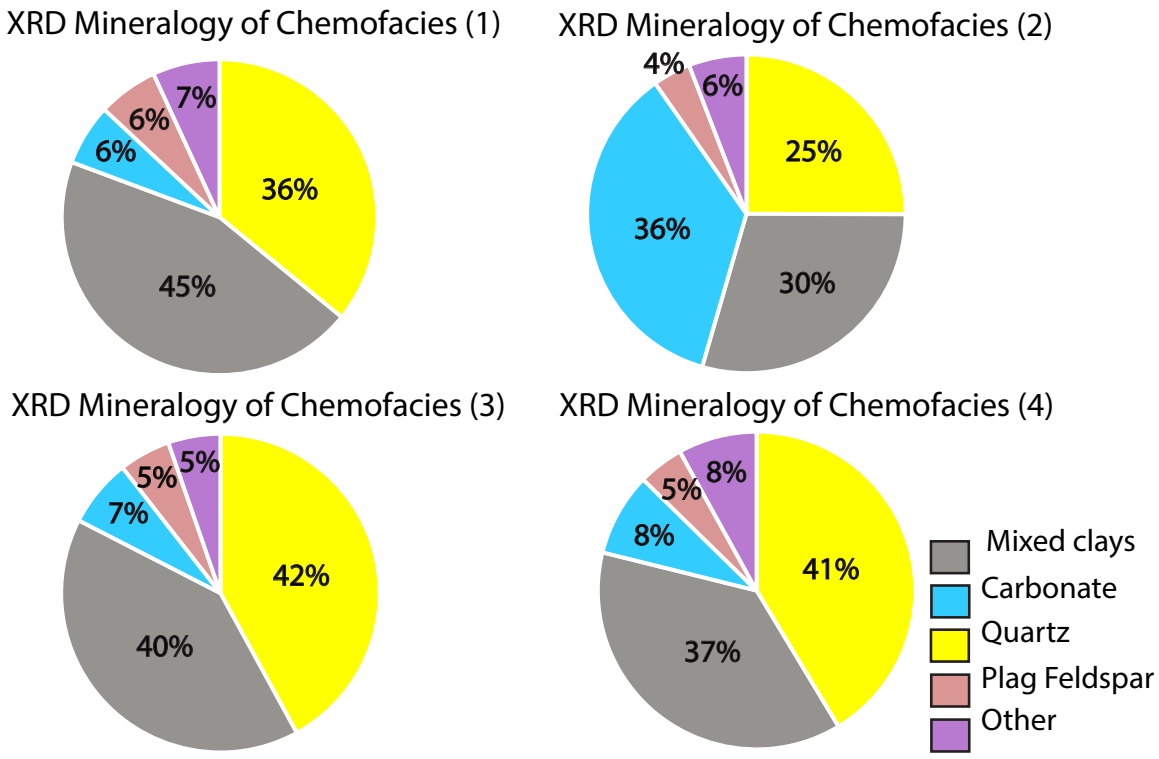

Figure 9: XRD mineral percentage pies calculated per chemofacies. Percentages are out of 100%. The "mixed clay" fraction (colored grey) accounts for both illite and kaolinite, and the "carbonate""fraction (colored blue) accounts for both calcite and ankerite. The small fraction of "other" minerals (colored purple) includes pyrite, siderite, and apatite.

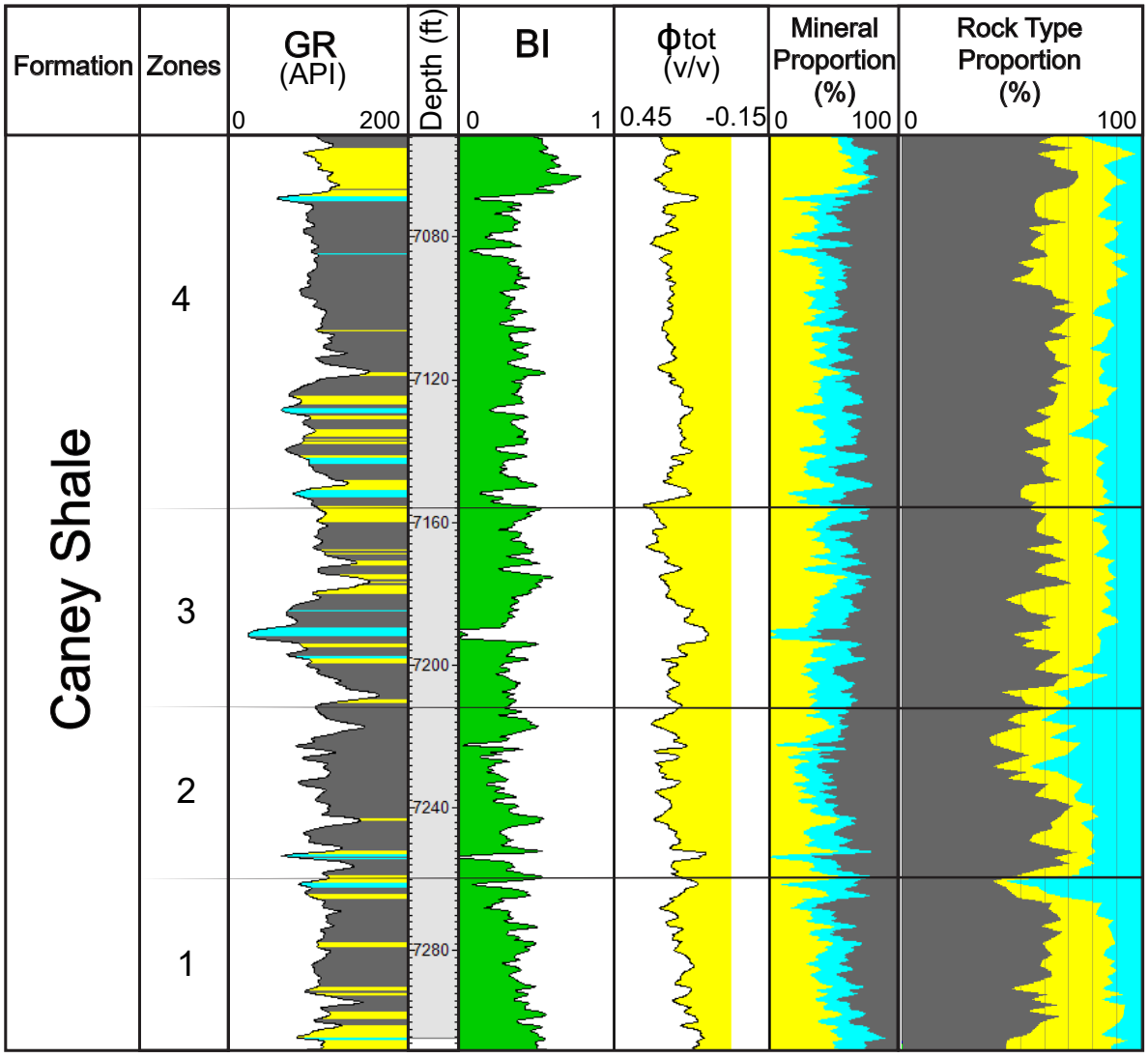

Figure 10: Vertical variability of rock type and petrophysical properties is shown next to zonations of the Caney Shale formations. Type logs for GR colored by rock type, BI increasing to the right, total porosity increasing to the left, and $\rho_{maa} - U_{maa}$ derived mineral log proportions are tied to the vertical rock type proportions of the entire Caney Shale interval, based on 59 well locations.

average bulk density of ~2.6 (Figure 11). At the base of the overlying Springer/Goddard Group, the GR response generally decreases, the porosity curves commonly shift to the right (decrease), the bulk density (RHOB) displays a peak increasing to the right, and the resistivity (RT) curve forms a distinct mound shape as it decreases in value near the top of the Caney Shale. The base of the Caney Shale, or the top of the Sycamore Formation, was interpreted according to the following log responses stratigraphically: an increase in the GR response due to change in lithology, a decrease in the RT and RHOB curves, and a separation of the porosity curves as well as a shift to the left (increase). Although the SP log is relatively constant and changes slowly with depth, it can be useful when there is a lack of GR or other log data. The SP curve generally displays a slight increase and decrease towards the top and base of the Caney Shale, respectively.

A high GR interval within the overlying Springer/Goddard Formation lies ~100-200 ft (30.5 m-61.0 m) above the top of the Caney Shale, and acts as a helpful marker when correlating the Mississippian section. This marker is generally 70-90 ft (21.3 m- 27.4 m) thick and is present nearly everywhere within the Ardmore basin, except for along its western edge. This high GR marker is additionally characterized by an increase in RT and NPHI.

The Caney Shale is divided into four laterally continuous zones, stratigraphically distinguished from the base to top of the Caney Shale as Zones 1 through 4. Four zones were also interpreted within the underlying Sycamore Formation to better understand the Mississippian stratigraphy; however these were not evaluated in terms of rock types and petrophysical properties. Stratigraphic cross-sections and structural-contour maps illustrate the complexity of the Mississippian section (Figures 12 and 13), and isopach maps (Figure 14; Appendix L) show the thickness variability for each zone. Cross-sections were flattened on the top of the Woodford Formation due to its unvarying log response and continuity across the

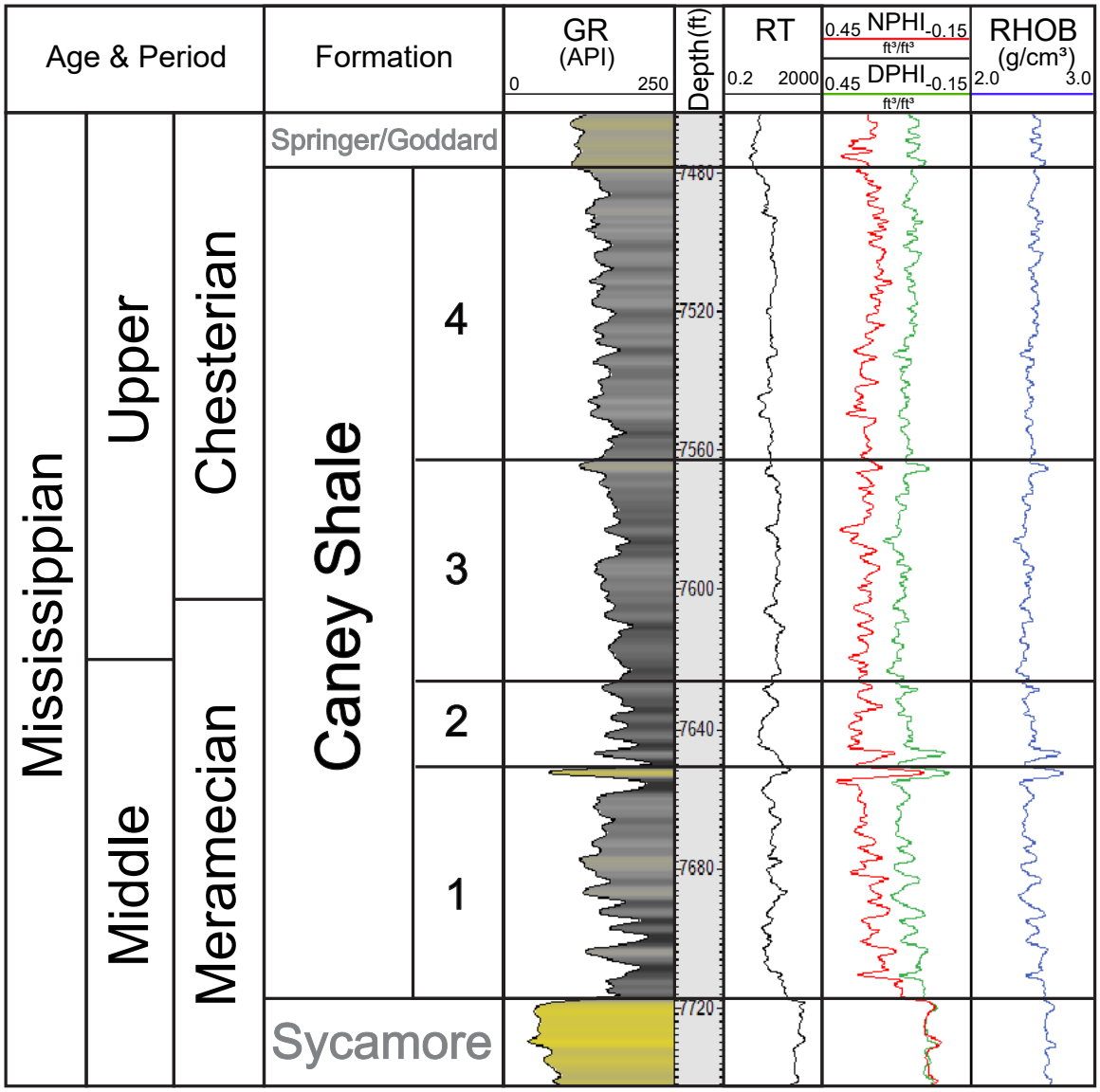

Figure 11: Example of typical log responses for the Caney Shale formation. Generalized age and period are shown in the first column, and formations and Caney Shale zonations are shown in the second column.

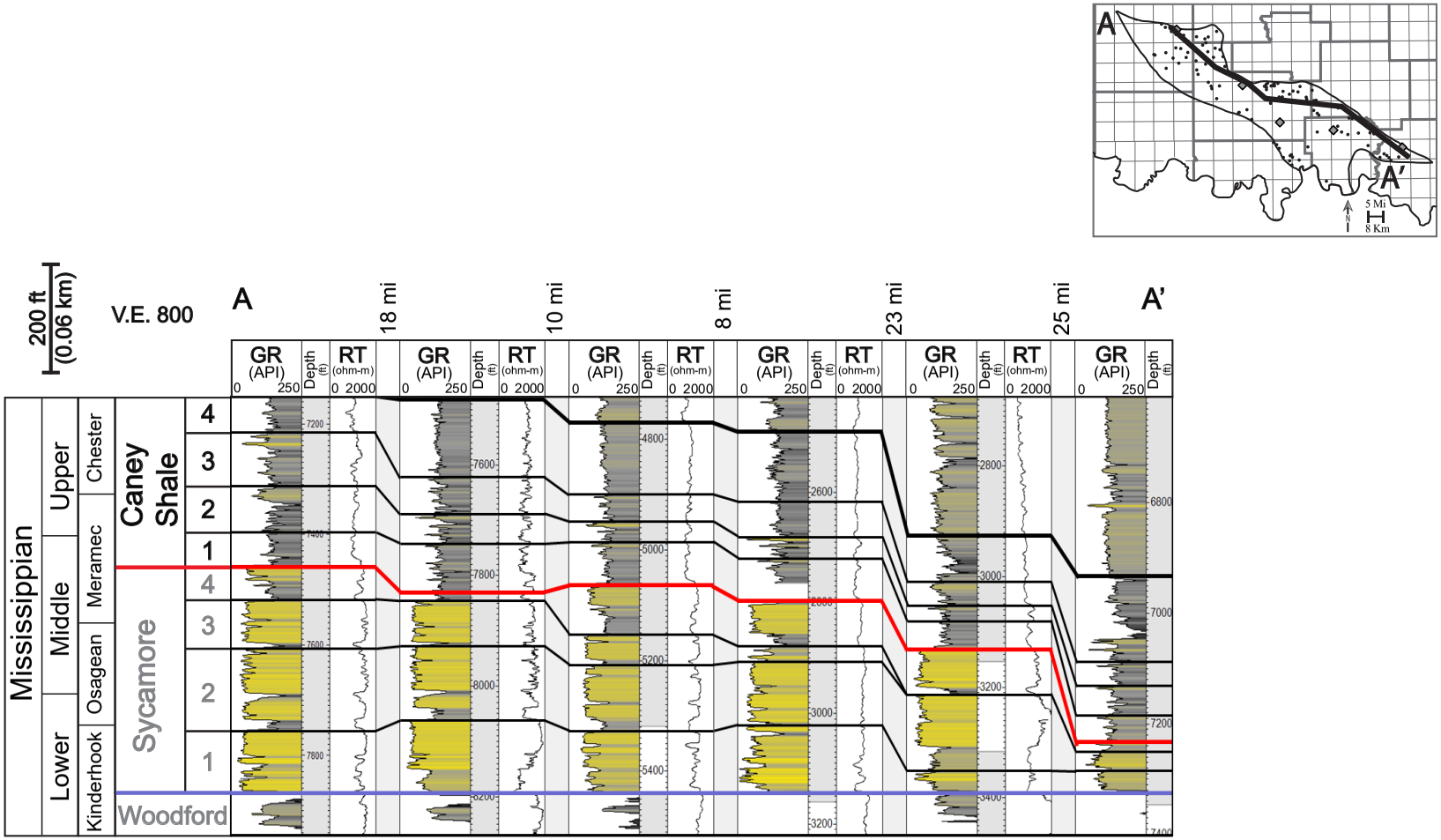

Figure 12: A northwest to southeast oriented stratigraphic cross-section of the Mississippian section flattened on the Woodford formation top is displayed. Zonations of the Caney Shale formation, as well as the Sycmore Formation, are correlated across the basin. Caney Shale zonations are characterized by decreasing upward GR responses and changes in RT, and Sycamore zonations are characterized by thickening and thinning low GR packages, often separated by thin high GR intervals. A generalized stratigraphic column (left) displays the ages, periods, and interpreted zonations. Well spacing distances are annotated above the cross section and between each well. A basemap with the location of A to A' is depicted in the top right corner.

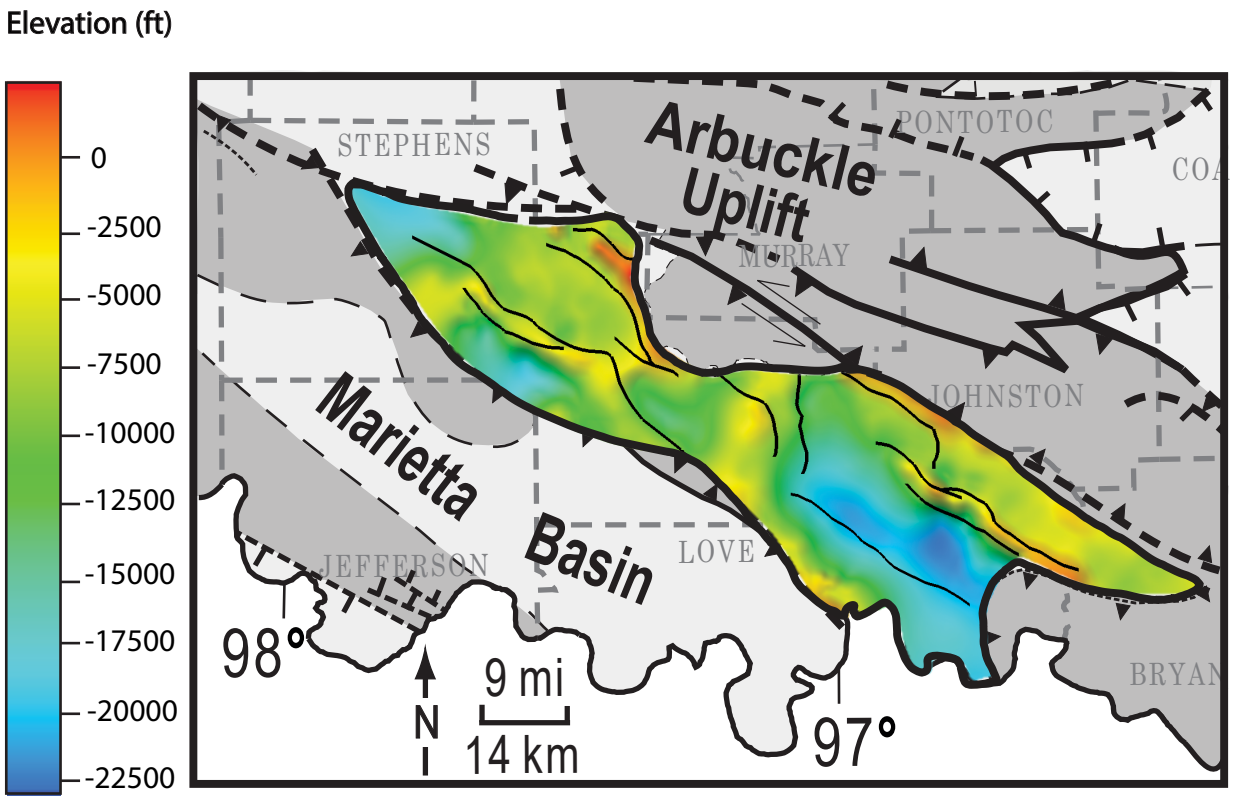

Figure 13: Structure-contour map of the Caney Shale formation across the Ardmore Basin. The highest areas of elevation are represented by the color red, and the lowest areas of elevation are represented by the color blue. The black lines on the map trace out several major faults that appear to correlate with structure. Structural highs correspond to major faults in the northern and southern portions of the basin.

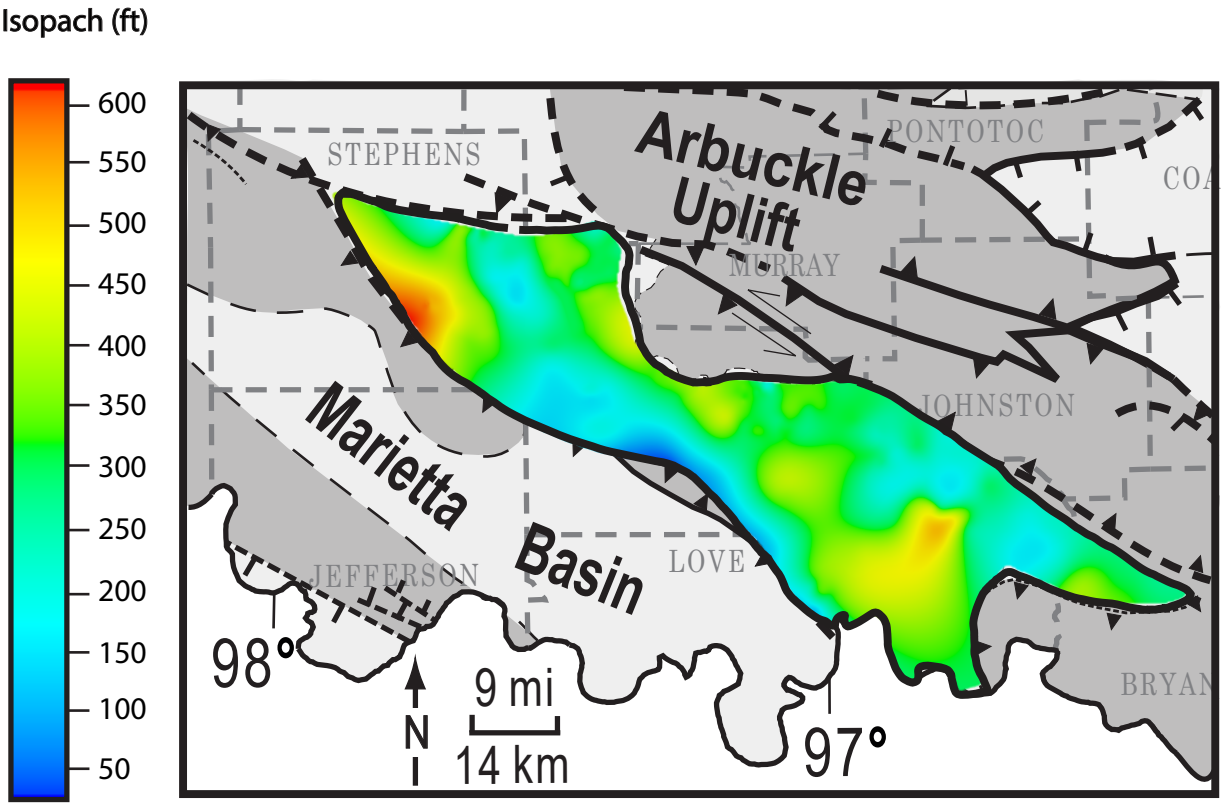

Figure 14: Isopach map of the Caney Shale formation across the Ardmore Basin. The thickest areas are represented by the color red, and the thinnest areas are represented by the color blue. The Caney Shale becomes thinnest towards the west flank of the basin, and generally becomes thicker eastward. A few peaks in thickness occur both in the northern and southern portions of the basin.

Ardmore Basin. The structural elevation ranges from 4 ft to -22,500 ft (1 m to -6,858 m) across the Ardmore Basin, with higher elevations often following fault traces, and the lowest elevations occurring towards the southern portion of the basin. The thickness of the Caney Shale ranges from 4 ft to 600 ft (1 m to 183 m), and approximately trends perpendicular to the elongation of the basin. Within the central portion of the basin, the southwestern flank ranges in thickness from ~20 ft to 140 ft (6 m to 43 m) and thickens from southwest to northeast. The thickest intervals of the Caney Shale occur near structural highs in both northern and southern portions of the basin. Isopach maps of Zones 1 to 4 (Appendix L) illustrate variability in zone thickness: Zone 4 ranges in thickness from 3-330 ft thick (0.9-100.5 m), Zone 3 ranges in thickness from 4-170 ft (1.2-51.8 m), Zone 2 ranges in thickness from 4-137 ft (1.2-41.8 m), and Zone 1 ranges in thickness from 9-104 ft (2.7-31.7 m). Zones 1-3 have an average thickness ranging from 50-68 ft (15.2-20.7 m), and Zone 4 is thickest with an average thickness of 128 ft (39.0 m).

3-D Model Grid

The interpreted zones were modeled across the Ardmore Basin using a proportional layering scheme, with each layer having a mean thickness of 2 ft (0.61 m), and an area of 500 x 500 ft (152 x 152 m). The grid was rotated 60.25 degrees to orient the model with the elongation of the basin, which stretches from northwest to southeast over 103 mi (165.7 km). The 3-D grid is composed of 105,481,008 cells, with 284 x 1086 x 342 cells in the I, J, and K directions.

Spatial Variability of Rock Types, Porosity, Brittleness Index, and Chemofacies

Rock types were generated, mapped, and modeled to evaluate their variability. The northern and southern portions of the Ardmore Basin has an abundance of mixed clays, especially in Zones 3 and 4 of the Caney Shale. The central portion of the basin, however, has a higher abundance of carbonate (~50%) compared to the ~20-30% carbonate in the northern and southern portions of the basin (Figure 15). The XRD mineral percentages support this finding, with the most carbonate rich area in the central portion of the basin (Figure 16; Appendix M). Zone 2 is the most carbonate-rich zone across the basin, with 31% carbonate compared to ~20% carbonate in Zones 1, 3, and 4. Overall, Zones 1-3 exhibit an increasing upwards carbonate content (decreasing upwards mixed-clay content) from the base to top of each zone, with each capped by an abundance of mixed-clays. The pulses in increasing carbonate abundance follow the decreasing upward GR pattern found in Zones 1-3 (Figure 15); furthermore, this trend is reflected in the elemental data by a decrease in detrital proxies, and an increase in carbonate proxies (Figure 17).

Zone 4 lacks the characteristics of Zones 1-3 and could potentially be interpreted as two separate zones. An additional zone was not interpreted due to discontinuity of GR markers across the basin. Zones 3 and 4 have a higher average GR than Zones 1 and 2 and have the highest percentage of mixed clays. There is a general increase in mixed clays from the bottom of the Caney Shale to the top. Overall, the three rock types do not show a strong lateral trend, and do not appear to correlate with structural lows or highs (Figure 18).

The stratigraphic variability of porosity reveals differences among the north, central, and southern portions of the basin. Within the northern portion of the basin, porosity general increases upwards from the base to top of Zone 1, followed by a dramatic ~2 ft (0.6 m) decrease in porosity right below the base of Zone 2. Porosity generally decreases upwards from base to

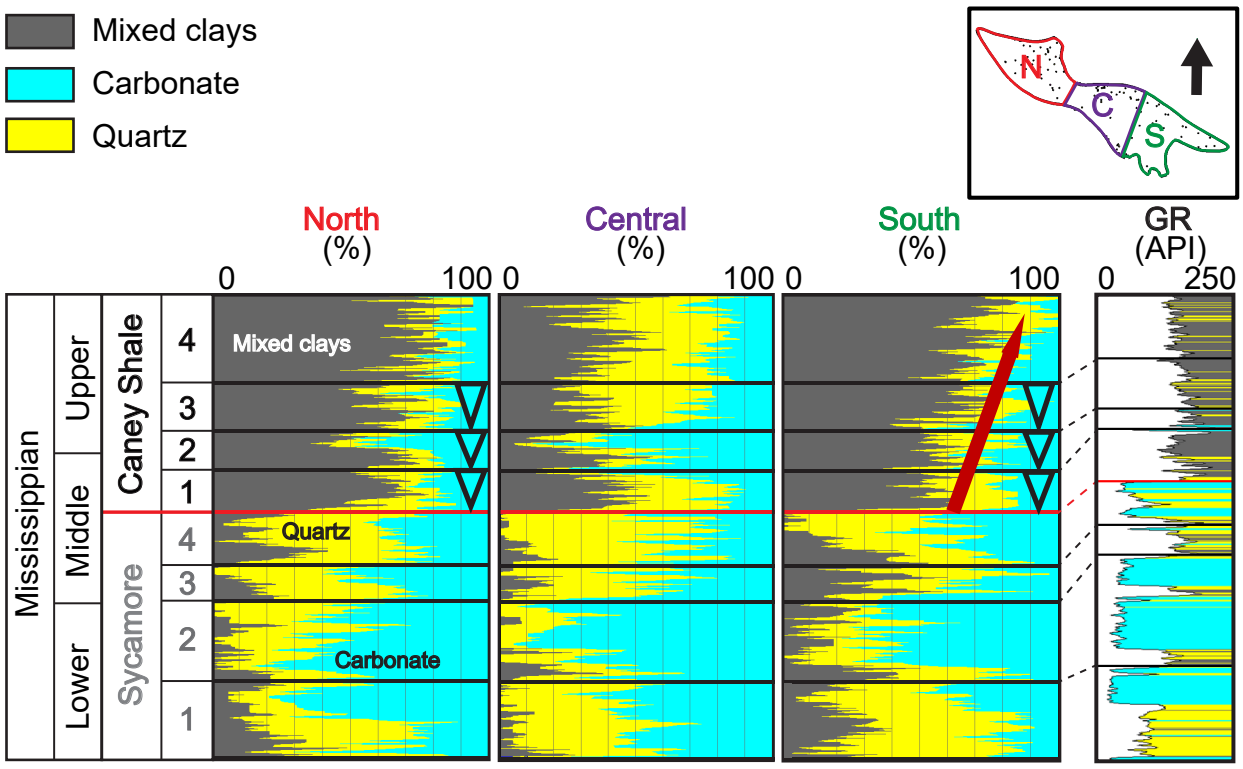

Figure 15: Vertical variability of rock type proportion curves for the northern, central, and southern portions of the basin. Perimeters for each vertical proportion curve are located in the upper-right map. North is denoted by "N", central is denoted by "C", and south is denoted by "S". A GR type log colored by rock type is displayed to the right to show the relationship between GR response and vertical rock type proportions. Blue triangles represent an upward increase of the carbonate rock type. The red arrow indicates and overall increase of the mixed clay rock type from the base to the top of the Caney Shale. A generalized stratigraphic column is displayed to the left with relative ages, formation names, and zonations.

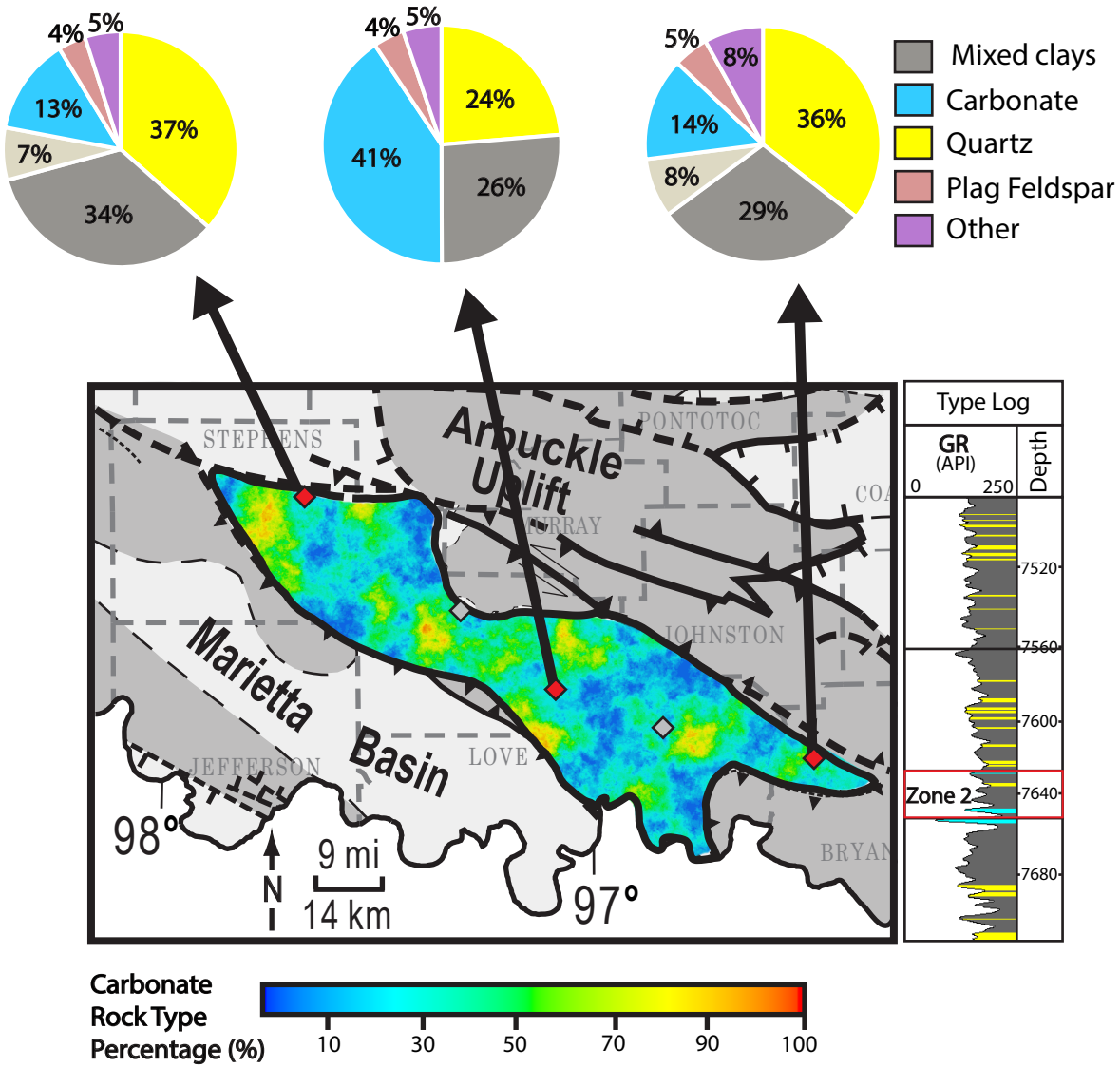

Figure 16: Carbonate rock type percentage map of zone 2 tied to XRD mineralogy percentage pies. Abundance of carbonate is represented by the warmer colors (yellow and red), and minimal carbonate abundance is represented by the cooler color (blue). A type log is displayed to the right, indicating the stratigraphic location.

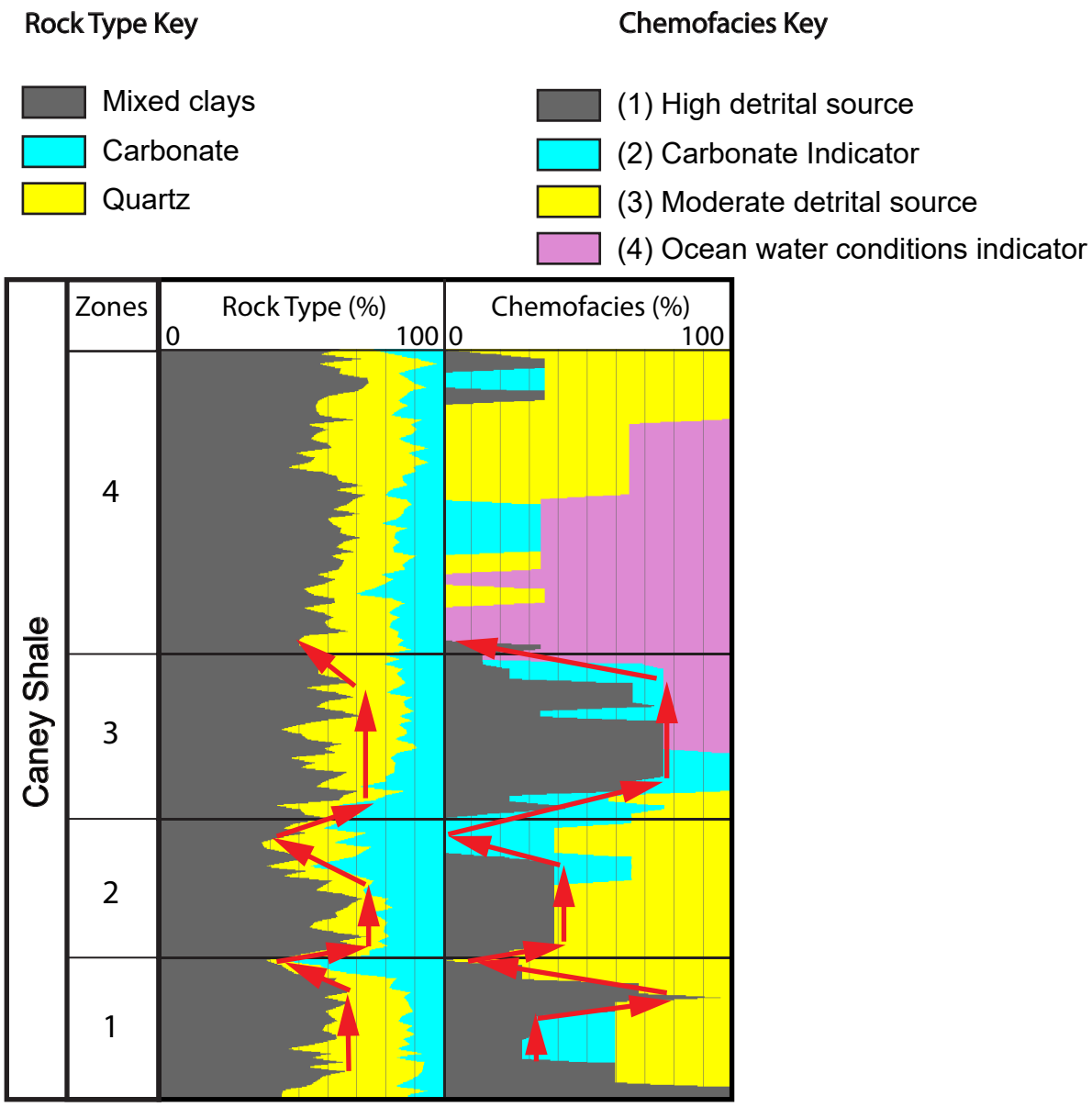

Figure 17: Displayed is the relationship between vertical proportions of rock types and chemofacies. Red arrows represent the general trend of rock type and chemofacies variability. Interpreted zones of the Caney Shale are displayed to the left. Similar patterns between chemfacies and rock type occurrence suggest that chemofacies are related to deposition.

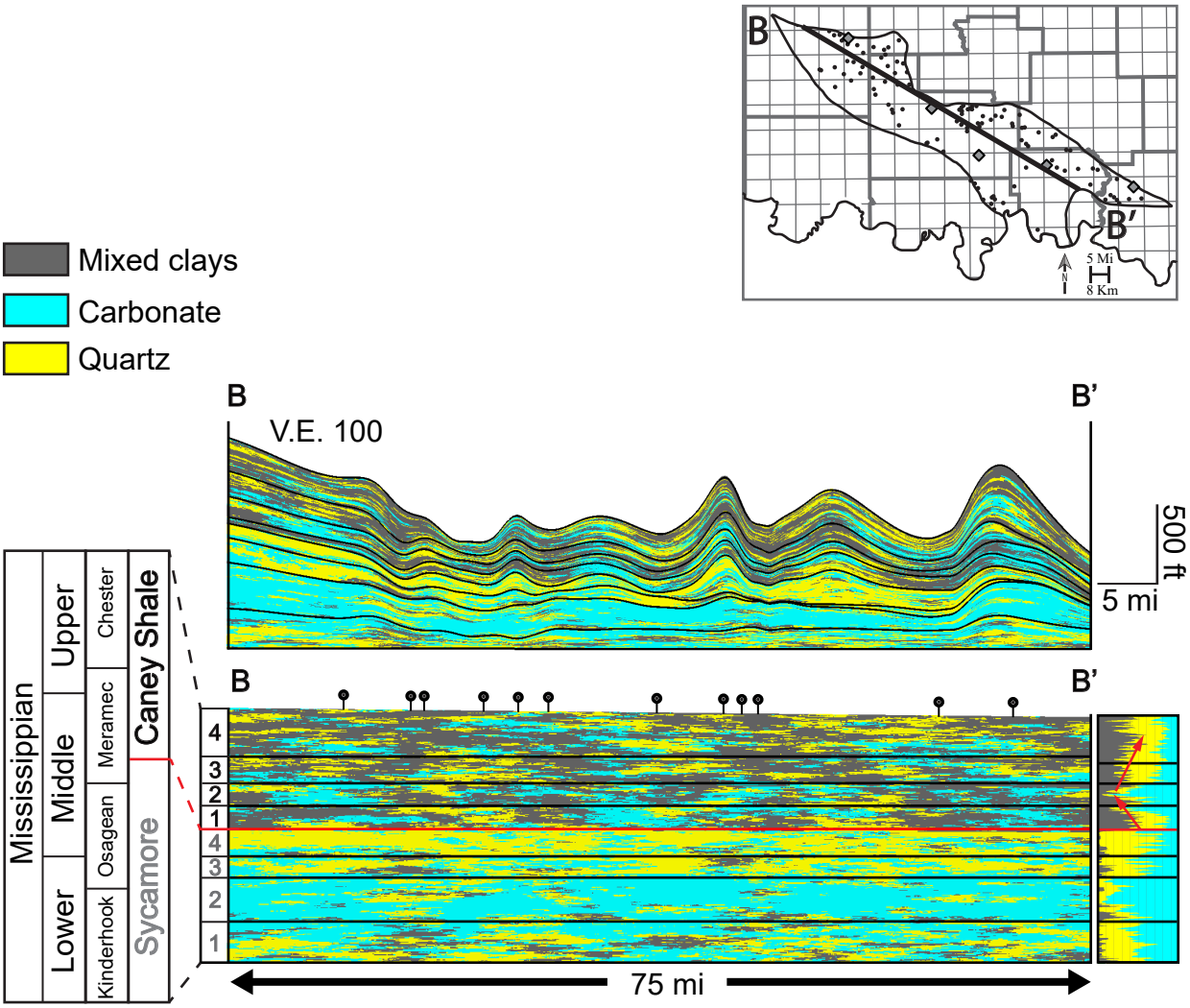

Figure 18: A northwest to southeast slice through the Caney Shale and Sycamore Formations displaying the spatial variability of ρmaa – Umaa derived rock types. The top cross section displays the structural complexity of the Ardmore Basin. Structure has been removed from the bottom cross section to better visualize the distribution of rock types. A vertical proportion curve has been displayed to the right to show a clear image of stratigraphic variability of rock types. The location of B to B' is plotted on the upper-right map.

top within Zone 2. Zone 3 and 4 within the northern portion of the basin do not show a defined trend compared to Zones 1 and 2. The northern portion of the basin displays an overall average porosity value of 15%. Zone 4 displayed the greatest average porosity of all the zones within the northern portion of the basin with a value of 23%. Zone 1 displayed the lowest average porosity with a value of 18%.

Within the central portion of the basin, porosity again increases upwards from base to top of Zone 1 and decreases right below the base of Zone 2. Zone 2 generally displays an approximate upwards decrease in porosity, with lowest porosity values being located just below the base of Zone 3. Some central wells reveal an approximate decrease in porosity from base to top of Zone 4, while others show no trend in porosity within this zone. The central portion of the basin revealed an overall average porosity of 13%. Zones 3 and 4 revealed the greatest average porosity of all the zones within the central portion of the basin, with a values of 21%. Zone 1 again displayed the lowest average porosity with a value of 17%.

The southern portion of the basin displays less of an upward increasing porosity trend from base to top within Zone 1, but still displays a decrease below the base of Zone 2, similar to that of the northern portion of the basin. Zone 2 does not display a definite trend from base to top but does display a decrease in porosity right below the base of Zone 3. Zones 3 and 4 within the southern portion of the basin do not display defined areas of increased or decreased porosity. The southern portion of the basin revealed an overall average porosity of 14%. Zones 3 and 4 displayed the greatest average porosity of all the zones within the southern portion of the basin, similar to that of the north and central portions of the basin, with a value of 22%. Zone 1 displayed the least average porosity at an average value of 16%.

Among the entire Ardmore basin, porosity approximately follows the decreasing upward GR pattern, with lower porosities moderately correlating to the carbonate rock type. Cumulative total porosity of the Caney Shale ranges from 1-61% with an average porosity of 21%. Each zone of the Caney Shale has an approximate average porosity of ~20% (Figure 19). Zone 4 displays the highest porosity with values reaching a maximum of 61%. The max porosity values of Zones 1, 2 and 3 are 35%, 36%, and 39%, respectively.

The stratigraphic variability of the brittleness model is a function of the rock type model variability. Areas classified as "ductile" (BI<50%) correlate to locations denoted as the mixed-clay rock type, while areas classified as "brittle" (BI>50%) correlate to locations classified as the quartz rock type (Figure 20). The most brittle zones were recorded as clay-rich Zones 3 and 4, while the least brittle zone was actually recorded as Zone 2, the most carbonate rich zone according to mineralogical and elemental analysis.

Chemofacies also display variability vertically within the Caney Shale. Chemofacies 1 and 3 are most prevalent across the basin, and appear in no particular pattern, but are often near each other stratigraphically. Chemofacies 2 appears often in short vertical sections, and vertical proportion curves reveal its dominance towards the top of increasing upwards GR curves within the Caney Shale zones. Chemofacies 4 is the third most prominent chemofacies, and it appears consistently in Wells 2, 3 and 4, often following the presence of Chemofacies 2; however, Chemofacies 2 sometimes appears stratigraphically higher than Chemofacies 4 as well. Chemofacies 4 appears in every well except the northern-most well, Well 1, and is the only chemofacies to not occur in every well.

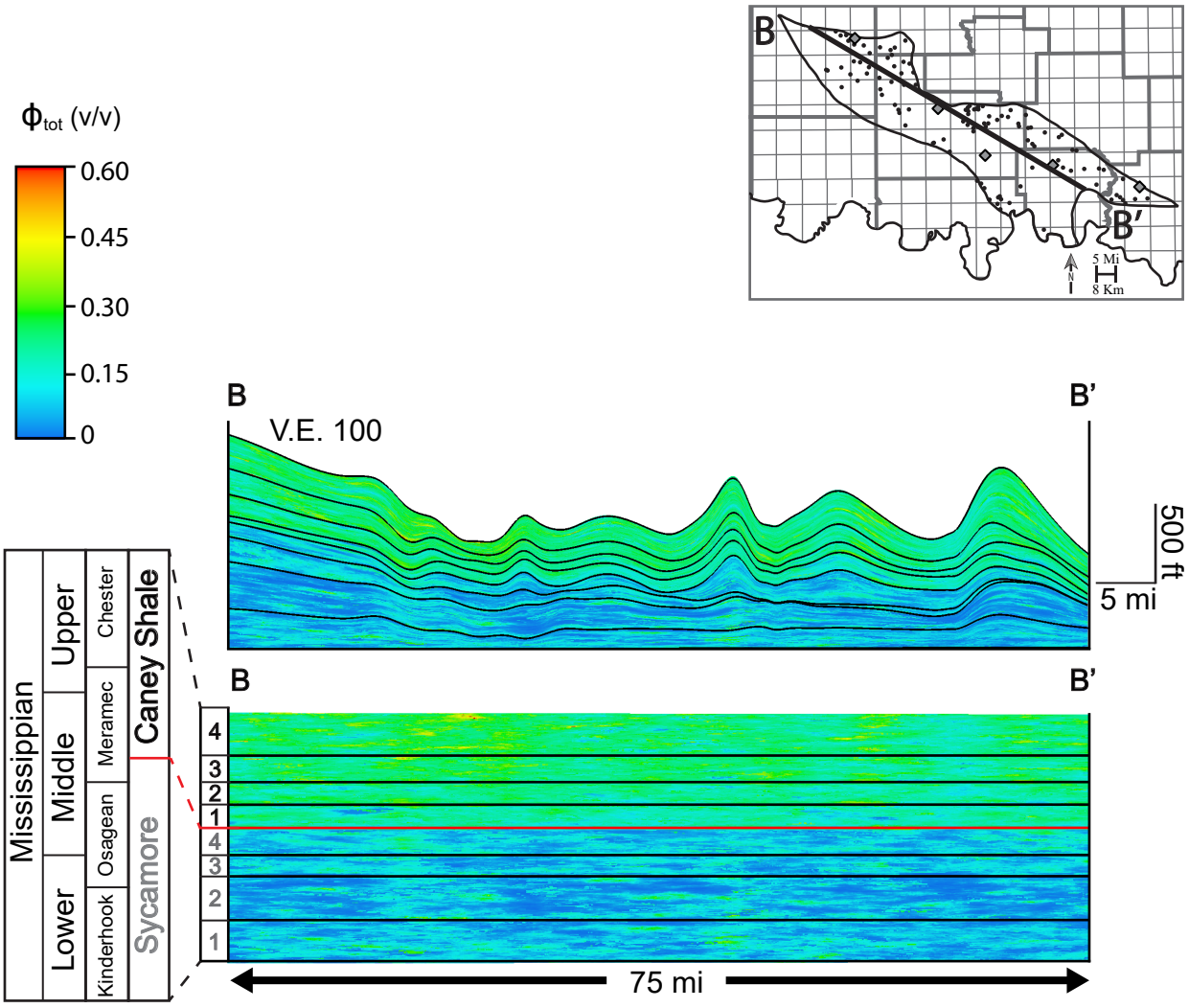

Figure 19: A northwest to southeast slice through the Caney Shale and Sycamore Formations displaying the spatial variability of porosity. The top cross section displays the structural complexity of the Ardmore Basin. Structure has been removed from the bottom cross section to better visualize the distribution of rock types. Red and yellow represent higher porosity values, and shades of blue represent lower porosity values. The location of B to B' is plotted on the upper-right map. The variability in porosity between the Caney Shale and the Sycamore Formation is apparent right at the base of the Caney Shale. Highest porosity values can be seen towards the left of the model in Zone 4.

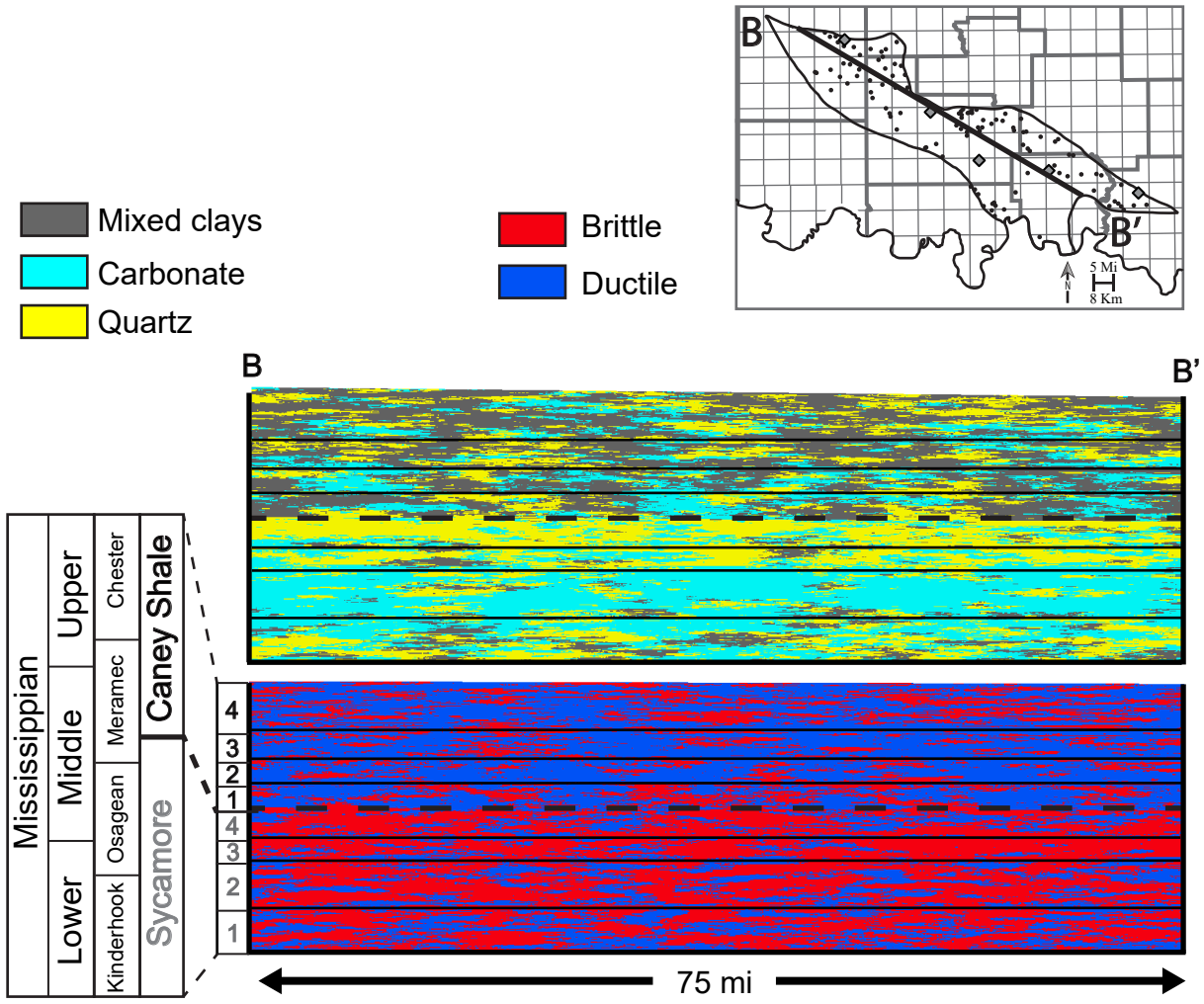

Figure 20: A northwest to southeast slice through the Caney Shale and Sycamore Formations displaying the spatial variability of rock types (top) compared to the brittleness model (bottom). For the brittleness model, red colors represent areas classified as "brittle", and blue colors represent areas classified as "ductile". The brittle classifications correlate with the quartz rock type while the ductile classifications correlate with the mixed clays rock type. Structure has been removed from the cross sections to better visualize the distribution of facies. The location of B to B' is plotted on the upper-right map. Caney Shale and Sycamore zonations are displayed to the right.

DISCUSSION

Chemofacies and Environmental Conditions

Chemofacies 1 (high detrital source) and 3 (moderate detrital source), which correlate with quartz and clay XRD results, respectively, are similar in abundance, which is reflected in the abundances of quartz and mixed clays within the rock-type model. Vertical proportion curves illustrate the presence of chemofacies 1 mainly in Zones 1, 2, and 3, separated at the top of each zone by chemofacies 2 and 3. This pattern reflects the vertical distribution of quartz, mixed-clays, and carbonate rock types. This correlation suggests that chemofacies are relatable to deposition. Chemofacies 2 (carbonate source) is associated with an increase in carbonate content and a decrease in GR value, and may be indicative of a shallow-marine environment. This chemofacies is likely associated with sediment deposited below a more oxic water column (improving bottom water conditions) as the presence of Mo and Co completely vanishes (Hemenway, 2018). Chemofacies 2 is likely the indicator of the top of a highstand systems tract (HST).

Chemofacies 4 is present in all wells except Well 1. Well 1 is the north-most well with cuttings in this study, suggesting that environmental conditions must have differed across the Ardmore Basin. Chemofacies 4 (assumed as an indicator of water oxygenation conditions) is within Zones 3 and 4, and is solely defined by the covariance of molybdenum and cobalt. The positive correlation between Mo and Co is unique to the dataset, as Mo does not positively correlate with any other recorded trace element from the dataset. The presence of chemofacies 4 may be interpreted in two different ways:

1) Detritally sourced molybdenum: The Mo peak does not only covary with Co, but also occurs where detrital proxies (Si, Al, K) are relatively high, and where carbonate proxies (Ca, Sr) are low. The combination of increased detrital proxies and the covariance with cobalt –commonly used as a detrital indicator –suggests that Mo could have originated from a detrital source rather than seawater; however, to generate a high detrital concentration of Mo, erosion from an igneous provenance would likely have to take place.
2) Euxinia/anoxia driven precipitation of molybdenum: During anoxic or euxinic conditions, Co is able to form insoluble cobalt sulfide (CoS) (Luther and Morse, 1999; Tribovillard et al. 2006; Simmons, 2019). In this state, Co may readily precipitate into the sediment through the formation of pyrite. XRD analysis reveals pyrite in low quantities through the Caney Shale, confirming this as a possible interpretation. While Co is often considered a weak indicator of paleoredox conditions due to its association with detrital deposition, it shows a weak correlation (R squared values ranging from 0.01-0.15) with Al, suggesting that there is likely not a relationship between them (Appendix N). Abundances of Mo near 200 ppm are often associated with euxinic or anoxic environments. Mo ranges from about ~120 to 140 ppm in chemofacies 4, which is relatively high compared to other dark shale formations (Simmons, 2019). Thus, an anoxic-euxinic water column is a more likely source of Mo in this study, as well as a source of leached Co.

Mo is often paired with other paleoredox sensitive elements such as U and V to investigate the presence of suboxic environments, however these elements do not correlate with Mo in this dataset.

Spatial Variability of Chemofacies

Well 1 is the northern-most well and is the only well lacking the presence of chemofacies 4. One interpretation is that chemofacies 4 bearing sediments did not reach the northern portion of the basin, resulting in its lack of concentration in Well 1. Chemofacies 4 appears consistently in Wells 2, 3 and 4, often following the presence of Chemofacies 2, however Chemofacies 2 sometimes appears stratigraphically higher than Chemofacies 4 as well. Chemofacies 4 appears in different stratigraphic locations within the Caney Shale, which is reasonable considering the large well spacing distance, structural complexity of the basin, and the potential of multiple sediment sources among the Ardmore Basin. Chemofacies 2 likely indicates many stages of shallow marine conditions during deposition of the Caney Shale. Chemofacies 1 and 3 are likely similar in composition to one another and may represent the presence of siliceous and clay-rich mudstone lithologies, respectively. These chemofacies often appear in conjunction with one another, presumably due to more similar depositional conditions than that of chemofacies 2 and 4.

Structure, Rock Types, and Mineralogy

Both the carbonate and quartz rock types are likely attributed mostly to calcareous shale and siliceous/silty shale, respectively. The quartz rock type cannot be assumed as sandstone, as the $\rho_{maa} - U_{maa}$ analysis does not account for grain size. Similarly, the carbonate rock type cannot be assumed as limestone. It is important to note that limestone beds and concretions have been recorded in the Caney Shale within the Arkoma Basin (Schad, 2004), so its presence in the Ardmore Basin should not be ruled out; however, a limestone lithology was not obvious in the

cuttings, and the Caney within the Ardmore Basin is commonly referred to as a "calcareous shale" rather than a limestone.

The variable thickness of the Caney Shale is likely a result of sea-level changes, as well as intense faulting and folding that occurred pre- and post-deposition (Granath, 1989; Allen, 2000). There were likely multiple nearshore sources depositing sediment into the basin during the late Mississippian, and the geometry of the basin was different than today. The structure of the middle portion of the basin displays a few areas of relatively high elevation (-2500 ft [-2500 m] to 620 ft [189 m]), potentially suggesting a shallow paleo sea-level. Similarly, the rock-type model, vertical proportion curves, and XRD mineralogy show an abundance of carbonate specifically within the central portion of the Ardmore Basin. Because the width of the central portion of the basin is much smaller than that of the northern and southern portions, it is possible that a shallow water environment may have been more easily maintained due to more proximal shorefaces.

Interpreted Depositional Environment

Zones 1-3 are interpreted to represent parasequences of a transgressive systems tract, likely resulting from both autocyclic and allocyclic sedimentation within a shallow- to deep-marine depositional environment. Mississippian-age sedimentation over the Ardmore basin was likely due to allogenic processes where global sea-level change and basin-wide tectonism was occurring; however, further isotopic studies are necessary for clarification. Based on the available data, different environmental interpretations are possible. First, the presence of chemofacies 2 (carbonate indicator) may suggest a shift towards a shallow-marine environment,

when local sea-level was at a lowstand. Chemofacies 4 may indicate a deeper marine setting during a local highstand, where base-level rise and resultant drowning of the carbonate system occurred (Schlager 1981; Catuneanu 2009). An alternative interpretation is one of "reciprocal sedimentation" where carbonates were deposited during periods of highstand, and clastics were deposited during periods of lowstand (Wilson 1967). Differentiation between the two hypotheses requires future investigation with additional data.

Porosity and Brittleness

The porosity of the Caney Shale varies vertically and laterally across the basin. The Caney Shale *appears* to have a high total porosity due to the relationship of the NPHI log with shale bound water. This owes to the separation displayed between the neutron and density porosity curves and is referred to as the shale effect (Schlumberger, 2015). Because the drill-cuttings indicate the Caney Shale as entirely shale in lithology, effective porosity was not calculated.

While the brittleness index (BI) calculations and resulting brittleness classification model revealed a correlation between brittleness and the quartz rock type, a few unexpected results must be addressed. The most brittle zones of the Caney Shale are Zones 3 and 4; however, these zones were most abundant in mixed clays. The most ductile zone is Zone 2, which is the most carbonate-rich zone. Because the BI calculation (Equation 4) accounted for both ankerite and calcite as an aggregate (the carbonate rock type), the potential of ankerite as a separate rock type could not be evaluated. The presence of dolomite tends to increase brittleness of shale (Wang and Gale, 2009), so investigating the effect of ankerite (similar in mineral structure to dolomite)

may reveal additional trends in brittleness of the Caney Shale. Thus, the relationship between brittleness and the carbonate rock-type, as well as porosity, requires further work.

CONCLUSION

XRD mineralogical analysis revealed a dominant composition of mixed-clays, quartz, and carbonate minerals within the Caney Shale of the Ardmore Basin. The mixed clay fraction is comprised of illite and kaolinite, while the carbonate fraction is composed of calcite and ankerite. These XRD results, along with ρ_{maa}-U_{maa} derived rock types correlate with four elementally derived chemofacies. Chemofacies 1 and 3 capture the presence of detrital input into the basin, while chemofacies 2 indicates carbonate mineral presence. The covariance between Mo and Co in chemofacies 4 can be interpreted in a few ways. The most plausible interpretation is that an euxinic to anoxic water column resulted in the precipitation of Mo from seawater into the underlying sediment, and the leaching of Co into sediment via the formation of pyrite.

Sea-level variation, faulting, and folding of the Mississippian strata likely resulted in the varying thicknesses and structure of the present-day Caney Shale. The central portion of the basin is thinner in width relative to the rest of the basin and encompasses some areas of higher elevation. This suggests the possibility of less accommodation space, and a shallower-sea level that could be more easily maintained than in the northern and southern portion. The rock-type model, vertical proportion curves, and XRD mineralogy reveal the central portion of the basin to be the most carbonate rich.

Four stratigraphic zones were correlated across the basin. Zones 1, 2, and 3 are characterized by a decreasing upward GR log response and an increasing upward carbonate

abundance, with each zone capped by an abundance of the mixed-clay rock type. According to XRD and ρ_{maa}-U_{maa} mineralogical analysis, Zone 2 displayed the greatest carbonate abundance of all the zones, with Zone 4 displaying the least amount of carbonate. Zone 4 was characterized by a more consistent, higher average GR than the underlying zones. These four zonations correlate with chemofacies, suggesting that elemental analysis can be tied to deposition.

The 3-D total porosity model reveals a range of 1-61% porosity, average porosity values of ~20% per zone of the Caney Shale, and maximum porosity values of 61% occurring within the clay-rich Zone 4. Evaluation of porosity from the northern, central, and southern portions of the basin revealed the northern portion to have the greatest average porosity at 15%. Among the entire Ardmore basin, porosity approximately follows the decreasing upward GR pattern, with lower porosities correlating to the carbonate rock type. Brittleness index models depicted brittleness within the quartz rock type, and greater ductility within the mixed clay rock type. Brittleness calculations did not account for carbonate presence, therefor a relationship was not assessed between the two.

REFERENCES

Andrews, R.D., 2007, Stratigraphy, production, and reservoir characteristics of the Caney Shale in southern Oklahoma: Shale Shaker, v. 58, pp. 9-25.

Allen, R.W., 2000. Complex structural features of the Ardmore Basin. *Shale Shaker Journal*, *51*, pp. 11-21.

Bornemann, E. and Doveton, J.H., 1981. Log normalization by trend surface analysis. *The log analyst*, *22*(04), pp. 3-9.

Cardott, B.J., 2017. Oklahoma shale resource plays. *Oklahoma Geology Notes*, *76*(2), pp.21-30.

Catuneanu, O., Abreu, V., Bhattacharya, J.P., Blum, M.D., Dalrymple, R.W., Eriksson, P.G., Fielding, C.R., Fisher, W.L., Galloway, W.E., Gibling, M.R. and Giles, K.A., 2009. Towards the standardization of sequence stratigraphy. *Earth-Science Reviews*, *92*(1-2), pp. 1-33.

Chatellier, J.Y., Quartero, E., Urban, M., Molgat, M., Deconinck, A. and Francus, P., 2011. Power and limitations of x-ray fluorescence from cuttings: a test in the Utica and Lorraine shales from Quebec. *Search and Discovery Article*, *40766*, pp. 10-13.

Cullen, A., 2019, My favorite… thin section: The Caney sandstone from Philip's Creek—one of Rick Andrews' favorite outcrops: Shale Shaker, v. 70, no. 4, pp. 168-180.

Dahl, T.W., Ruhl, M., Hammarlund, E.U., Canfield, D.E., Rosing, M.T. and Bjerrum, C.J., 2013. Tracing euxinia by molybdenum concentrations in sediments using handheld X-ray fluorescence spectroscopy (HHXRF). *Chemical geology*, *360*, pp. 241-251.

"Defining Porosity." *Schlumberger*, 9 Sept. 2015, https://www.slb.com/resource-library/oilfield-review/defining-series/defining-porosity.

Doveton, J. H., 1994. Numerical Methods for Mineral Estimation from Well Logs, *AAPG Datapages/Archives*, Special Publications of SEPM, pp. 123-133.

Elias, M.K., 1956, Upper Mississippian and Lower Pennsylvanian formations of south-central Oklahoma: AAPG Petroleum Geology of Southern Oklahoma, v. 1, pp. 56-134.

Emerson, S.R. and Huested, S.S., 1991. Ocean anoxia and the concentrations of molybdenum and vanadium in seawater. *Marine Chemistry*, *34*(3-4), pp. 177-196.

Granath, Jim., 1989, Structural evolution of the Ardmore Basin, Oklahoma: Progressive deformation in the foreland of the Ouachita Collision. Tectonics, 8, pp. 1015-1036

Hardisty, L., Pranter, M.J., Devegowda, D., Marfurt, K.J., Sondergeld, C., Rai, C., Gupta, I., Han, H., Dang, S., McLain, C.T. and Larese, R.E., 2021. Stratigraphic variability of Mississippian Meramec chemofacies and petrophysical properties using machine learning

and geostatistical modeling, STACK trend, Anadarko Basin, Oklahoma. *Interpretation*, *9*(3), pp. T987-T1007.

Harris, R.W., Jr., 1971, Palynology of the Sand Branch Member of the Caney Shale Formation (Mississippian) of southern Oklahoma: Norman, University of Oklahoma, unpublished PhD dissertation, 216 p.

Hayatdavoudi, A., Durugbor, N.C., Ghalambor, A., and C. Okoye. "Prediction of Average Cutting Size While Drilling Shales." Paper presented at the SPE/IADC Drilling Conference, New Orleans, Louisiana, March 1987. doi: https://doi.org/10.2118/16101-MS

Hemenway, M.A., 2018. Application of handheld ED-XRF for high-resolution chemostratigraphy in texturally homogeneous carbonate mudstones: Salina A-1 Carbonate (Silurian), Michigan Basin, *Masters Theses*, 77 p.

Jarvie, D.M., Hill, R.J., Ruble, T.E. and Pollastro, R.M., 2007. Unconventional shale-gas systems: The Mississippian Barnett Shale of north-central Texas as one model for thermogenic shale-gas assessment. *AAPG bulletin*, *91*(4), pp. 475-499.

Kamann, P.J., 2006, Surface-to-subsurface correlation and lithostratigraphic framework of the Caney Shale (including the "Mayes" Formation) in Atoka, Coal, Hughes, Johnston, Pittsburg, and Pontotoc Counties, Oklahoma: Stillwater, Oklahoma, Oklahoma State University, unpublished M.S. thesis, 259 p.

Katende, A., Rutqvist, J., Benge, M., Seyedolali, A., Bunger, A., Puckette, J.O., Rhin, A. and Radonjic, M., 2021. Convergence of micro-geochemistry and micro-geomechanics towards understanding proppant shale rock interaction: A Caney shale case study in southern Oklahoma, USA. *Journal of Natural Gas Science and Engineering*, *96*, p. 104296.

Macqueen, J.B., 1967. Some methods for quantification of the multivariate observations, western management science institute, university of california. Technical report, Working paper 96, pp. 281-297.

Martin, K.G., 2019. X-Ray Fluorescence Applications in Mudrock Characterization: Investigations into Middle Devonian Stratigraphy, Appalachian Basin, USA. West Virginia University, Masters Theses, 151 p.

Morse, J.W. and Luther Iii, G.W., 1999. Chemical influences on trace metal-sulfide interactions in anoxic sediments. *Geochimica et Cosmochimica Acta*, *63*(19-20), pp. 3373-3378.

Milad, B., Slatt, R. and Fuge, Z., 2020. Lithology, stratigraphy, chemostratigraphy, and depositional environment of the Mississippian Sycamore rock in the SCOOP and STACK area, Oklahoma, USA: Field, lab, and machine learning studies on outcrops and subsurface wells. *Marine and Petroleum Geology*, *115*, 18 p.

Miller, J.C., M.J. Pranter, and A.B. Cullen, 2019, Regional stratigraphy and organic richness of the Mississippian Meramec and associated strata, Anadarko Basin, central Oklahoma: Oklahoma City Geological Society, Shale Shaker, v. 70, p. 50-79.

Pearce, T.H. and Jarvis, I., 1992. Applications of geochemical data to modelling sediment dispersal patterns in distal turbidites; late Quaternary of the Madeira abyssal plain. *Journal of Sedimentary Research*, *62*(6), pp. 1112-1129.

Pearson, K., 1901. Principal components analysis. *The London, Edinburgh, and Dublin Philosophical Magazine and Journal of Science*, *6*(2), p. 559.

Pranter, M.J., Hurley, N.F. and Davis, T.L., 2004. Anhydrite distribution within a shelf-margin carbonate reservoir: San Andres Formation, vacuum field, New Mexico, USA. *Petroleum Geoscience*, *10*(1), pp. 43-52.

Radonjic, M., Luo, G., Wang, Y., Achang, M., Cains, J., Katende, A., Puckette, J., Grammer, M. and King, G.E., 2020, December. Integrated microstructural characterisation of caney shale, OK. In *Unconventional Resources Technology Conference, 20–22 July 2020* (pp. 2157-2174). Unconventional Resources Technology Conference (URTEC).

Rowe, H., Hughes, N. and Robinson, K., 2012. The quantification and application of handheld energy-dispersive x-ray fluorescence (ED-XRF) in mudrock chemostratigraphy and geochemistry. *Chemical geology*, *324*, pp. 122-131.

Sarle, W.S., 1983. *Cubic clustering criterion*. SAS Technical Report A-108. Cary, NC: SAS Institute Inc, 51 p.

Schad, S. T., 2004, Hydrocarbon potential of the Caney Shale in southeastern Oklahoma: M.S. thesis, University of Tulsa, Tulsa, Oklahoma, 576 p.

Schlager, W., 1981. The paradox of drowned reefs and carbonate platforms. *Geological Society of America Bulletin*, *92*(4), pp. 197-211.

Schwartzapfel, J.A., 1990, Biostratigraphic investigations of Late Paleozoic (Upper Devonian to Mississippian) radiolaria within the Arbuckle Mountains and Ardmore Basin of south-central Oklahoma: Dallas, Texas, unpublished PhD dissertation, University of Texas, 475 p.

Shier, D.E., 2004. Well log normalization: Methods and guidelines. *Petrophysics-The SPWLA Journal of Formation Evaluation and Reservoir Description*, *45*(03), p. 13.

Simmons, J., 2019. *A Geochemical Analysis of Upper Cretaceous Tuscaloosa Marine Shale Core, Lambert H-1* (Doctoral dissertation, University of Louisiana at Lafayette), 80 p.

Sloss, L.L., 1963. Sequences in the cratonic interior of North America. *Geological Society of America Bulletin*, *74*(2), pp. 93-114.

Suneson, N., 1996, The geology of the Ardmore Basin in the Lake Murray State Park area, Oklahoma; an introduction and field-trip guide. Norman, OK: Oklahoma Geological Survey, Norman, OK, United States, pp. 2-96.

Taff, J.A., 1901. Description of the Coalgate quadrangle. US Geol. Survey geologic Atlas, Folio, 74, p. 1903.

Trevino, A., 2016. Introduction to K-means Clustering. *Oracle AI & Data Science Blog, Blogs.oracle.com*

Tribovillard, N., Algeo, T.J., Lyons, T. and Riboulleau, A., 2006. Trace metals as paleoredox and paleoproductivity proxies: an update. *Chemical geology*, *232*(1-2), pp. 12-32.

Turner, B.W., 2016, Utilization of chemostratigraphic proxies for generating and refining sequence stratigraphic frameworks in mudrocks and shales, Dissertation, University of Oklahoma, Norman, Oklahoma, p. 32–35.

Vine, J.D. and Tourtelot, E.B., 1970. Geochemistry of black shale deposits; a summaryreport. *Economic Geology*, *65*(3), pp. 253-272.

Wilson, J.L., 1967. Cyclic and reciprocal sedimentation in Virgilian strata of southern New Mexico. *Geological Society of America Bulletin*, *78*(7), pp. 805-818.

Well Name	Well API #	County	S/T/R	Operator	Caney Top Depth (ft)	Sycamore Top Depth (ft)
Well 1	35137245210000	Stephens	12 01N 05W	Sun Expl & Prod	7947	8202
Well 2	35019229130000	Carter	03 03S 01W	Amoco	4768	5057
Well 3	35019211280000	Carter	04 05S 02E	Signal Oil & Gas	15739	16124
Well 4	35095203740000	Marshall	18 05S 05E	Amoco	5824	6280
Well 5	35013000130000	Bryan	15 06S 08E	Pasotex	4452	4661

Appendix A: A table of the 5 key wells with drill-cuttings and their corresponding well API numbers, county names, section, township, and range values, operators, and top and base depths of the Caney Shale.

Appendix B: Cuttings Description Sheets

Tools used for cuttings description and analysis include tweezers for handling small chips, triangular metal trays, a binocular microscope with fluorescent and plane light, lighter fluid for testing the presence of organic material, and hydrochloric acid to test for the presence of calcite. The presence of any key features, as well as caving material, were noted frequently.

Cuttings Description Sheet 7/15/2021

Well Name: A-1 Hefner

API: 35137245210000

Caney Interval: 9082 ft-9335 ft

Depth (ft)	Lithology								Grain Sizes							Color					Description
	Clay Rich MS	Calcareous MS	Dolomitic MS?	Interbedded	Siliceous MS	Silty MS	LS	SS	CL	Silt	VF	F	M	C	VC	Black	Dark grey	Grey	Light grey	Beige	
9440									CL										X		100 ft below base of Caney. pyrite- altered sulfur present, caving material present, light grey mudstone, possible limestone
9430									CL										X		
9420									CL										X		
9410									CL										X		
9400									CL									X			
9390									CL									X			
9380									CL									X			
9370									CL									X			few calcite crystal grains- maybe indicative of a calcite vein? Some pyrite- altered sulfur present, less caving
9360									CL									X			material present, light grey mudstone fizzes, darker grey grains do not. So, possibly an interbedded calcareous and noncalcareous mudstone. Some black, vitreous grains- maybe organics
9350									CL									X			
9340									CL									X			
9330									CL									X			Base of Caney, Top of Sycamore?
9320									CL									X			
9310									CL									X			less caving material than before. All grains seem to efferece readily. few calcite crystal grains- maybe indicative of a calcite vein? Some pyrite- altered sulfur present, less caving material present, Some black, vitreous grains- maybe organics.
9300									CL									X			
9290									CL									X			
9280									CL									X			
9270									CL									X			
9260									CL									X			less caving material, appears to be slightly darker in color, few black vitreous grains, fizzes.
9250									CL									X			
9240									CL									X			
9230									CL									X			
9220									CL									X			
9210									CL									X			
9200									CL								X				darker thank before, the cuttings are finer here. Some altered pyrite/sulfur grains present. Little caving material. Slow efferecing.
9190									CL								X				
9180									CL								X				
9170									CL								X				
9160									CL								X				dark grey-black mudstone. Many more vitreous grains. Some sulfur grains.
9150									CL												
9140									CL												
9130									CL												
9120									CL												
9110									CL												
9100									CL												some sulfur grains, less than before, still looks massive. Very slow fizz, possibly due to presence of dolomite or ferroan dolomite. Gamma has a strong decreasing peak.
9090									CL												
9080									CL												

Appendix B1: Drill-cuttings description sheet for Well 1. Lithology, grain size, chip color, and a basic descriptions are noted.

Cuttings Description Sheet 8/10/2021

Well Name: Matha Speake #1-3

API: 35019229130000

Caney Interval: 5690ft- 5970ft

Depth (ft)	Lithology								Grain Sizes							Color					Description
	Clay Rich MS	Calcareous MS	Dolomitic MS?	Interbedded	Siliceous MS	Silty MS	LS	SS	CL	Silt	VF	F	M	C	VC	Black	Dark grey	Grey	Light grey	Beige	
5690									CL									x			some pyrite flakes
5700									CL									x			
5710									CL									x			caving material
5720									CL									x			dark grey, massive looking silicceous (likely) shale
5730									CL									x			
5740									CL									x			black, some vitreous looking flakes
5750									CL									x			
5760									CL									x			fizzes rapidly
5770									CL									x			
5780									CL										x		lighter grey shale
5790									CL										x		
5800									CL										x		
5810									CL									x			
5820									CL									x			
5830									CL									x			
5840									CL									x			
5850									CL									x			grey, possible calcite vein
5860									CL									x			little caving
5870									CL									x			chips appear o separate in thin flakes. Has caving material present. No pyrite here
5880									CL									x			
5890									CL									x			
5900									CL									x			
5910									CL									x			massive grey shale
5920									CL									x			some vitreous looking flakes, some calcite crystals, maybe remnant of calcite vein, thinly bedded- breaks in plates
5930									CL									x			
5940									CL									x			
5950									CL									x			dark grey
5960									CL									x			grey
5970									CL									x			

Appendix B2: Drill-cuttings description sheet for Well 2. Lithology, grain size, chip color, and a basic descriptions are noted.

Cuttings Description Sheet 10/14/2021

Well Name: City of Ardmore #1

API: 35019211280000

Caney Interval: 16620- 16990ft

Depth (ft)	Lithology								Grain Sizes							Color					Description
	Clay Rich MS	Calcareous MS	Dolomitic MS?	Interbedded	Siliceous MS	Silty MS	LS	SS	CL	Silt	VF	F	M	C	VC	Black	Dark grey	Grey	Light grey	Beige	
16580									CL										x		white caving material
16590									CL										x		
16600									CL										x		
16610									CL										x		
16620									CL										x		
16630									CL									x			fizzes slowly
16640									CL								x				
16650									CL								x				dark grey, uniform cuttings
16660									CL								x				
16670									CL									x			
16680									CL									x			
16690									CL									x			
16700									CL									x			
16710									CL									x			lighter grey shale
16720									CL									x			
16730									CL									x			
16740									CL									x			no sign of calcite veins
16750									CL								x				
16760									CL								x				
16770									CL							x					
16780									CL							x					very dark, black shale chips with few small white grains of caving material, no fizz
16790									CL								x				
16800									CL								x				overall these chips appear darker than the previous wells
16810									CL								x				
16820									CL								x				
16830									CL								x				
16840									CL								x				white and brown caving material, material is limited for next several packets
16850									CL								x				
16860									CL									x			
16870									CL									x			
16880									CL									x			
16890									CL									x			
16900									CL									x			
16910									CL								x				
16920									CL								x				
16930									CL								x				some fizzing, however most grains in this packet do not fizz
16940									CL								x				
16950									CL								x				
16960									CL								x				
16970									CL								x				
16980									CL								x				
16990									CL								x				Base of Caney
17000									CL							x					
17010									CL							x					fizzes more rapidly
17020									CL										x		
17030									CL										x		
17040									CL										x		
17050									CL									x			
17060									CL									x			
17070									CL										x		very light grey cuttings
17080									CL										x		

Appendix B3: Drill-cuttings description sheet for Well 3. Lithology, grain size, chip color, and a basic descriptions are noted.

Cuttings Description Sheet 8/10/2021

Well Name: Albert Purser #1

API: 35095203740000

Caney Interval: 7225ft- 6475ft

Depth (ft)	Lithology								Grain Sizes							Color					Description
	Clay Rich MS	Calcareous MS	Dolomitic MS?	Interbedded	Siliceous MS	Silty MS	LS	SS	CL	Silt	VF	F	M	C	VC	Black	Dark grey	Grey	Light grey	Beige	
6400									CL									x			No reaction at all.
6410									CL									x			
6420									CL									x			No reaction, no caving material
6430									CL									x			
6440									CL									x			
6450									CL									x			some vitreous grains
6460									CL									x			this should be the top of caney, base of goddard
6470									CL									x			several vitreous grains
6480									CL									x			some vitreous/carbonaceous grains, possible dolomite presence
6490									CL									x			
6500									CL									x			no fizz at all
6510									CL									x			
6520									CL									x			slightly lighter grey in color, very slow fizz, possibly dolomitic?
6530									CL									x			
6540									CL									x			
6550									CL									x			no reaction at all, little to no caving material
6560									CL									x			
6570									CL									x			
6580									CL									x			most grains non-reactive
6590									CL									x			tiny calcite vein running through a shale grian
6600									CL									x			
6610									CL									x			
6620									CL									x			
6630									CL									x			no reaction still, little to no caving material
6640									CL									x			few split calcite/shale grains- evidence of calcite vein
6650									CL									x			
6660									CL									x			
6670									CL									x			
6680									CL									x			evidence of calcite vein adhered to shale, few vitreous/carbonaceous looking grains
6690									CL									x			
6700									CL									x			
6710									CL									x			
6720									CL									x			very unifom, little to no caving material
6730									CL									x			
6740									CL									x			
6750									CL									x			
6760									CL									x			more muscovite and quartz caving material
6770									CL									x			
6780									CL									x			some altered muscovite with hematite staining, some quartz crystals
6790									CL									x			
6800									CL									x			
6810									CL									x			
6820									CL									x			
6830									CL									x			
6840									CL									x			mix of reaction with acid and no reaction. Lots of muscovite caving material.
6850									CL									x			
6860									CL								x				darker grey
6870									CL								x				
6880									CL									x			
6890									CL									x			some carbonaceous looking material
6900									CL									x			
6910									CL									x			no reaction, maybe visible thin beds here,
6920									CL									x			
6930									CL									x			some muscovite caving material, generally no reaction with HCl-some very slow reaction occuring, maybe presence of dolomite
6940									CL									x			
6950									CL								x				calcareous, little to no caving material
6960									CL								x				darker grey, most grains no reaction, test with lighter fluid- no reaction
6970									CL									x			reacts with HCl
6980									CL									x			
6990									CL									x			calcite vein? reacts with acid. A calcite crystal is adhered to a shale grain
7000									CL									x			
7010									CL									x			no reaction, no HC shows when tested with lighter fluid
7020									CL									x			no reaction with HCl
7030									CL									x			
7040									CL									x			no reaction with HCl.
7050									CL									x			
7060									CL									x			Most grains have no fizz
7070									CL									x			
7080									CL									x			slightly calcareous- less fizzing than before
7090									CL								x				
7100									CL								x				darker grey
7110									CL									x			likely siliceous
7120									CL									x			
7130									CL									x			some limestone/light colored caving material. All the shale is non-calcareous
7140									CL									x			
7150									CL									x			breaks in plates, generally not fizzing very much- most grains not calcareous
7160									CL									x			
7170									CL									x			getting slightly darker grey in color, reacts well with acid
7180									CL									x			
7190									CL									x			
7200									CL									x			these cuttings are uniform in color. Still calcareous, but fizzes much less rapidly. Size of cuttings: 1-5 mm
7210									CL									x			
7220									CL									x			
7230									CL									x			nonuniform mix of calcareous shale and limestone grains
7240									CL									x			
7250									CL										x		
7260									CL										x		
7270									CL										x		
7280									CL										x		
7290									CL										x		light grey, very reactive with acid.
7300									CL									x			darker grey, increase in clay content?
7310									CL										x		
7320									CL										x		near 100 feet below the base of caney: Sycamore Limestone- fizzes rapidly, light grey to grey

Appendix B4: Drill-cuttings description sheet for Well 4. Lithology, grain size, chip color, and a basic descriptions are noted.

Cuttings Description Sheet 7/09/2021

Well Name: John Traina #1

API: 35013000130000

Caney Interval: 5260-5440 ft

Depth (ft)	Lithology								Grain Sizes							Color					Description
	Clay Rich Mudstone	Calcareous Mudstone	Dolomitic Mudstone?	Interbedded	Siliceous Mudstone	Silty Mudstone	Limestone	Sandstone	CL	Silt	VF	F	M	C	VC	Black	Dark grey	Grey	Light grey	Beige	
5240									CL								x				
5245									CL								x				
5250									CL								x				some vitreous black grains present
5255									CL								x				
5260									CL								x				
5265									CL								x				
5270									CL								x				
5275									CL								x				
5280									CL								x				vitreous black grains
5285									CL								x				vitreous black grains
5290									CL								x				
5295									CL								x				
5300									CL								x				some calcite veins within the shale grains are present
5305									CL								x				
5310									CL								x				most grains in this section did not react with acid, however a few grains still fizzed slowly
5315									CL								x				
5320									CL								x				
5325									CL								x				
5330									CL								x				
5335									CL								x				
5340									CL								x				overall the cuttings packets are starting to look like a mixture of dark grey grains and slightly lighter grey grains. The lighter grains are less indurated and may be more clay rich. The darker grains are well indurated and difficult to break.
5345									CL								x				some dark red tinted grains appearing; possible hematite staining
5350									CL								x				
5355									CL								x				
5360									CL								x				frequent grains of white caving material
5365									CL								x				
5370									CL								x				
5375									CL								x				
5380									CL								x				still a mixed calcareous/siliceous mudstone.
5385									CL								x				
5390									CL									x			
5395									CL									x			
5400									CL									x			
5405									CL									x			chips of a calcite vein are found here. Otherwise the lithology remains partially light grain and darker, less calcareous grains.
5410									CL									x			
5415									CL									x			
5420									CL									x			
5425									CL									x			
5430									CL									x			some beige looking, possibly silty grains that fizz with HCl
5435									CL									x			
5440									CL									x			
5445									CL									x			
5450									CL									x			
5455									CL									x			
5460									CL									x			
5465									CL									x			an equal parts mixture of lighter grey and darker grey grains. The lighter grains tend to fizz more rapidly. Some of the darker grains still have a slow fizz. Some of the lighter colored grains appear beige
5470									CL												

Appendix B5: Drill-cuttings description sheet for Well 5. Lithology, grain size, chip color, and a basic descriptions are noted.

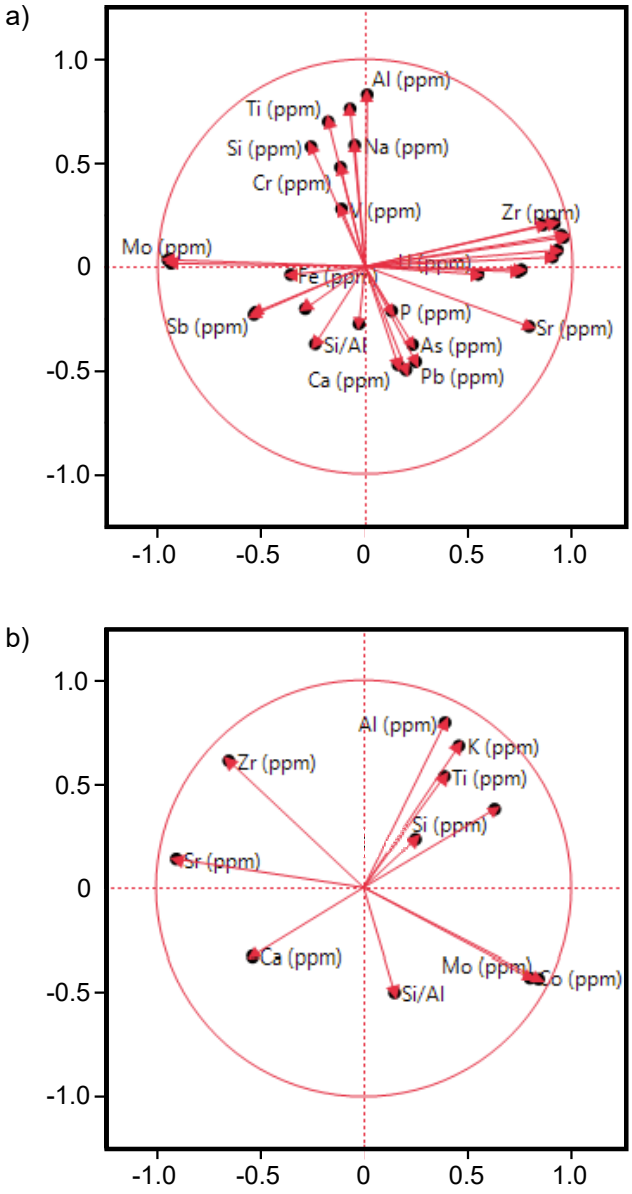

Appendix C: Developed in 1901 by Karl Pearson (Pearson, 1901), PCA is a dimension-reduction tool that allows for analysis of individual variables within a large dataset. This method is helpful for determining the weight of individuality each element has with respect to another element. Shown above are Principal component analysis (PCA) biplots of major and minor elements. Vectors near one another represent variables with positive correlations, while vectors that diverge with a large angle between them represent variables that negatively correlation. Magnitude of vectors depicts the weight of contribution a particular variable has. a) displays a PCA biplot for all 29 major and minor elements prior to ind element selection. b) displays a PCA biplot for 9 index elements and 1 ratio, selected based on strong negative and positive correlative relationships.

	Na	Al	Si	P	S	K	Ca	Ba	Ti	V	Cr	Mn	Fe	Co	Ni	Cu	Zn	As	Pb	Th	Rb	U	Sr	Y	Zr	Nb	Mo	Sn	Sb
Na	1	0.47	0.56	-0.1	-0	0.41	-0.3	-0.1	0.21	0.07	0.59	0.15	-0.2	0.11	0.02	-0	0.01	-0.1	-0.2	-0	-0	0.03	-0.3	-0.1	-0	-0	0.13	-0	-0.1
Al	0.47	1	0.51	-0.2	-0.2	0.66	-0.4	-0.2	0.47	0.15	0.49	-0.1	0.03	0.05	0.08	-0.1	-0.1	-0.2	-0.2	0.17	0.15	-0.1	-0.3	0	0.11	0.2	0.05	-0.2	-0.1
Si	0.56	0.51	1	-0.2	0.26	0.51	-0.7	-0.1	0.18	0.25	0.68	0.23	-0.1	0.1	0.01	0.09	0.06	-0.1	-0.1	-0.1	-0.1	0	-0.5	-0.2	-0.1	-0.1	0.16	0.05	0.17
P	-0.1	-0.2	-0.2	1	-0.2	-0.1	0.2	0.08	-0.1	-0.1	-0.1	-0	-0.1	-0	0.03	-0	0.01	-0	-0.1	0.03	0.03	0.07	0.12	0	0.06	0.03	-0	-0	-0.1
S	-0	-0.2	0.26	-0.2	1	0.02	-0.2	0.24	-0.3	-0.1	0.29	0.25	-0	0.25	-0.2	-0.1	-0	0.04	0.19	-0.3	-0.3	-0.1	-0.2	-0.3	-0.3	-0.4	0.29	0.4	0.39
K	0.41	0.66	0.51	-0.1	0.02	1	-0.3	-0.3	0.45	0.02	0.45	-0.2	-0.1	0.07	0.09	0.09	0.09	-0.1	-0.2	0.15	0.14	-0.1	-0.2	0.05	0.14	0.11	0.08	-0	-0.1
Ca	-0.3	-0.4	-0.7	0.2	-0.2	-0.3	1	0.06	-0.1	-0.2	-0.5	-0	-0.2	-0.2	0.05	-0.1	-0.1	0.08	0.04	0.06	0.08	0.12	0.69	0.21	0.11	0.11	-0.3	-0.1	-0.2
Ba	-0.1	-0.2	-0.1	0.08	0.24	-0.3	0.06	1	-0.9	-0.5	-0	0.56	-0.2	-0.1	0.07	0.22	0.22	0.16	0.24	0.03	0.06	0.15	0.17	-0	-0.1	-0.1	-0.1	0.11	0.17
Ti	0.21	0.47	0.18	-0.1	-0.3	0.45	-0.1	-0.9	1	0.52	0.15	-0.5	0.22	0.08	-0	-0.3	-0.3	-0.2	-0.2	0.05	-0	-0.2	-0.2	0.08	0.25	0.2	0.05	-0.2	-0.2
V	0.07	0.15	0.25	-0.1	-0.1	0.02	-0.2	-0.5	0.52	1	0.22	-0.1	0.19	0.07	-0.1	-0.2	-0.2	-0.1	-0.1	-0.1	-0.1	0	-0.2	-0.1	-0.1	-0	0.09	0.1	0.08
Cr	0.59	0.49	0.68	-0.1	0.29	0.45	-0.5	-0	0.15	0.22	1	-0	-0.1	0.28	-0.1	-0	-0	-0.1	-0.2	-0.2	-0.2	-0	-0.5	-0.3	-0.4	-0.3	0.36	0.19	0.22
Mn	0.15	-0.1	0.23	-0	0.25	-0.2	-0	0.56	-0.5	-0.1	-0	1	0	-0.1	0	0.07	0.09	0.13	0.22	-0	-0	0.11	-0	0.01	-0	-0.1	-0.1	0.13	0.22
Fe	-0.2	0.03	-0.1	-0.1	-0	-0.1	-0.2	-0.2	0.22	0.19	-0.1	0	1	0.44	-0.4	-0.3	-0.3	-0	0.17	-0.2	-0.3	-0.4	-0.4	-0.2	-0.1	-0.2	0.32	0.23	0.16
Co	0.11	0.05	0.1	-0	0.25	0.07	-0.2	-0.1	0.08	0.07	0.28	-0.1	0.44	1	-0.8	-0.6	-0.6	-0.2	-0.2	-0.9	-0.9	-0.4	-0.7	-0.8	-0.8	-0.8	0.95	0.51	0.43
Ni	0.02	0.08	0.01	0.03	-0.2	0.09	0.05	0.07	-0	-0.1	-0.1	0	-0.4	-0.8	1	0.71	0.7	0.24	0.27	0.82	0.83	0.44	0.52	0.73	0.66	0.72	-0.8	-0.3	-0.4
Cu	-0	-0.1	0.09	-0	-0.1	0.09	-0.1	0.22	-0.3	-0.2	-0	0.07	-0.3	-0.6	0.71	1	0.94	0.14	0.13	0.67	0.7	0.48	0.37	0.54	0.47	0.55	-0.6	-0.2	-0.2
Zn	0.01	-0.1	0.06	0.01	-0	0.09	-0.1	0.22	-0.3	-0.2	-0	0.09	-0.3	-0.6	0.7	0.94	1	0.14	0.13	0.62	0.66	0.47	0.37	0.51	0.42	0.49	-0.5	-0.1	-0.1
As	-0.1	-0.2	-0.1	-0	0.04	-0.1	0.08	0.16	-0.2	-0.1	-0.1	0.13	-0	-0.2	0.24	0.14	0.14	1	0.84	0.16	0.11	0.03	0.2	0.19	0.07	0.11	-0.2	0.03	-0
Pb	-0.2	-0.2	-0.1	-0.1	0.19	-0.2	0.04	0.24	-0.2	-0.1	-0.2	0.22	0.17	-0.2	0.27	0.13	0.13	0.84	1	0.2	0.14	0.03	0.16	0.22	0.13	0.12	-0.2	0.18	0.11
Th	-0	0.17	-0.1	0.03	-0.3	0.15	0.06	0.03	0.05	-0.1	-0.2	-0	-0.2	-0.9	0.82	0.67	0.62	0.16	0.2	1	0.99	0.41	0.59	0.84	0.83	0.92	-0.9	-0.4	-0.4
Rb	-0	0.15	-0.1	0.03	-0.3	0.14	0.08	0.06	-0	-0.1	-0.2	-0	-0.3	-0.9	0.83	0.7	0.66	0.11	0.14	0.99	1	0.45	0.61	0.83	0.81	0.89	-0.9	-0.4	-0.4
U	0.03	-0.1	0	0.07	-0.1	-0.1	0.12	0.15	-0.2	0	-0	0.11	-0.4	-0.4	0.44	0.48	0.47	0.03	0.03	0.41	0.45	1	0.4	0.25	0.25	0.42	-0.4	-0.2	-0.2
Sr	-0.3	-0.3	-0.5	0.12	-0.2	-0.2	0.69	0.17	-0.2	-0.2	-0.5	-0	-0.4	-0.7	0.52	0.37	0.37	0.2	0.16	0.59	0.61	0.4	1	0.64	0.51	0.57	-0.7	-0.3	-0.4
Y	-0.1	0	-0.2	0	-0.3	0.05	0.21	-0	0.08	-0.1	-0.3	0.01	-0.2	-0.8	0.73	0.54	0.51	0.19	0.22	0.84	0.83	0.25	0.64	1	0.83	0.87	-0.8	-0.4	-0.5
Zr	-0	0.11	-0.1	0.06	-0.3	0.14	0.11	-0.1	0.25	-0.1	-0.4	-0	-0.1	-0.8	0.66	0.47	0.42	0.07	0.13	0.83	0.81	0.25	0.51	0.83	1	0.86	-0.8	-0.5	-0.5
Nb	-0	0.2	-0.1	0.03	-0.4	0.11	0.11	-0.1	0.2	-0	-0.3	-0.1	-0.2	-0.8	0.72	0.55	0.49	0.11	0.12	0.92	0.89	0.42	0.57	0.87	0.86	1	-0.8	-0.5	-0.6
Mo	0.13	0.05	0.16	-0	0.29	0.08	-0.3	-0.1	0.05	0.09	0.36	-0.1	0.32	0.95	-0.8	-0.6	-0.5	-0.2	-0.2	-0.9	-0.9	-0.4	-0.7	-0.8	-0.8	-0.8	1	0.59	0.52
Sn	-0	-0.2	0.05	-0	0.4	-0	-0.1	0.11	-0.2	0.1	0.19	0.13	0.23	0.51	-0.3	-0.2	-0.1	0.03	0.18	-0.4	-0.4	-0.2	-0.3	-0.4	-0.5	-0.5	0.59	1	0.83
Sb	-0.1	-0.1	0.17	-0.1	0.39	-0.1	-0.2	0.17	-0.2	0.08	0.22	0.22	0.16	0.43	-0.4	-0.2	-0.1	-0	0.11	-0.4	-0.4	-0.2	-0.4	-0.5	-0.5	-0.6	0.52	0.83	1

Appendix D: Correlation table displaying the numerical elemental relationships in a color coded format. All 29 major and trace elements are cross plotted. Red and orange colors represent elements that negatively correlate, and yellow and green colors represent elements that positively correlate.

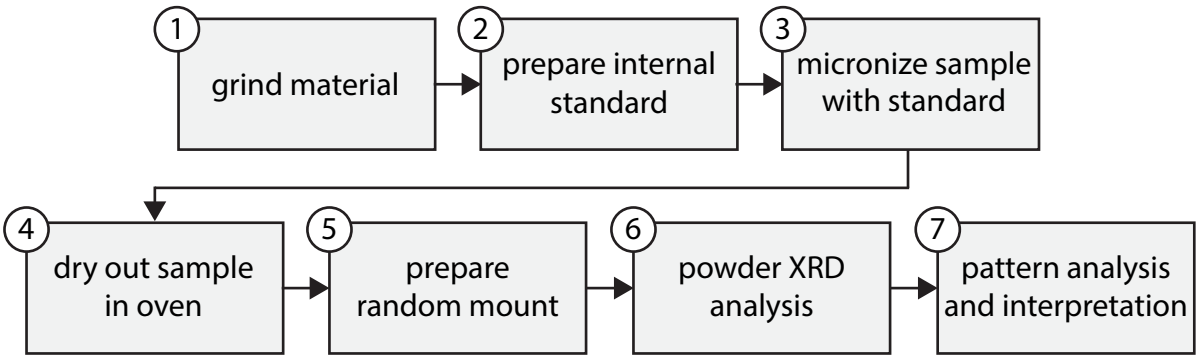

Appendix E: General workflow of powder X-ray Diffraction (XRD) methodology. (Modified from Poppe et al., 2005)

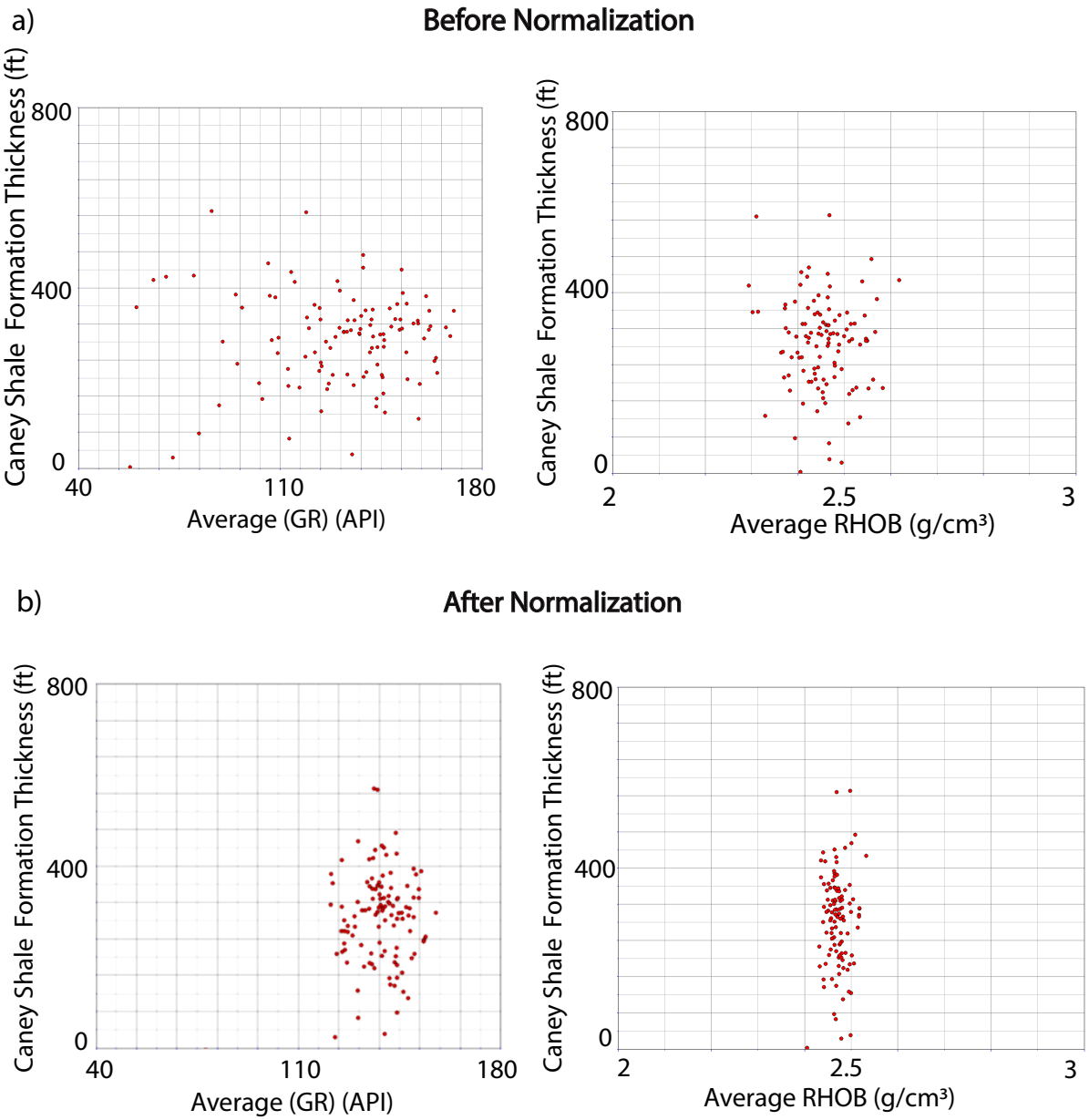

Appendix F: Normalization of well-logs is critical when working with log data from many vendors and vintages because it removes inaccuracy within the log curve data (Shier, 2004). Potential well-log errors include inaccurate tool measurements from ineffective calibration, drift in tool response, improperly scaled curves, improperly recorded borehole environments, etc. (Shier, 2004). Displayed are graphs of log data versus the Caney shale formation thickness. Each point represents one well from the study area. a) shows the GR log data versus formation thickness (left) and the RHOB log data versus formation thickness (right) prior to normalization. b) shows the resultant data spread after normalization.

Appendix G: X-ray diffraction (XRD) patterns and mineral percentage pies.

To prepare samples for analysis, the clay size fraction (< 2μm) separation began with grounding 1 gram of drill-cuttings chips via a mortar and pestle . Crushed material was transfered to solution and mixed with an internal standard used for calibration. Each sample was placed in a micronizer for 5 minutes to further disaggregate the sample. The suspended materials were placed directly into an oven for 3-4 hours. The dry samples were removed from the oven and were applied to a glass slide in a random orientation using a metal spatula.

Prior to conducting pattern interpretation, a 0.15 degree 2-theta shift was applied to each pattern. Mineralogies were interpreted based on standard d-spacing values (Poppe et al., 2005). XRD results were compared to Katende et al. (2021).

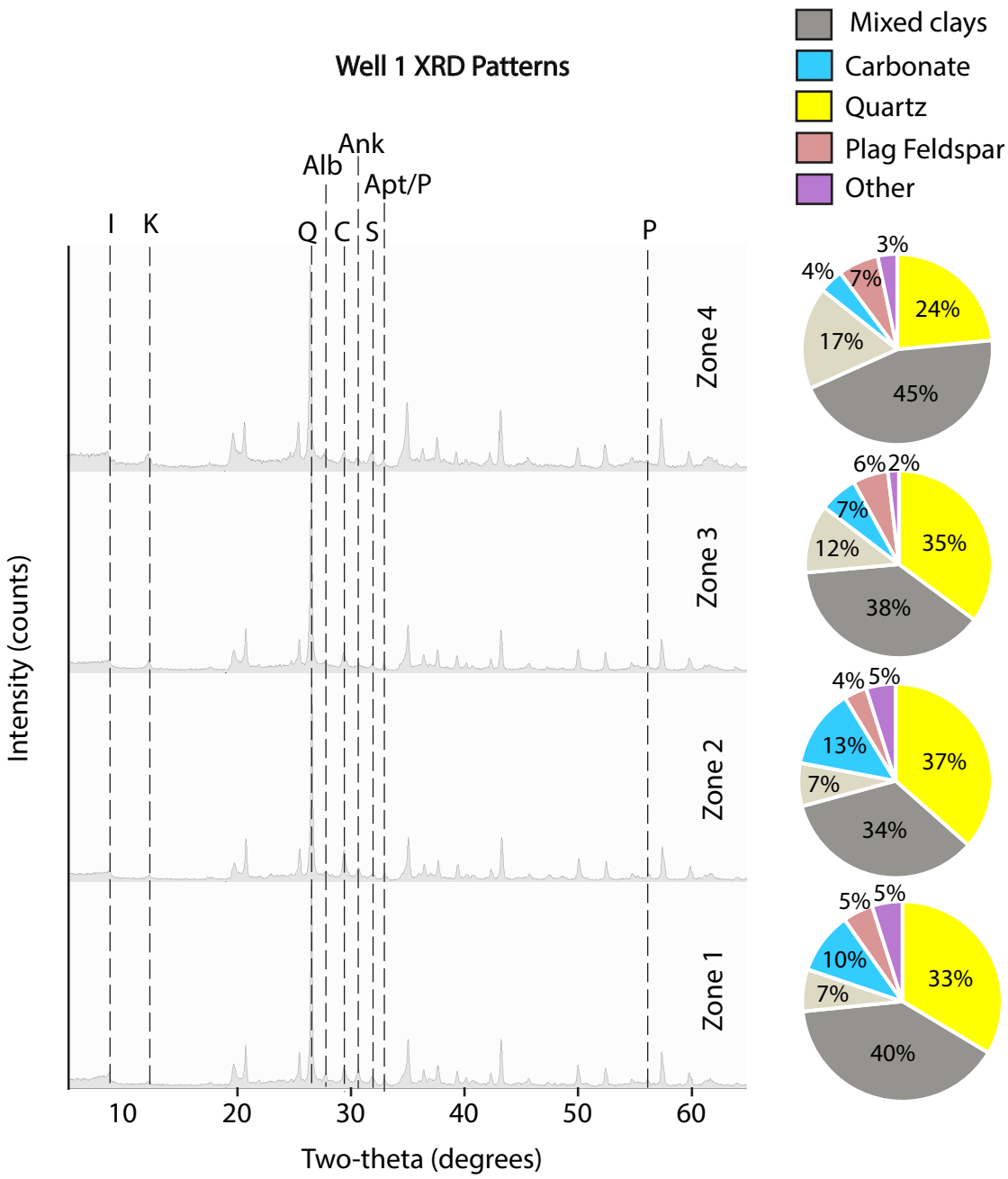

Appendix G1: Well 1 XRD patterns and resultant mineral percentage pies for zones 1-4 of the Caney Shale. Quartz is indicated by (Q), mixed clays account for both illite (I) and kaolinite (K), and carbonate accounts for both calcite (C) and ankerite (Ank). Plagioclase feldspar accounts mostly for albite (Alb), while the small faction of other minerals include apatite (Apt), siderite (S), and pyrite (P).

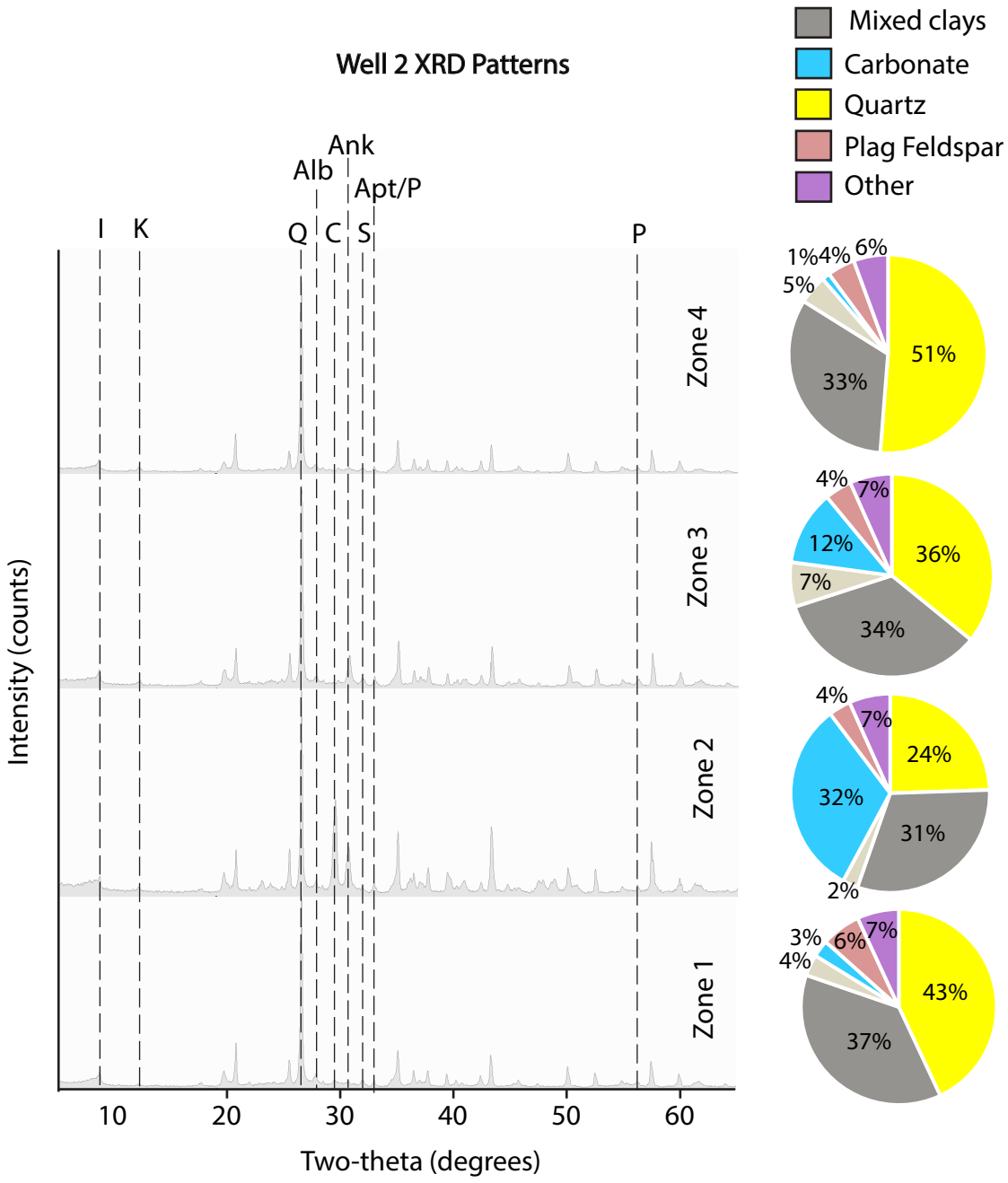

Appendix G2: Well 2 XRD patterns and resultant mineral percentage pies for zones 1-4 of the Caney Shale. Quartz is indicated by (Q), mixed clays account for both illite (I) and kaolinite (K), and carbonate accounts for both calcite (C) and ankerite (Ank). Plagioclase feldspar accounts mostly for albite (Alb), while the small faction of other minerals include apatite (Apt), siderite (S), and pyrite (P).

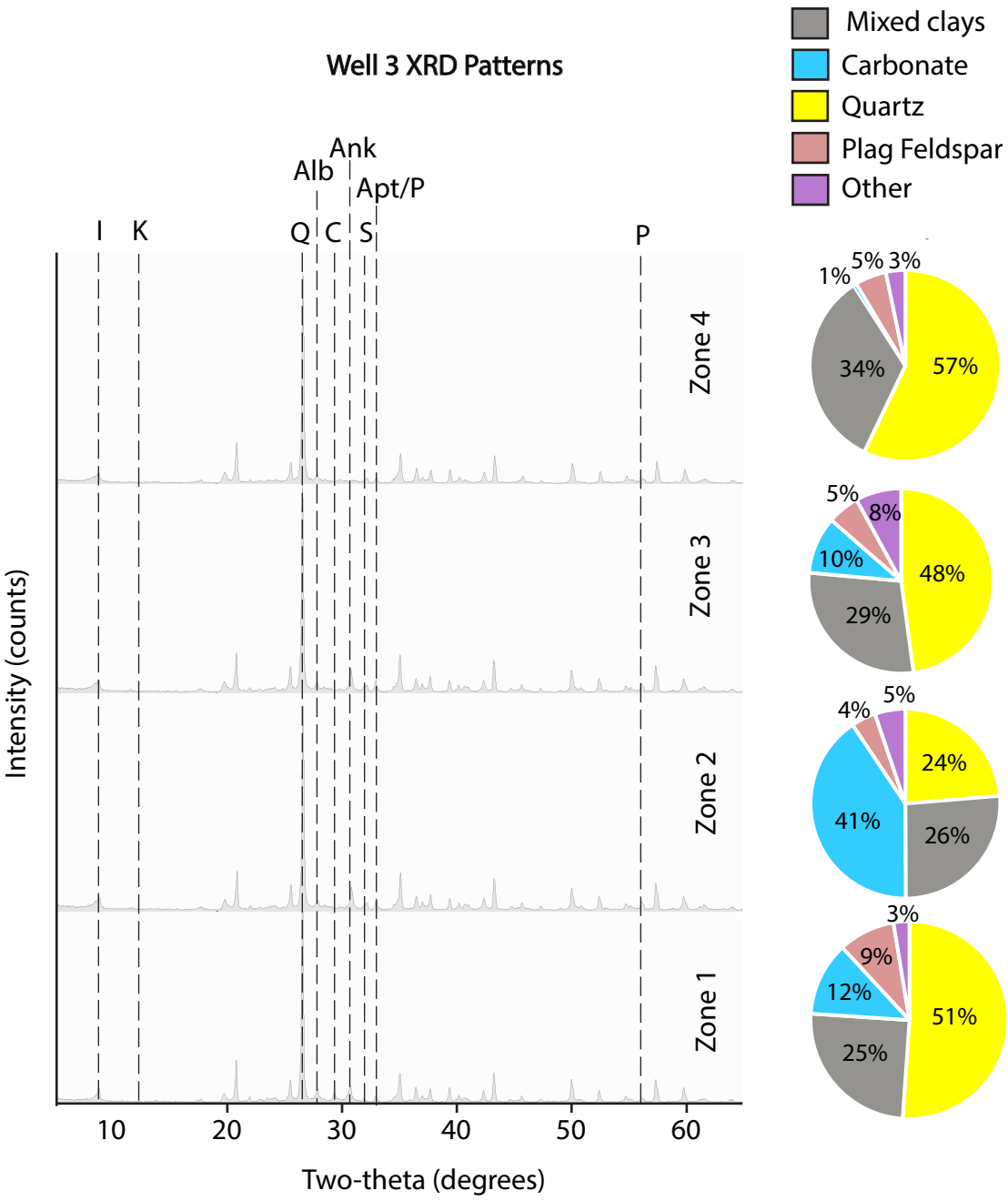

Appendix G3: Well 3 XRD patterns and resultant mineral percentage pies for zones 1-4 of the Caney Shale. Quartz is indicated by (Q), mixed clays account for both illite (I) and kaolinite (K), and carbonate accounts for both calcite (C) and ankerite (Ank). Plagioclase feldspar accounts mostly for albite (Alb), while the small faction of other minerals picture included apatite (Apt), siderite (S), and pyrite (P). Note that kaolinite (K) is absent from the XRD patterns.

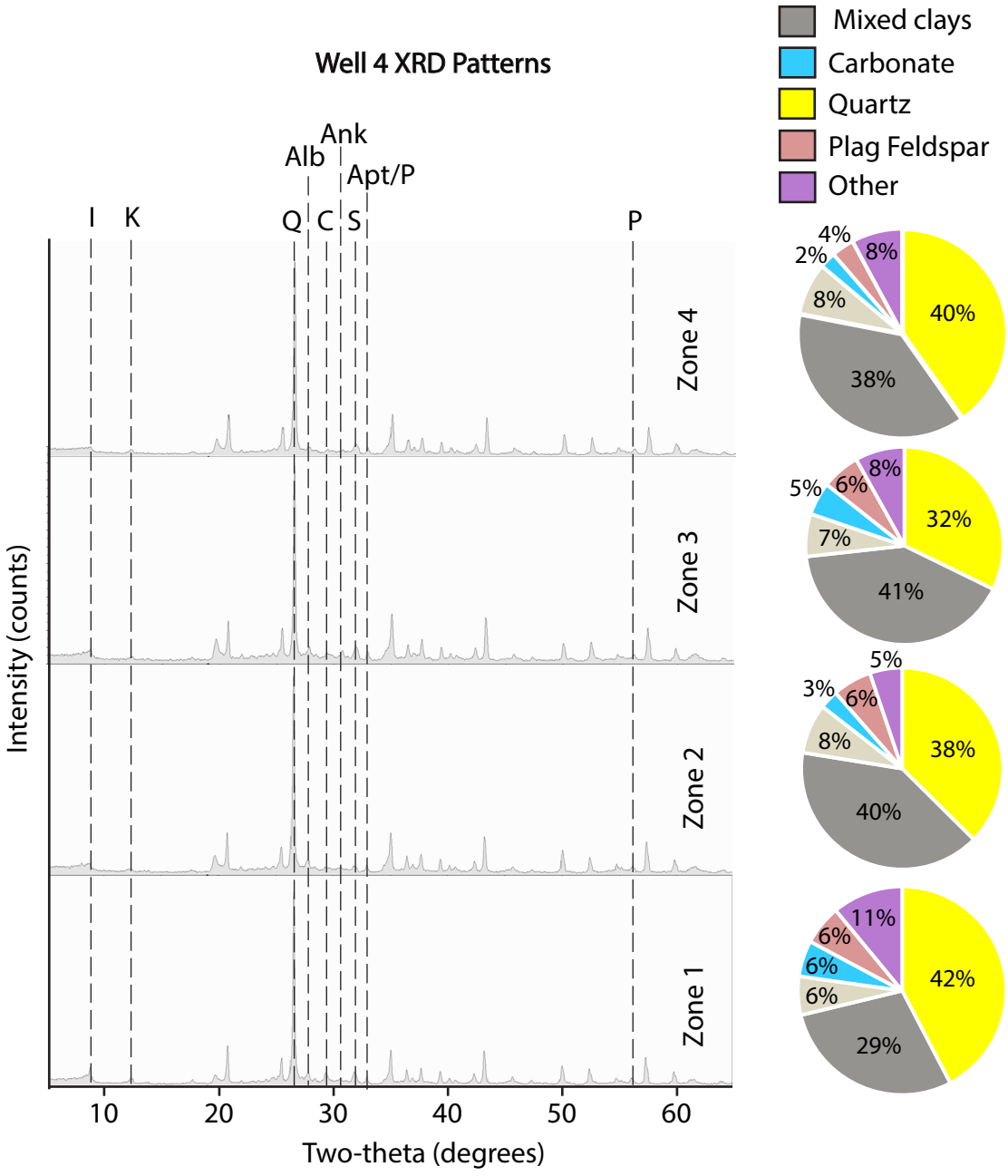

Appendix G4: Well 4 XRD patterns and resultant mineral percentage pies for zones 1-4 of the Caney Shale. Quartz is indicated by (Q), mixed clays account for both illite (I) and kaolinite (K), and carbonate accounts for both calcite (C) and ankerite (Ank). Plagioclase feldspar accounts mostly for albite (Alb), while the small faction of other minerals picture included apatite (Apt), siderite (S), and pyrite (P).

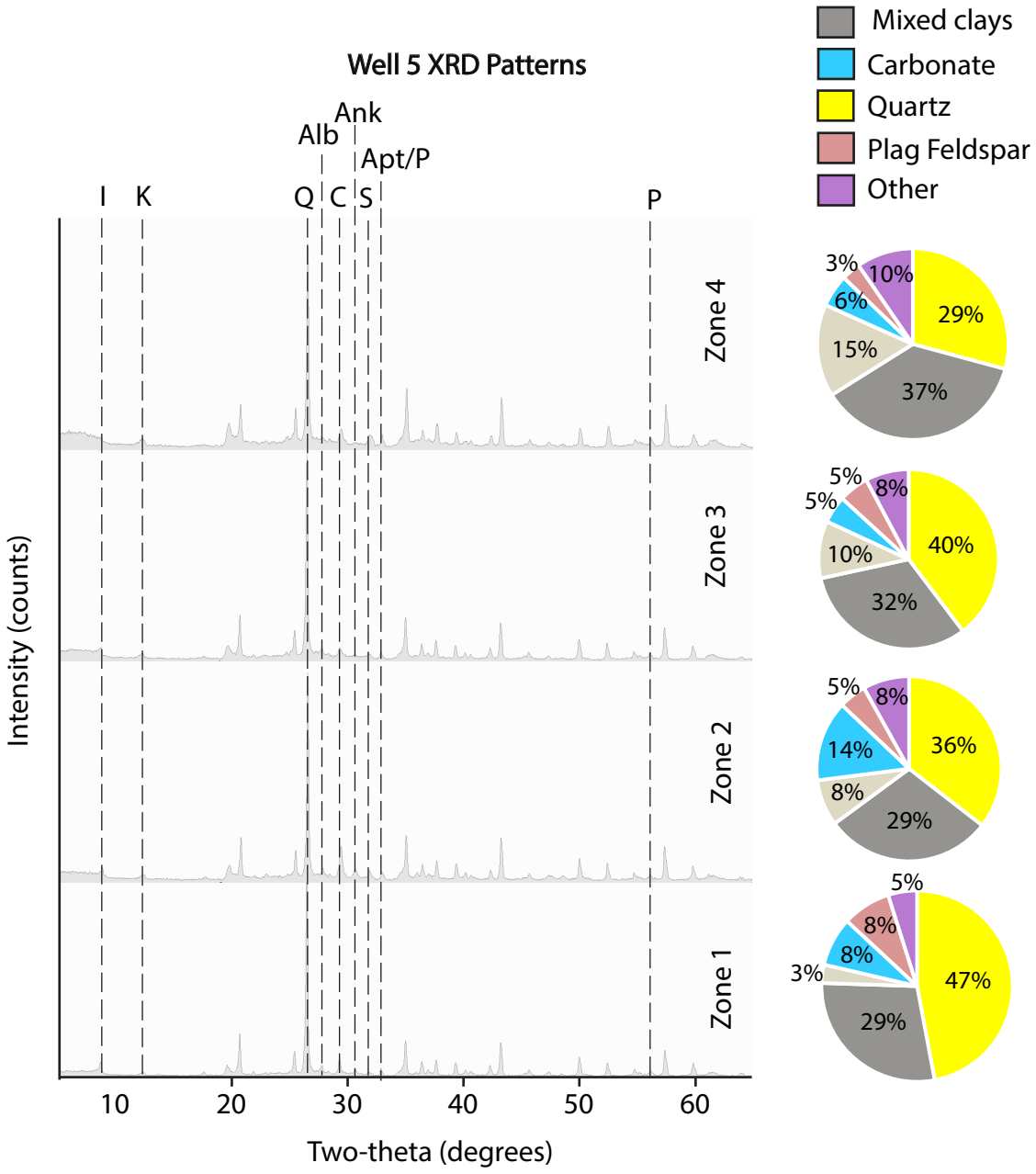

Appendix G5: Well 5 XRD patterns and resultant mineral percentage pies for zones 1-4 of the Caney Shale. Quartz is indicated by (Q), mixed clays account for both illite (I) and kaolinite (K), and carbonate accounts for both calcite (C) and ankerite (Ank). Plagioclase feldspar accounts mostly for albite (Alb), while the small faction of other minerals picture included apatite (Apt), siderite (S), and pyrite (P).

Appendix H: XRF elemental profiles for 9 index elements and 1 ratio. Major elements were analyzed for a period of 90 seconds at 15 kV accelerating voltage, and trace elements were analyzed for 60 seconds at 40 kV accelerating voltage. Unit correction from KeV to ppm was conducted using a mudrock standard conversion process developed by Rowe et al. (2012).

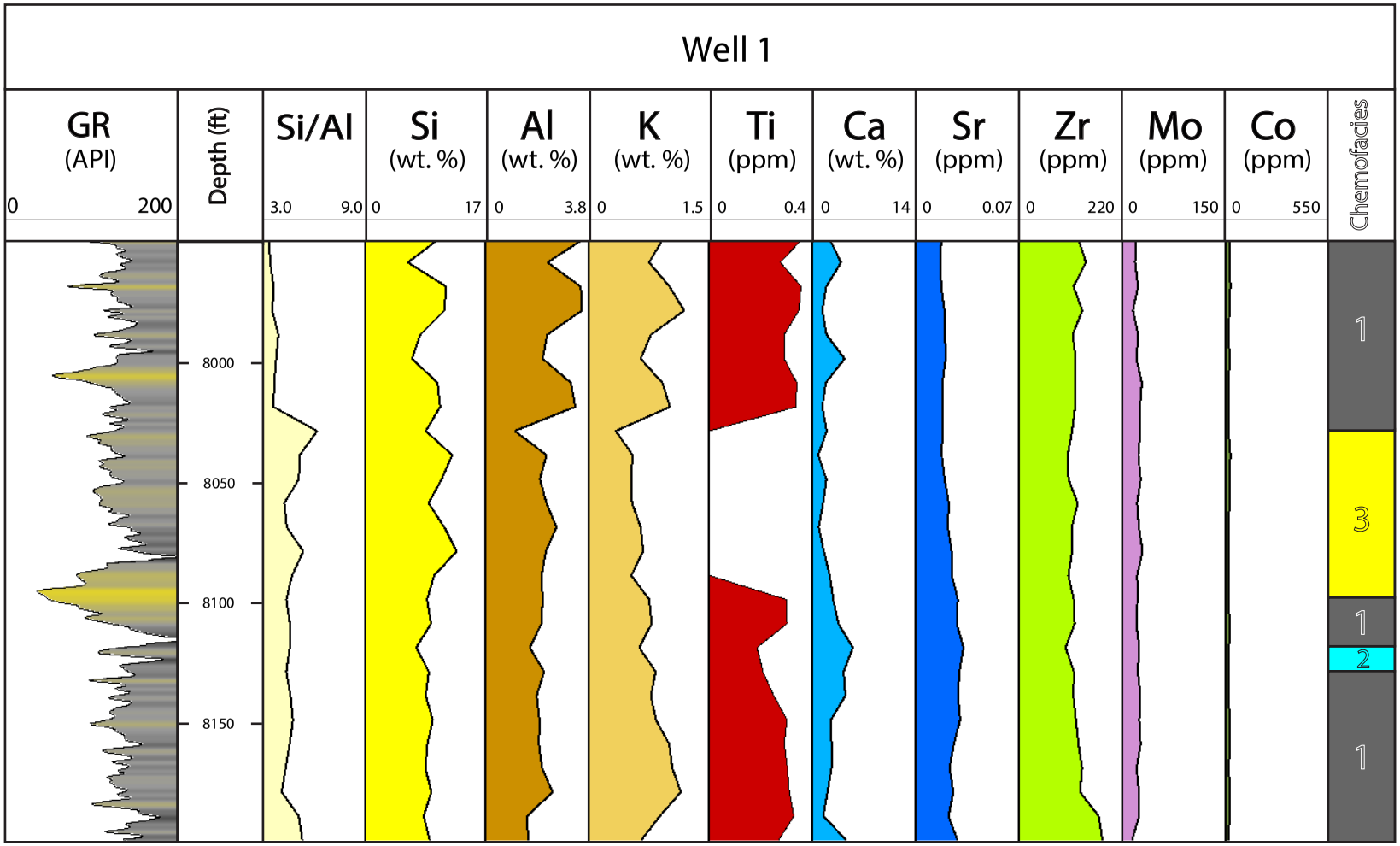

Appendix H1: Well 1 elemental profiles for 9 index elements and 1 ratio used to interpret chemofacies in the right most column. Well 1 is the only well in which chemofacies 4 is absent. Major elements are displayed in wt% and trace elements are displayed in ppm. Chemofacies 1 indicates a high detrital source, chemofacies 2 indicates a carbonate presence, chemofacies 3 indicates a moderate detrital source, and chemofacies 4 indicates ocean water conditions.

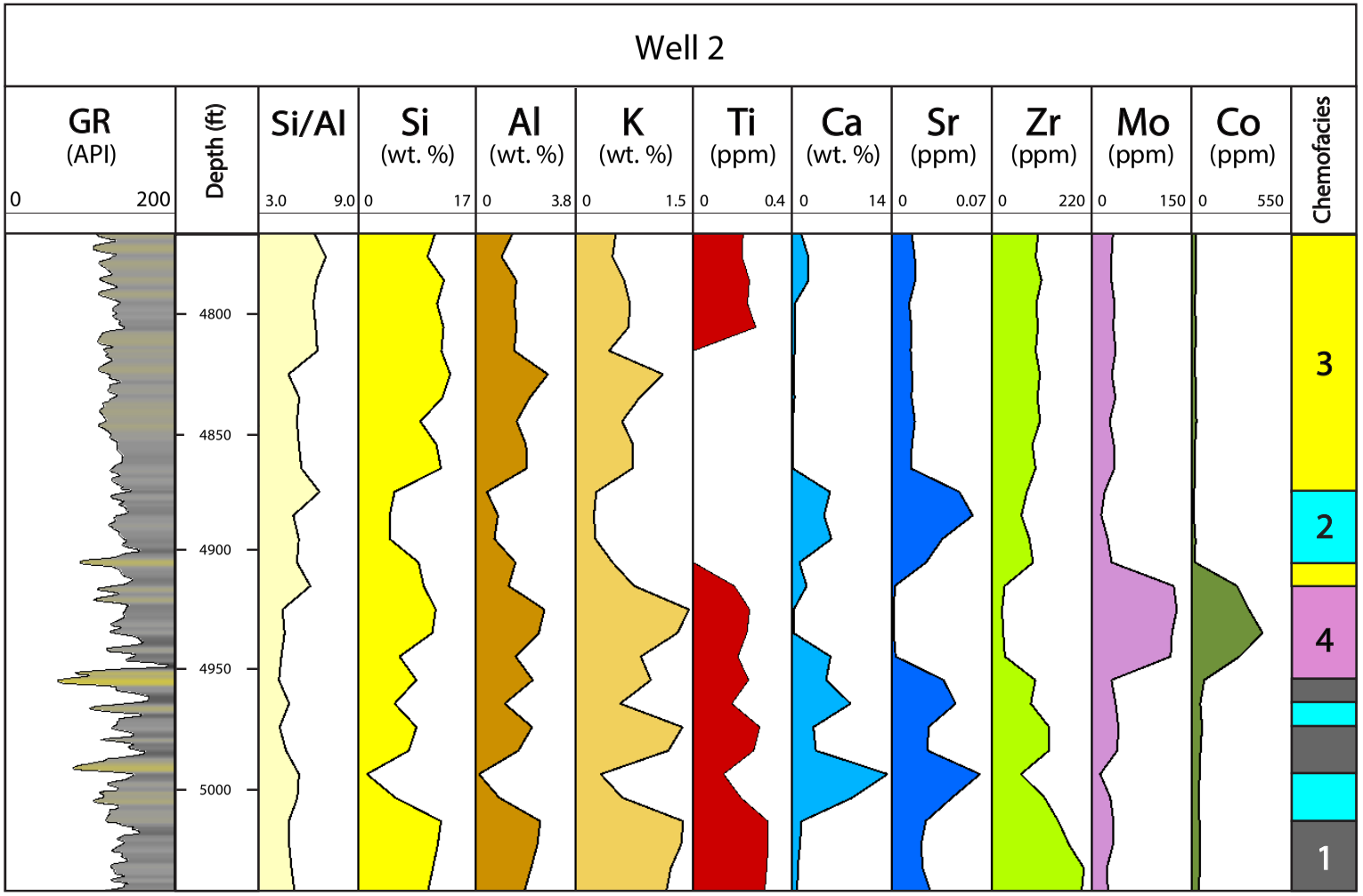

Appendix H2: Well 2 elemental profiles for 9 index elements and 1 ratio used to interpret chemofacies in the right most column. Major elements are displayed in wt% and trace elements are displayed in ppm. Chemofacies 1 indicates a high detrital source, chemofacies 2 indicates a carbonate presence, chemofacies 3 indicates a moderate detrital source, and chemofacies 4 indicates ocean water conditions.

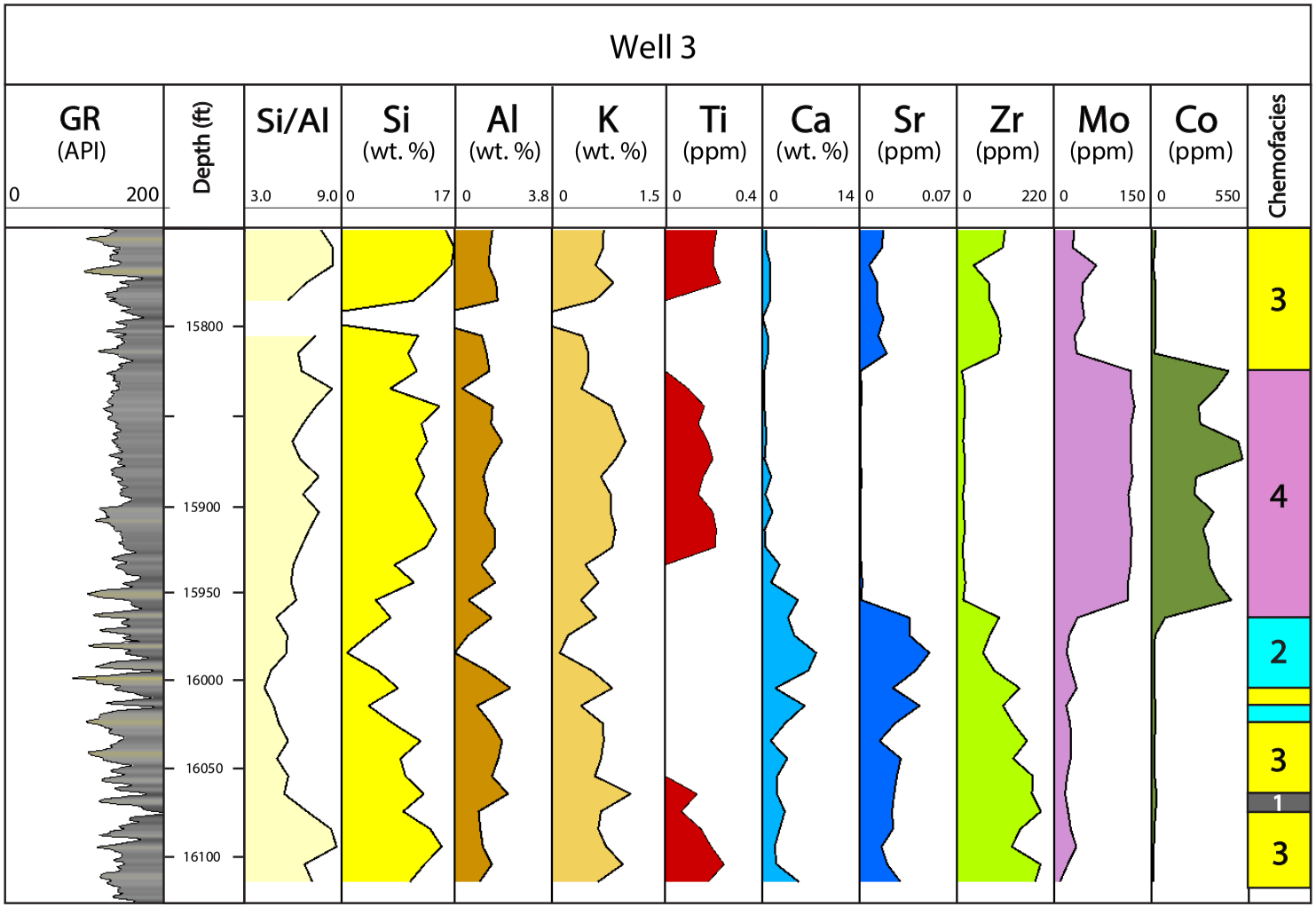

Appendix H3: Well 3 elemental profiles for 9 index elements and 1 ratio used to interpret chemofacies in the right most column. Major elements are displayed in wt% and trace elements are displayed in ppm. Chemofacies 1 indicates a high detrital source, chemofacies 2 indicates a carbonate presence, chemofacies 3 indicates a moderate detrital source, and chemofacies 4 indicates ocean water conditions.

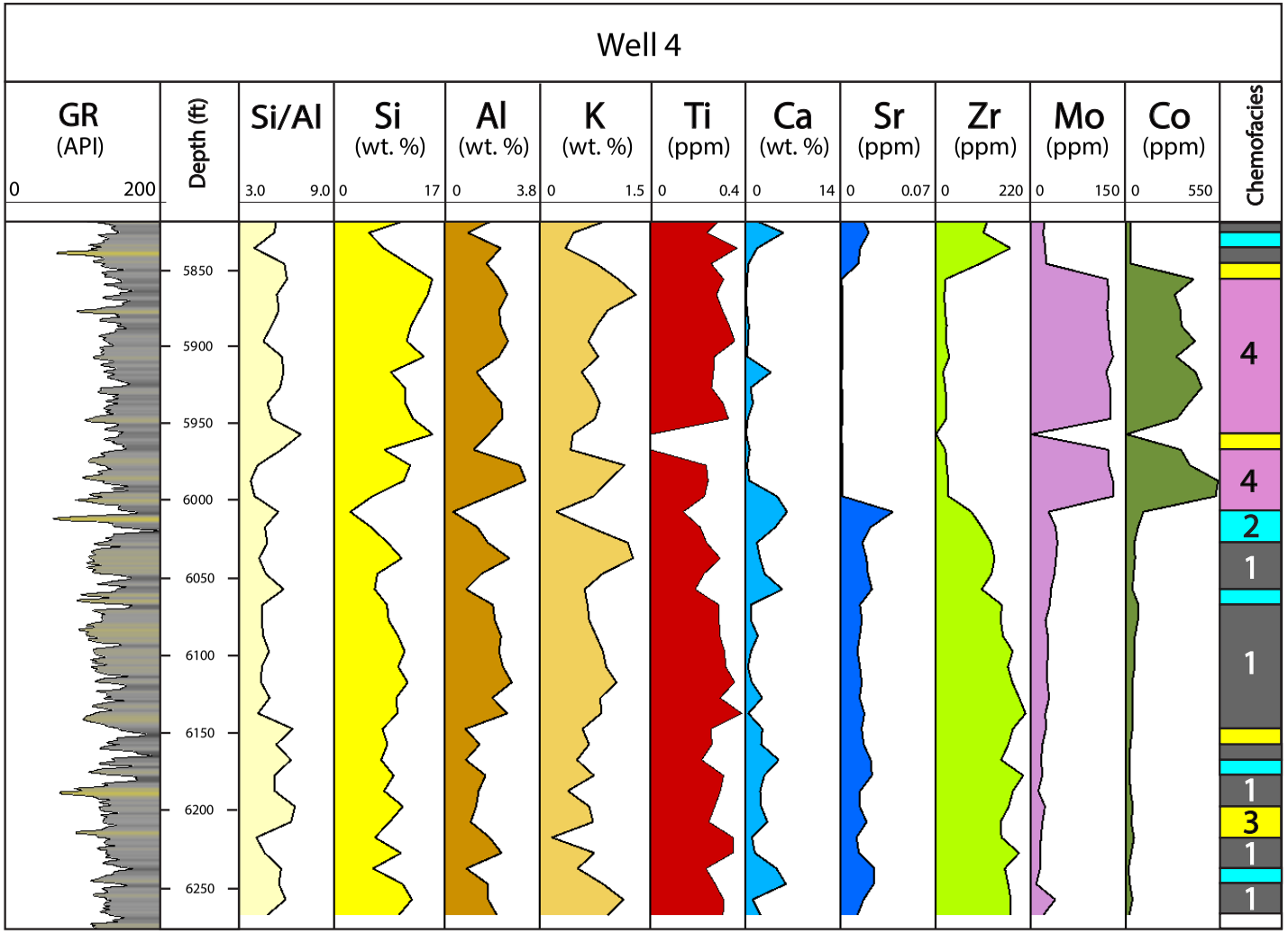

Appendix H4: Well 4 elemental profiles for 9 index elements and 1 ratio used to interpret chemofacies in the right most column. Major elements are displayed in wt% and trace elements are displayed in ppm. Chemofacies 1 indicates a high detrital source, chemofacies 2 indicates a carbonate presence, chemofacies 3 indicates a moderate detrital source, and chemofacies 4 indicates ocean water conditions.

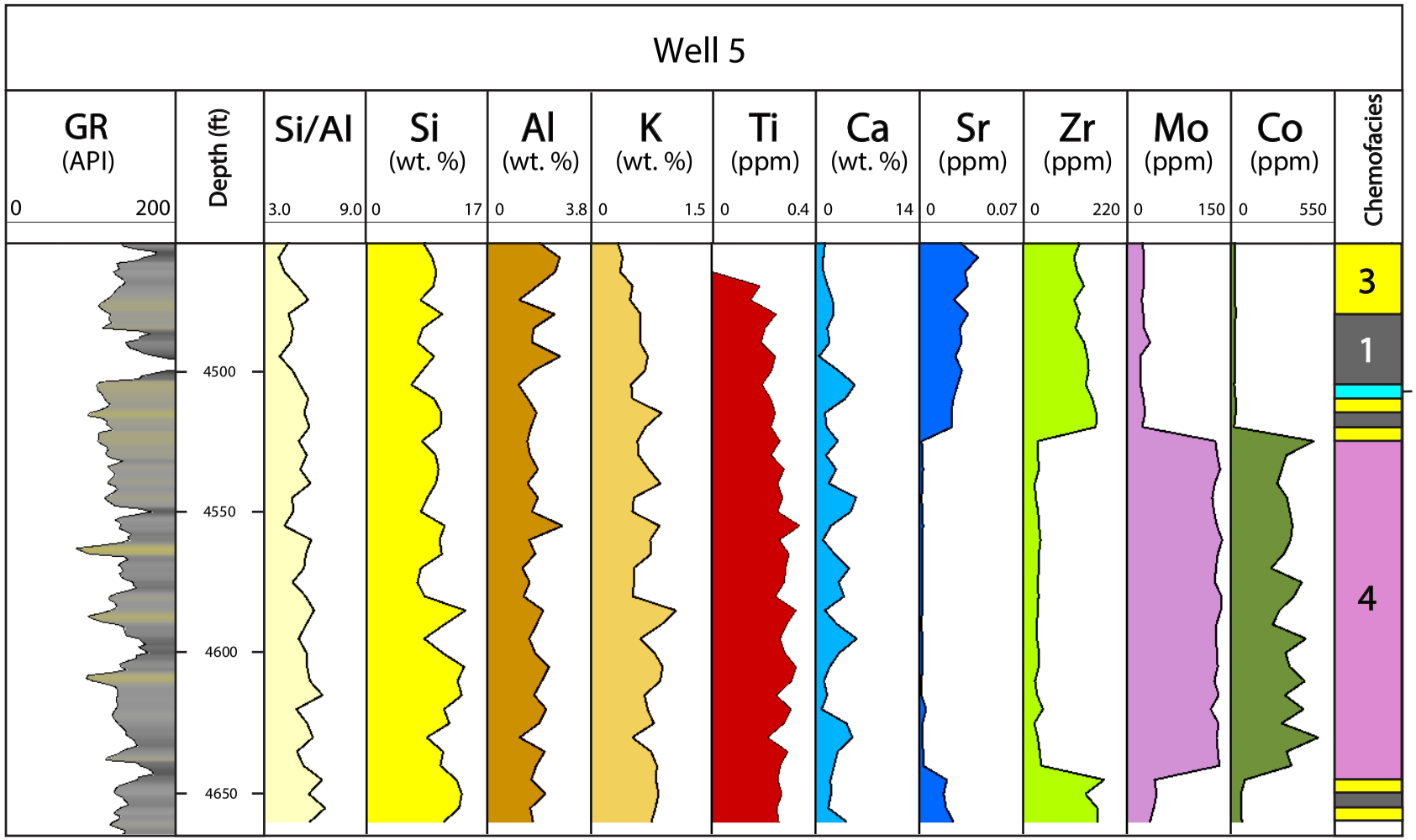

Appendix H5: Well 5 elemental profiles for 9 index elements and 1 ratio used to interpret chemofacies in the right most column. Major elements are displayed in wt% and trace elements are displayed in ppm. Chemofacies 1 indicates a high detrital source, chemofacies 2 indicates a carbonate presence, chemofacies 3 indicates a moderate detrital source, and chemofacies 4 indicates ocean water conditions.

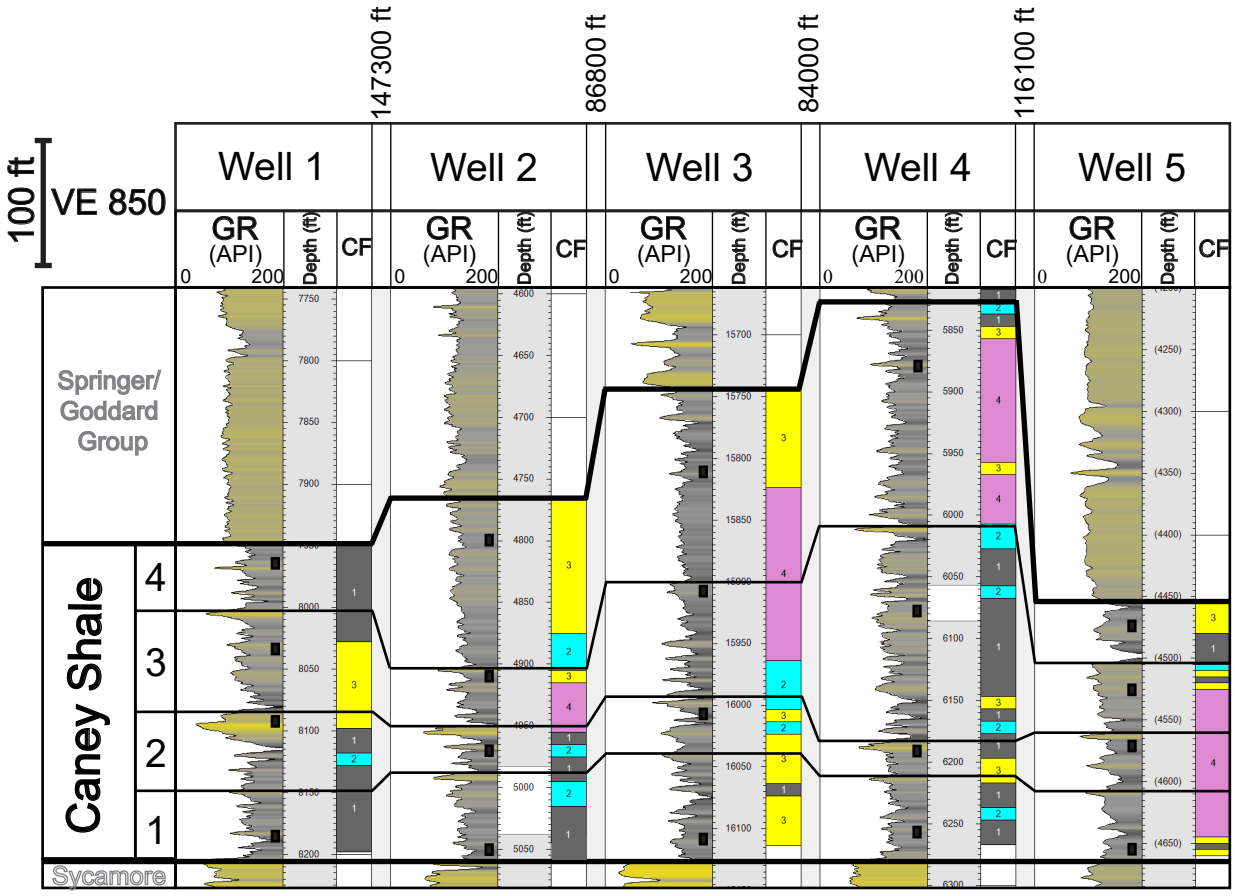

Appendix I: Locations of XRD sampling per zone per well are depicted by the black squares plotted on the GR log. Chemofacies are displayed to the right of each well to show the relationship between XRD sampling and chemofacies occurance.

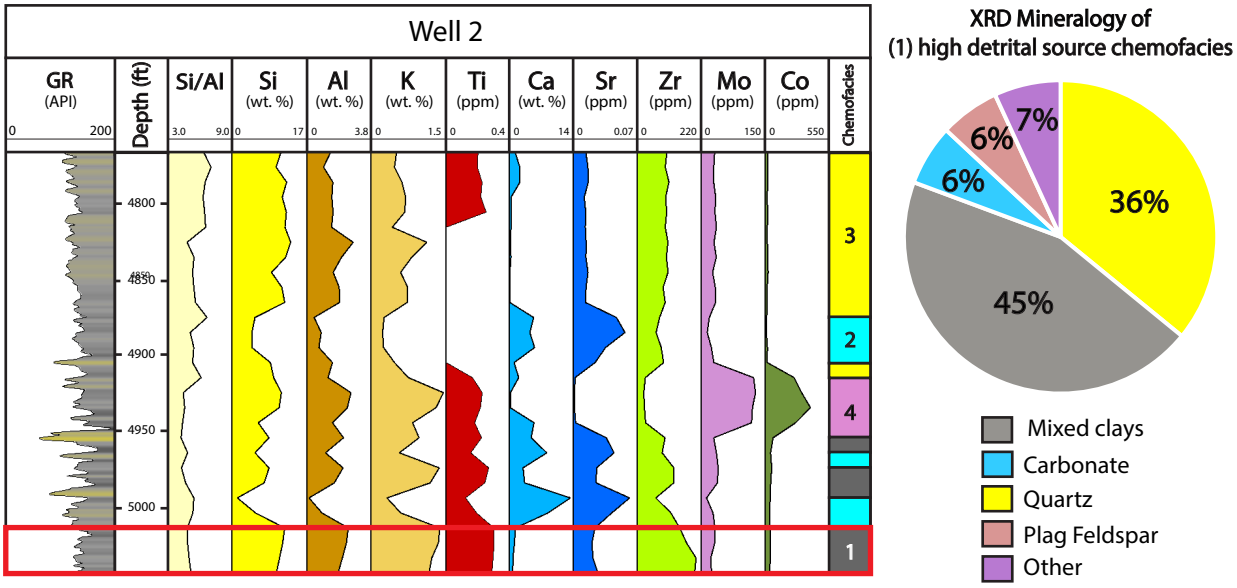

Appendix J1: Chemofacies 1 elemental curve patterns, stratigraphic distribution, and corresponding XRD mineralogy for Well 2.

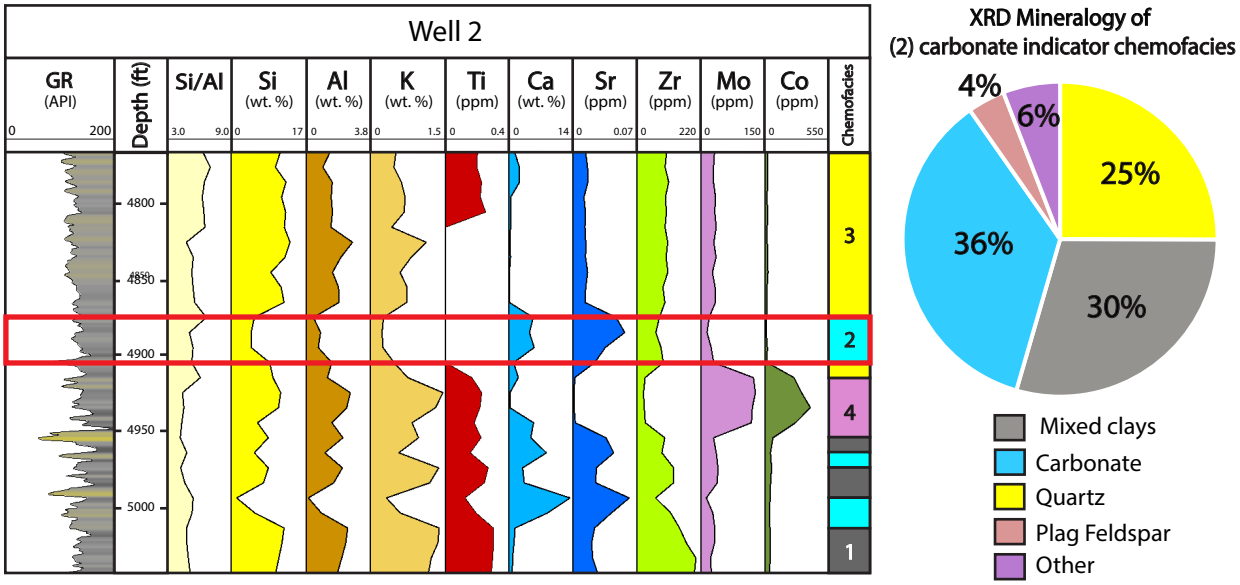

Appendix J2: Chemofacies 2 elemental curve patterns, stratigraphic distribution, and corresponding XRD mineralogy for Well 2.

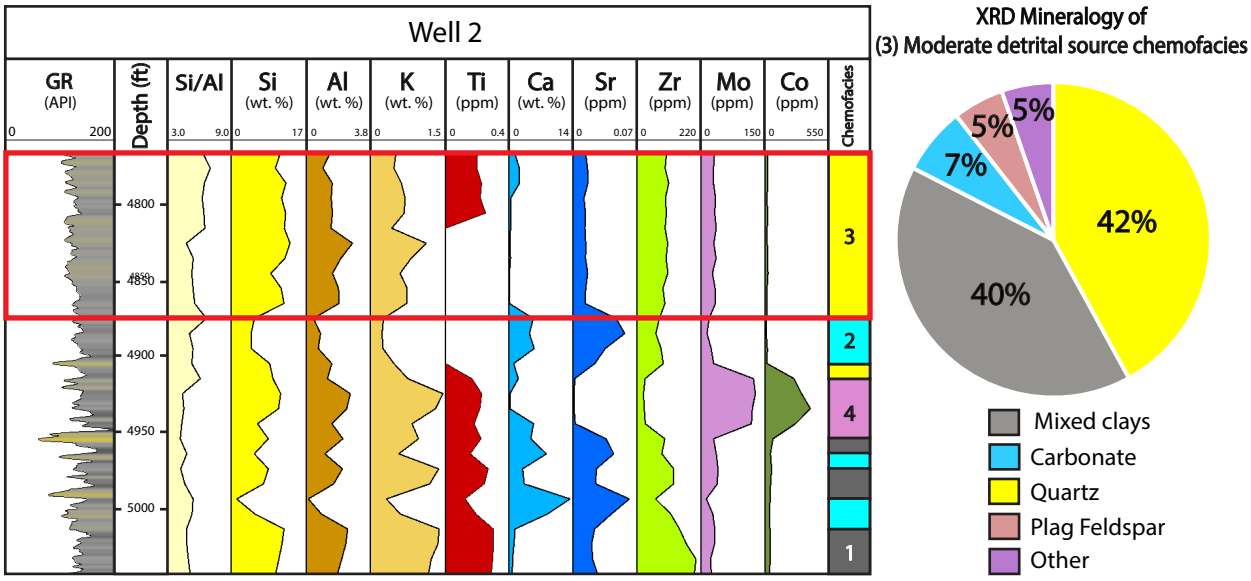

Appendix J3: Chemofacies 3 elemental curve patterns, stratigraphic distribution, and corresponding XRD mineralogy for Well 2.

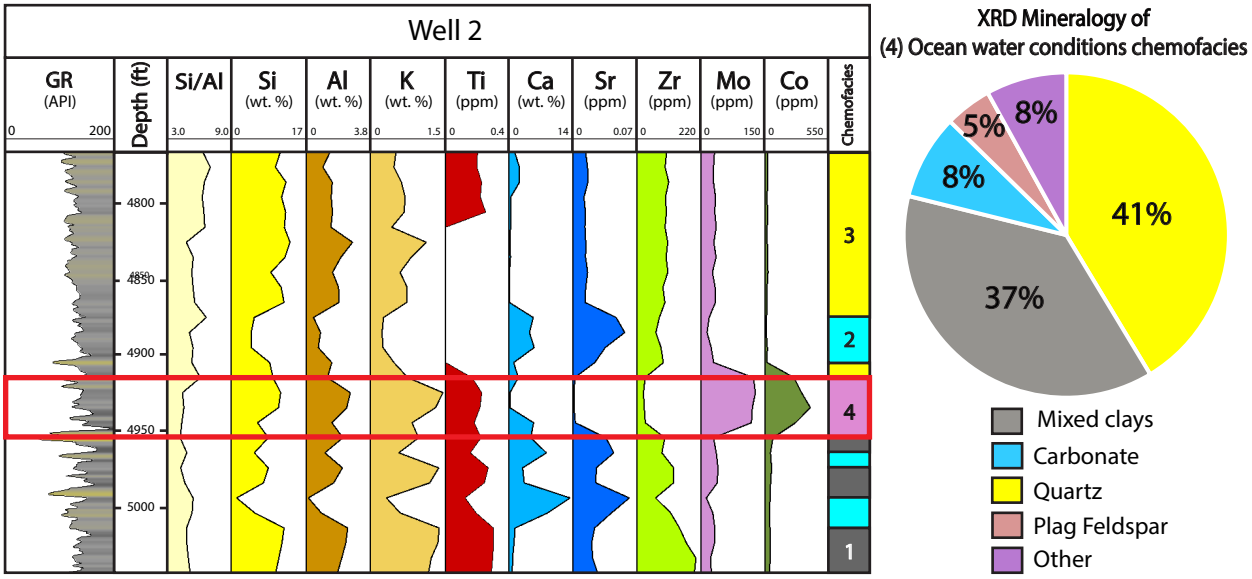

Appendix J4: Chemofacies 4 elemental curve patterns, stratigraphic distribution, and corresponding XRD mineralogy for Well 2.

Caney Shale Formation

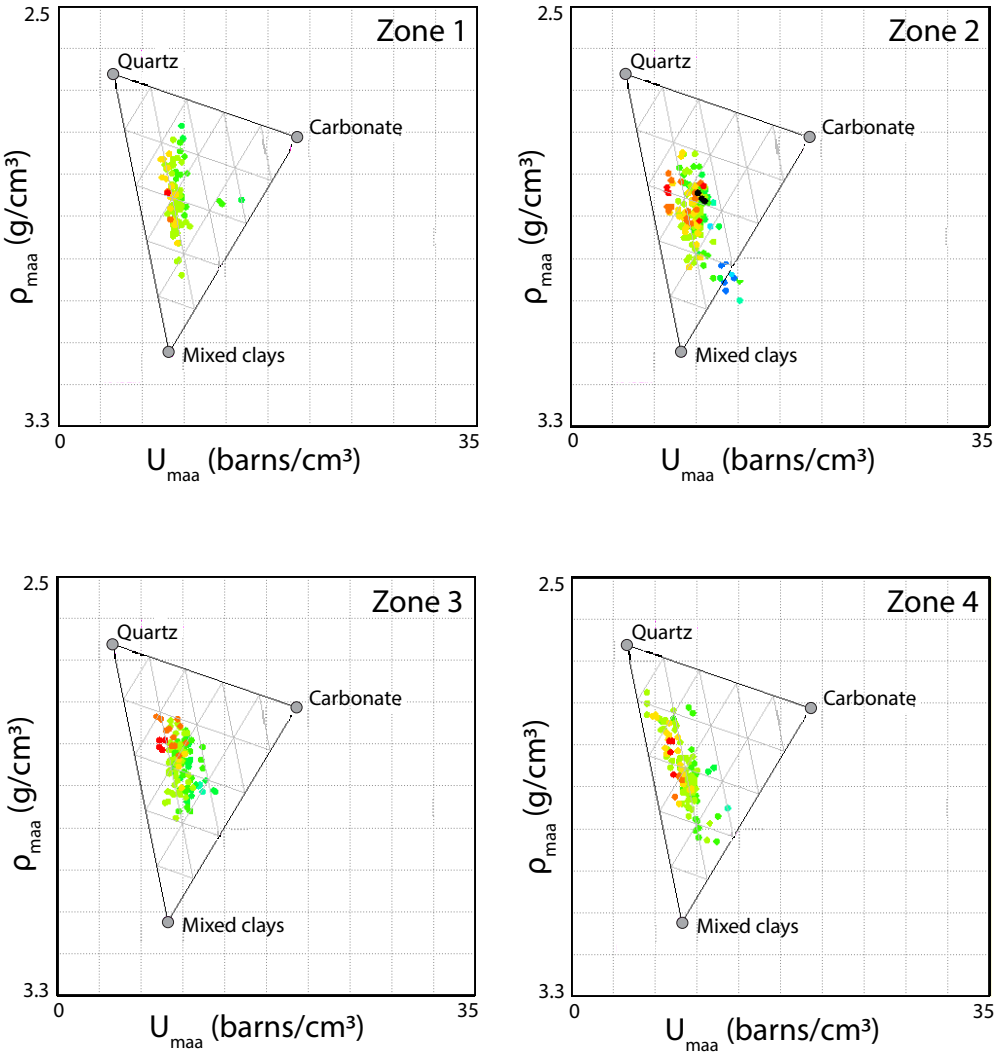

Appendix K1: The ρ_{maa}-U_{maa} analysis of the Caney Shale per zone of a type well located in the northern portion of the Ardmore Basin. ρ_{maa}-U_{maa} values plot lower on the 3 end-member mineral template for the Caney Shale than they do for the Sycamore Formation displayed in Appendix J2, indicating a difference in lithology.

Sycamore Formation

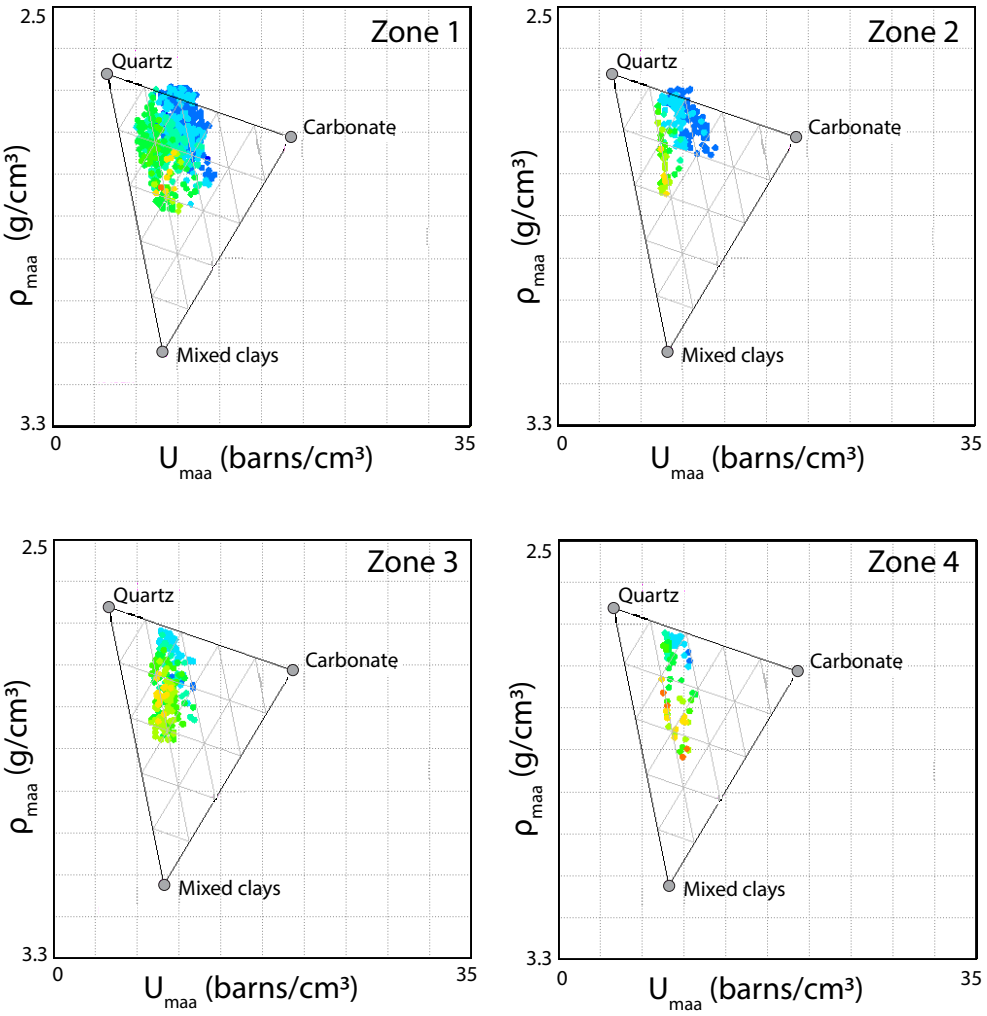

Appendix K2: ρ_{maa}-U_{maa} analysis of the Sycamore Formation per zone of a type well located in the northern portion of the Ardmore Basin. ρ_{maa}-U_{maa} values plot higher on the 3 end-member mineral template for the Sycamore Formation than they do for the Caney Shale formation displayed in Appendix J1, indicating a difference in lithology.

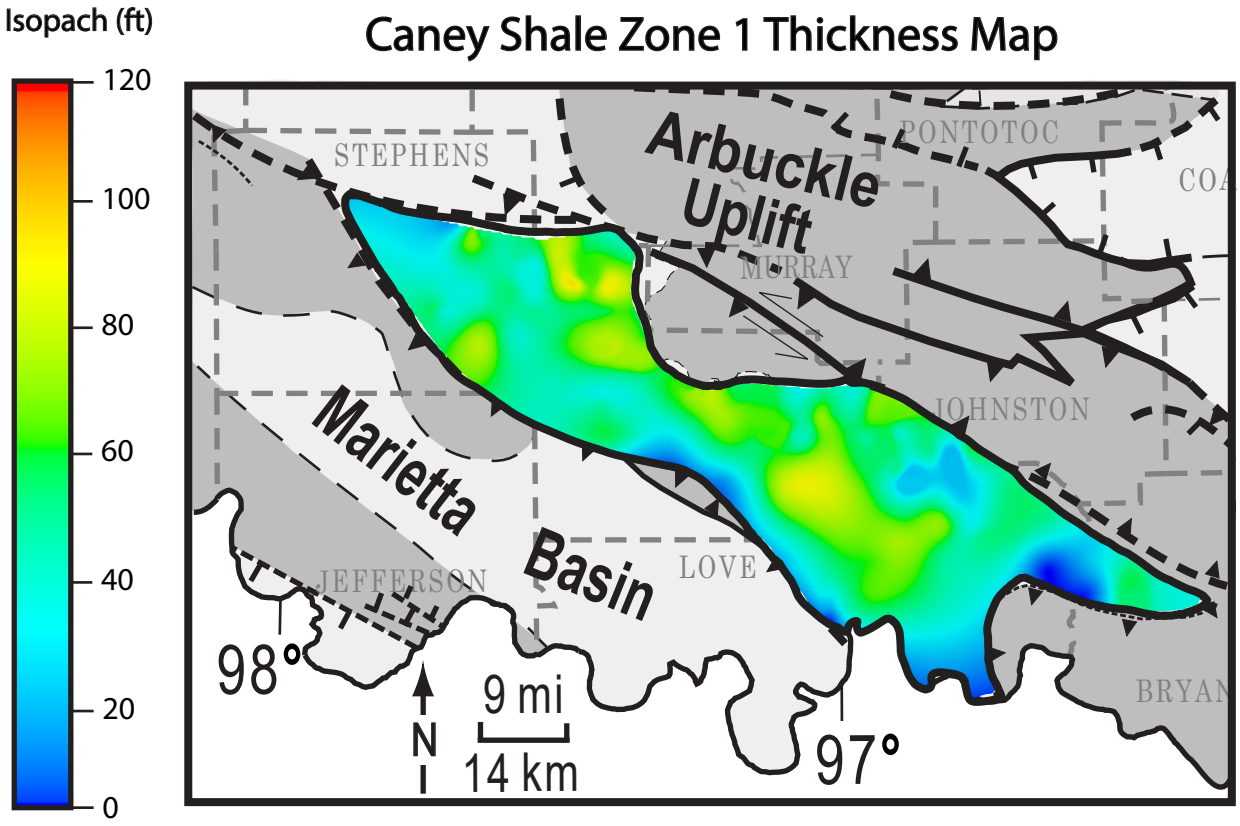

Appendix L1: Caney Shale isopach map for zone 1. Thinner portions of the Caney Shale are represented by the color blue, and thicker portions are represented by yellow and red.

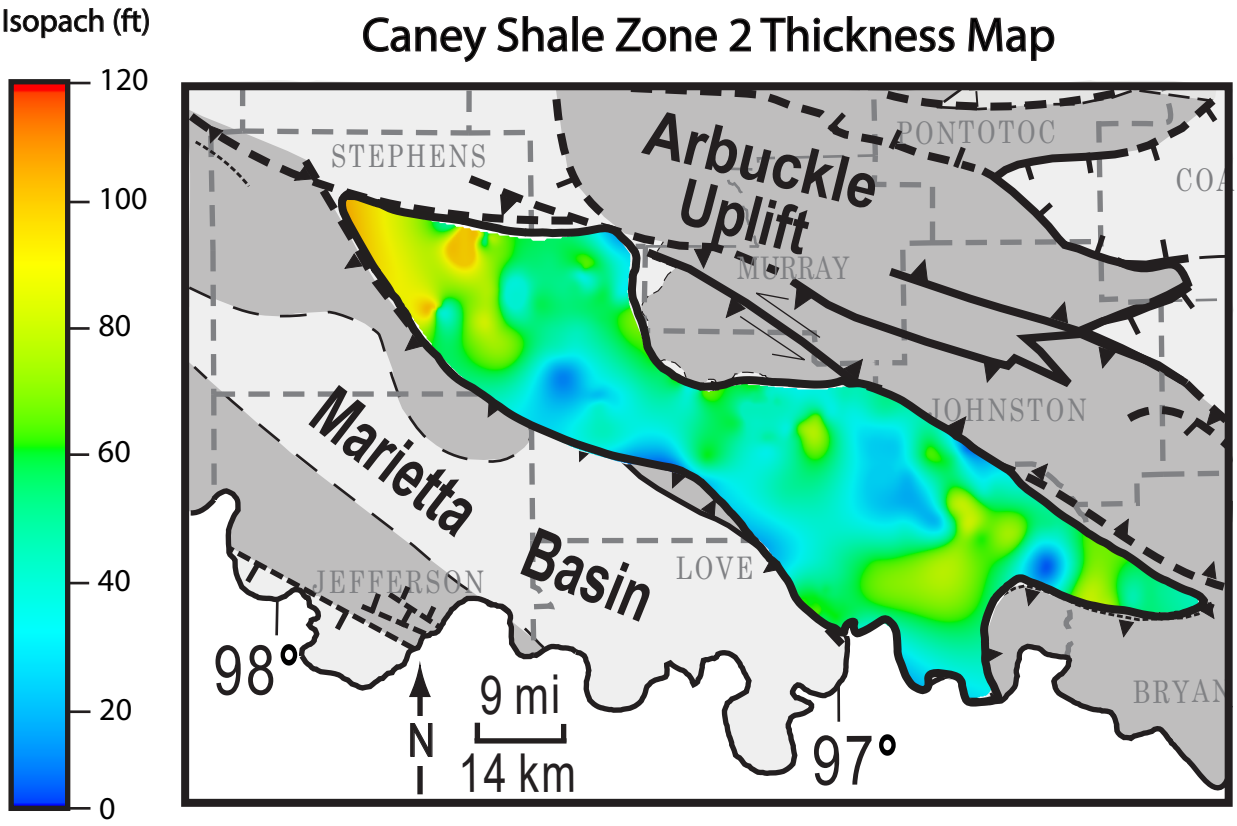

Appendix L2: Caney Shale isopach map for zone 2. Thinner portions of the Caney Shale are represented by the color blue, and thicker portions are represented by yellow and red.

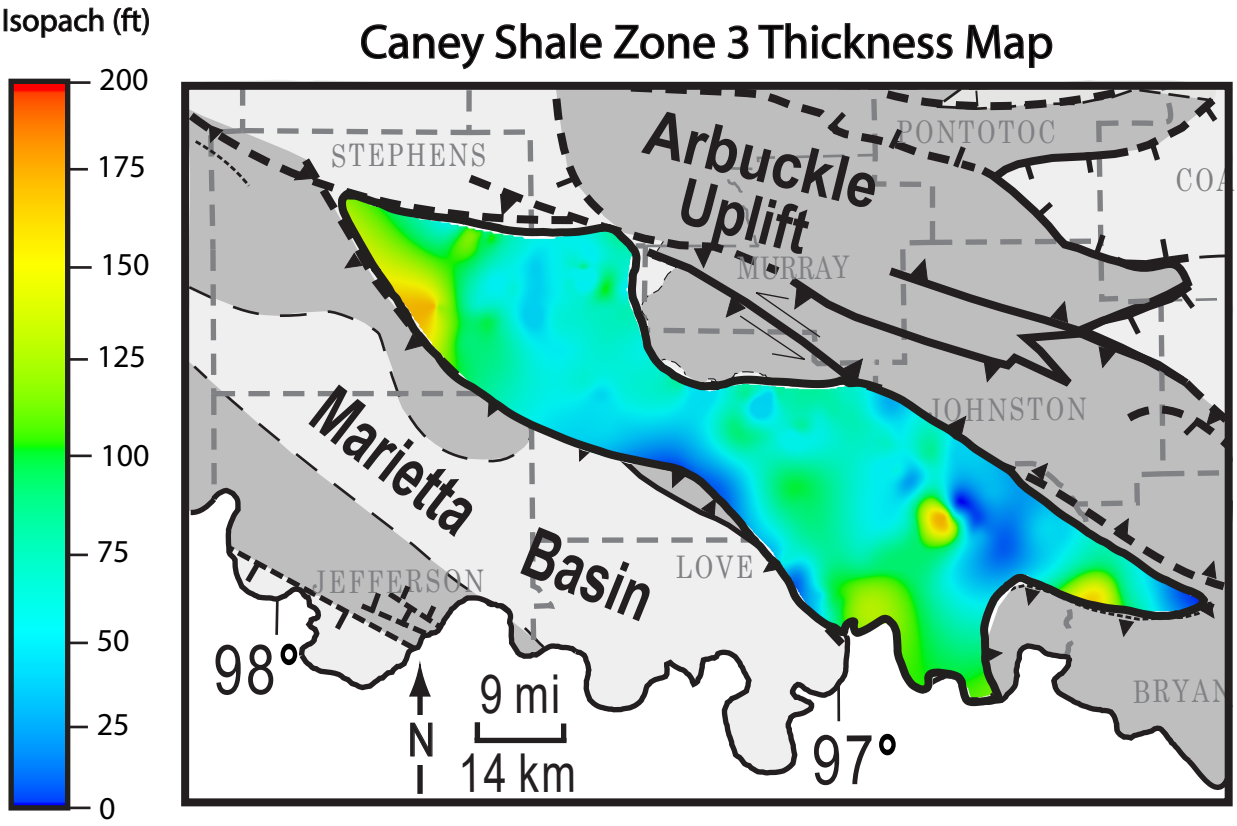

Appendix L3: Caney Shale isopach map for zone 3. Thinner portions of the Caney Shale are represented by the color blue, and thicker portions are represented by yellow and red.

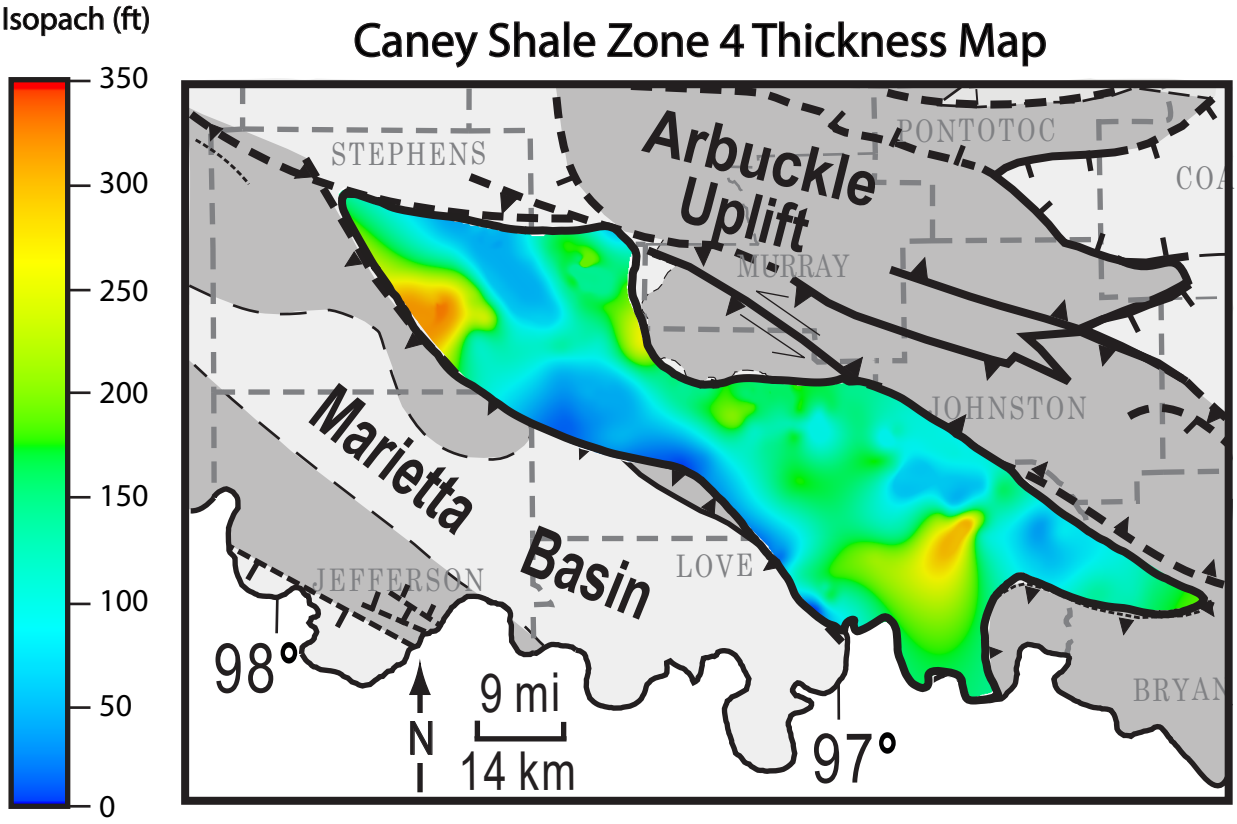

Appendix L4: Caney Shale isopach map for zone 4. Thinner portions of the Caney Shale are represented by the color blue, and thicker portions are represented by yellow and red. Thickest portions of the Caney Shale occur in this zone.

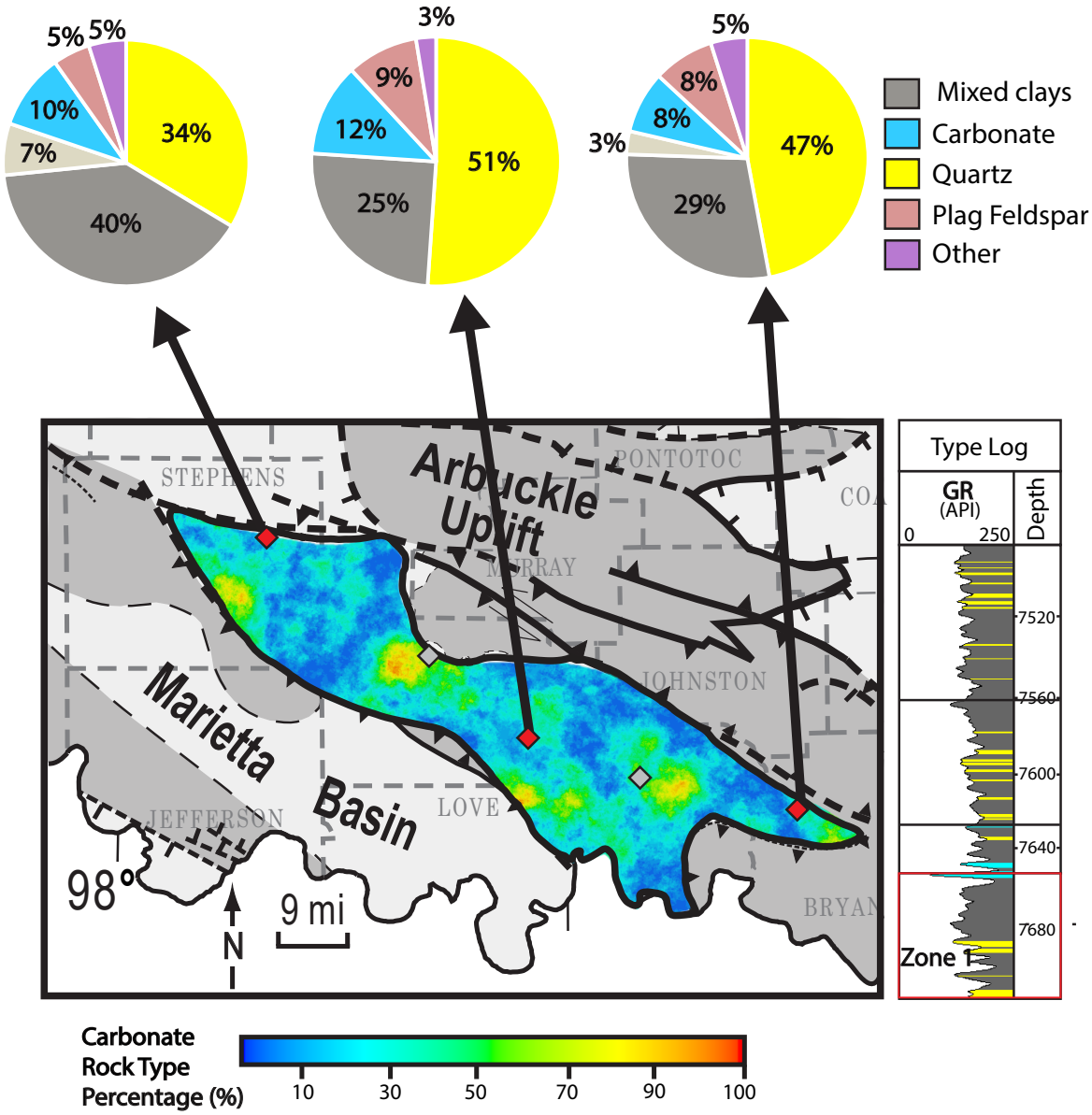

Appendix M1: ρ_{maa}-U_{maa} derived carbonate rock type percentage map for zone 1 of the Caney Shale. A GR type log colored by rock type is displayed to the right to show the stratigraphic location. Blue indicates areas with low carbonate abundance, and red indicates high carbonate abundance. XRD mineral percentage pies are displayed above to tie rock types to mineralogical anlayses. Zone 1 displays a moderate abundance of carbonate compared to the other zones.

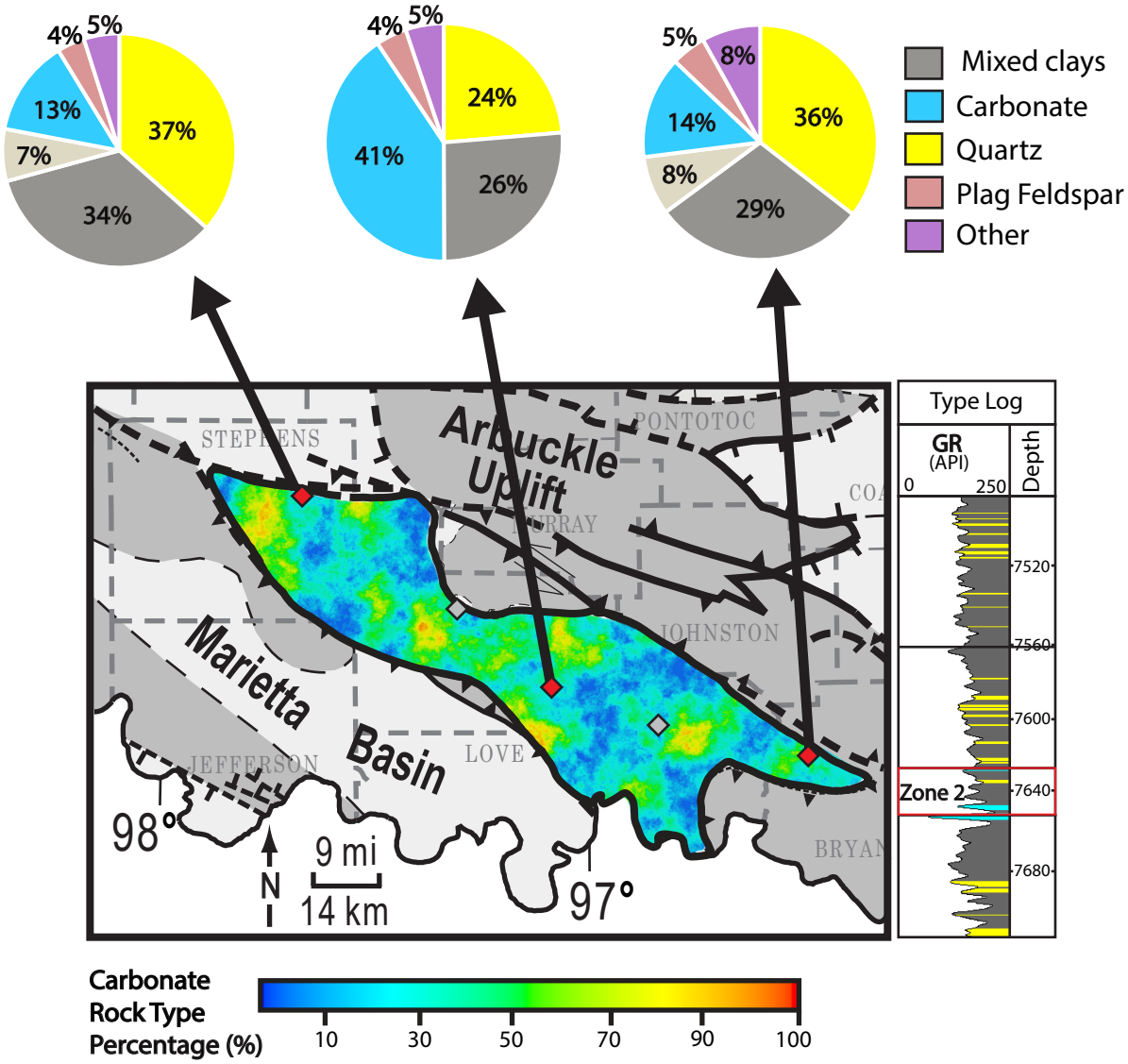

Appendix M2: ρ_{maa}-U_{maa} derived carbonate rock type percentage map for zone 2 of the Caney Shale. A GR type log colored by rock type is displayed to the right to show the stratigraphic location. Blue indicates areas with low carbonate abundance, and red indicates high carbonate abundance. XRD mineral percentage pies are displayed above to tie rock types to mineralogical anlayses. Zone 2 displays a high abundance of carbonate compared to the other zones, especially in the central portion of the basin.

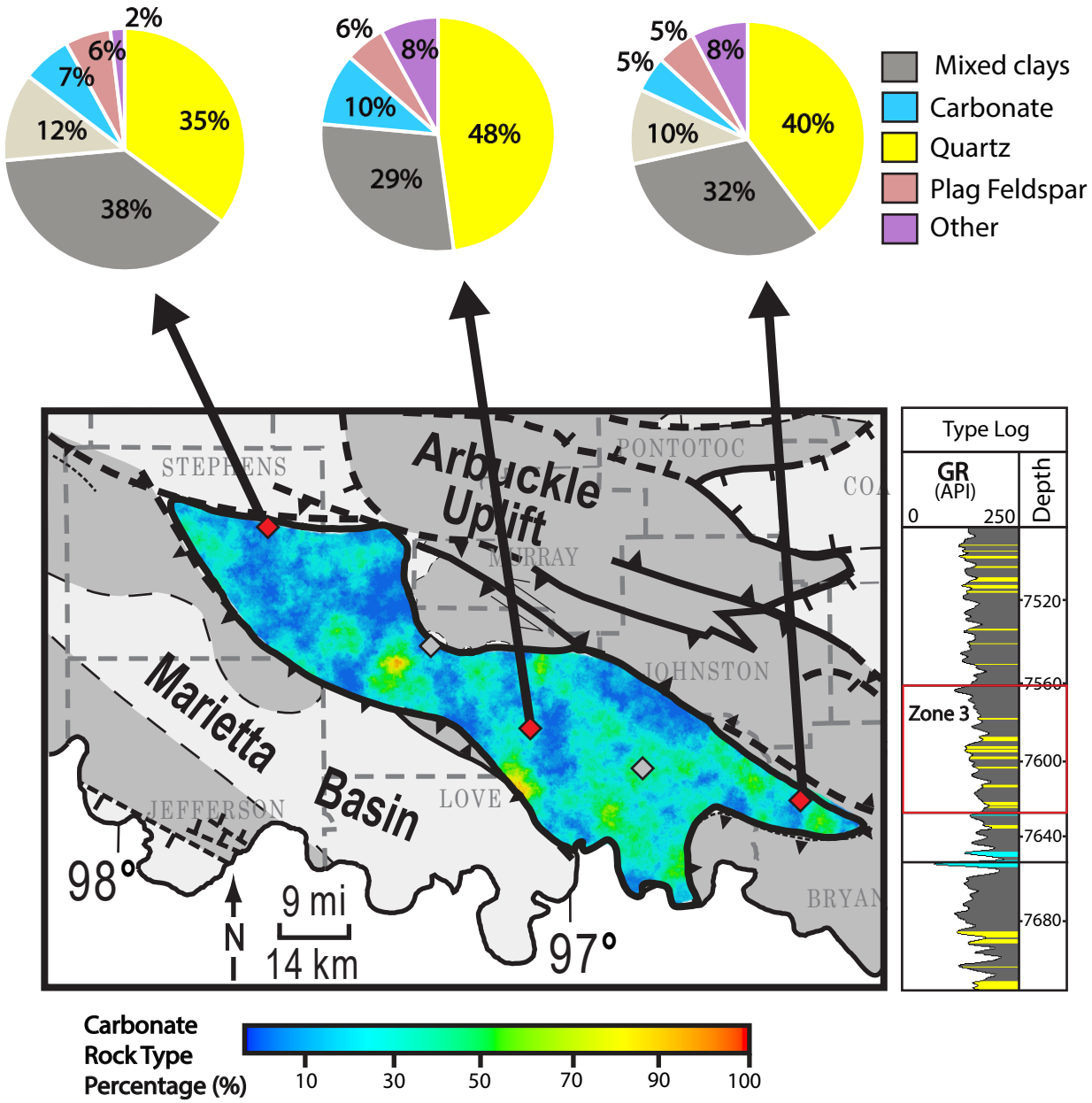

Appendix M3: ρ_{maa}-U_{maa} derived carbonate rock type percentage map for zone 3 of the Caney Shale. A GR type log colored by rock type is displayed to the right to show the stratigraphic location. Blue indicates areas with low carbonate abundance, and red indicates high carbonate abundance. XRD mineral percentage pies are displayed above to tie rock types to mineralogical anlayses. Zone 3 displays a lower abundance of carbonate compared to the other zones.

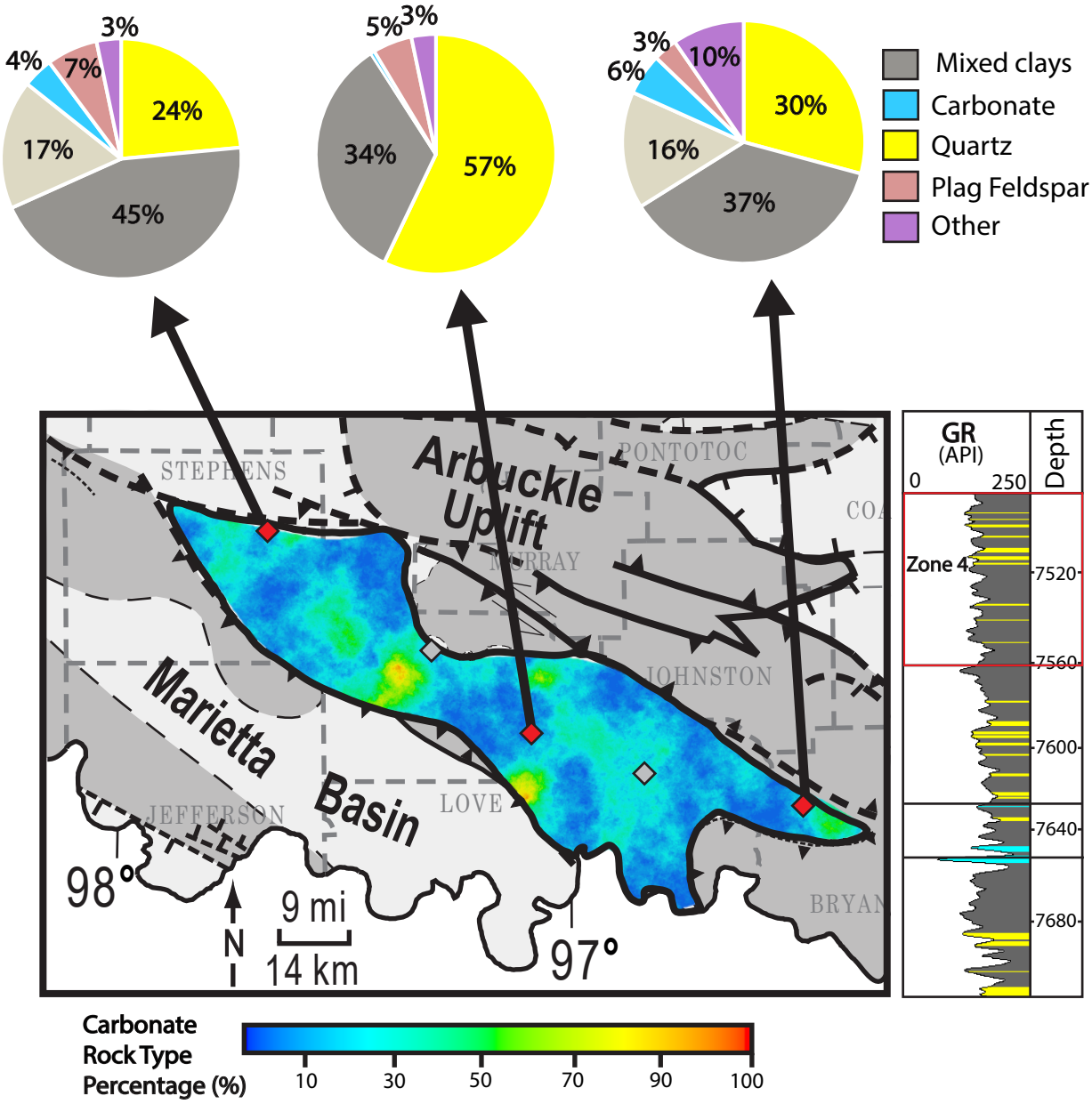

Appendix M4: ρ_{maa}-U_{maa} derived carbonate rock type percentage map for zone 4 of the Caney Shale. A GR type log colored by rock type is displayed to the right to show the stratigraphic location. Blue indicates areas with low carbonate abundance, and red indicates high carbonate abundance. XRD mineral percentage pies are displayed above to tie rock types to mineralogical anlayses. Zone 4 displays the lowest carbonate abundance, and the highest abundance of mixed clays and quartz.

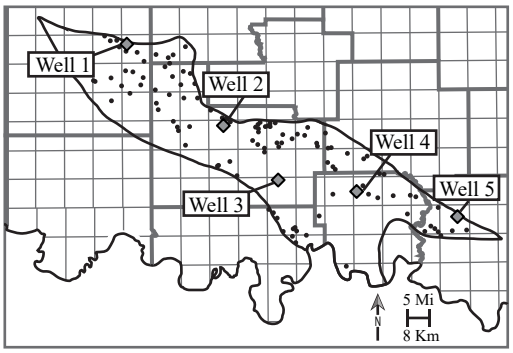

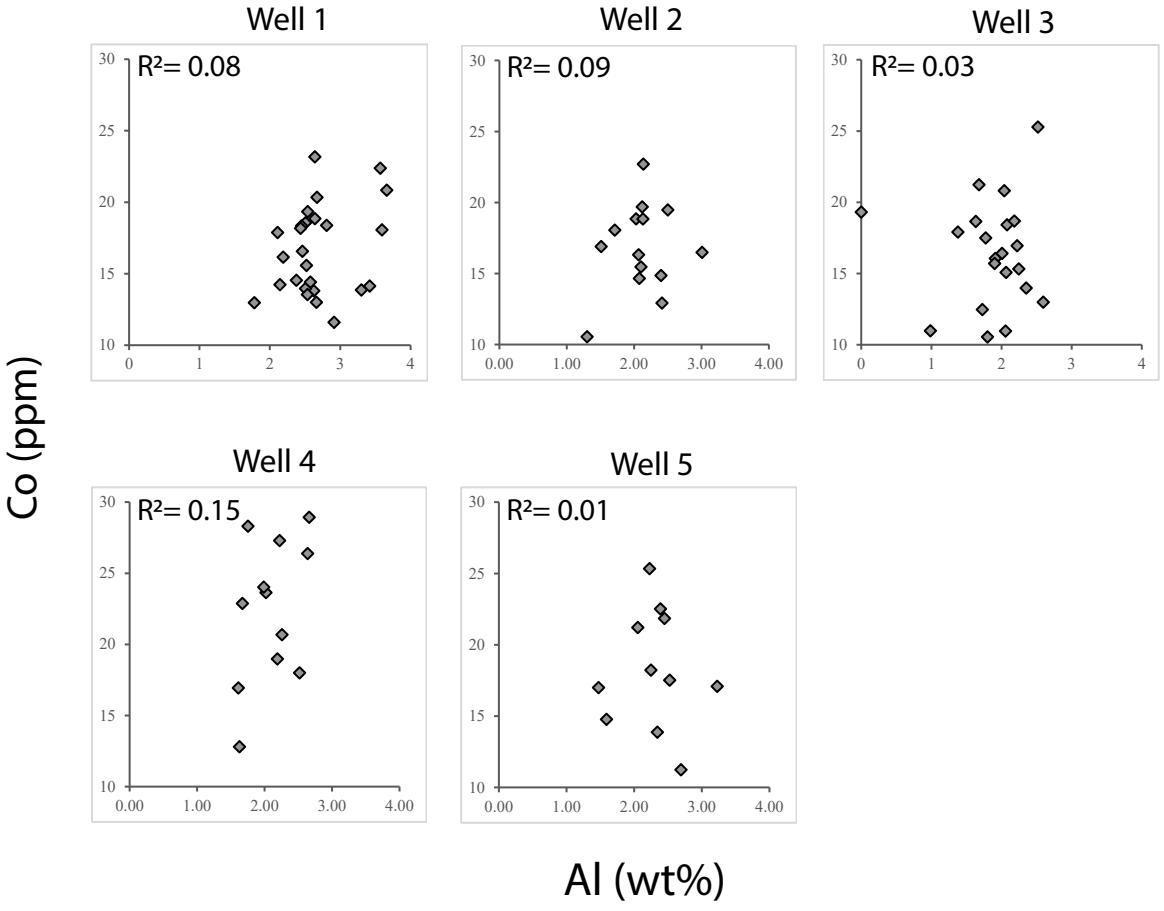

Appendix N: Cross plots of aluminum (Al) versus cobalt (Co) for each well with elemental data display a non-correlative relationship, indicating that Al and Co are likely sourced from different origins. Well locations are shown on the map in the upper-right corner.